THE OPTIMIZATION OF A TIME-RESOLVED, VESICLE-BASED FLUORESCENCE ASSAY FOR THE ACTIVITY OF THE LIPID KINASE PI4K-IIIBETA AND THE EFFECT OF LIPID TRANSFER PROTEINS ON ENZYME ACTIVITY

Marcelo Muniz Correa, BSc

Department of Chemistry and Centre for Biotechnology

A thesis submitted to the Department of Chemistry and Centre for Biotechnology

in partial fulfillment of the requirements for the degree

of Master of Science (Gene Biotechnology)

Brock University

St. Catharines, Ontario

August 2023

Abstract

Human PI4K-IIIβ is an 89 kDa phosphatidylinositol (PI) kinase that phosphorylates its substrate headgroup at position C-4, thus producing PI(4)P. This phosphoinositide is the most abundant in the *trans*-Golgi network where it is essential for secretory vesicle formation, as well as the precursor for other phosphoinositides that are crucial for intracellular signalling. Among others, phosphoinositide homeostasis in eukaryotic membranes rely on PI kinases and PI transfer proteins (PITPs). In yeast, the PITP Sec14p is known to exchange PI and phosphatidylcholine between lipid bilayers *in vitro* and proposed to present PI to be phosphorylated by the PI4-kinase Pik1 in a heterotypic ligand exchange fashion. However, the precise mechanism by which this interaction occurs has yet to be elucidated. To explore how and if PITPs and PI4K-IIIβ work as hypothesized, we expressed and purified recombinant human PI4K-IIIβ in *Escherichia coli* and assayed lipid kinase activity using an optimized real-time, vesicle-based fluorescence assay. After comparing different affinity tags, deletion mutants and expressing cell lines, GST-tagged wild-type PI4K-IIIβ was chosen and expressed in Rosetta 2(DE3) cells with a 2.5-fold increase in the native protein yield when compared to other methods. Proteins were further purified by an addition heat shock protein removal wash. The resulting PI4K-IIIβ displayed activity comparable to the commercially available, insect cell expressed counterpart. Optimization of the activity assay afforded a robust assay that displayed protein concentration dependent response while using unilamellar liposomes as the substrate. Agreeing with previous reports, the activity of PI4K-IIIβ was greatly reduced by wortmannin and increased by Triton X-100. The activity of PI4K-IIIβ was tested in the presence of active human PITPα and PITPβ, as well as yeast Frequenin and Sec14p, but none of them elicited a reproducible enhancement on PI(4)P production by PI4K-IIIβ. A similar pattern was observed with the human PI3-kinase, PIK3C3.

Our results demonstrate that a PI presentation model based on heterotypic exchange may not occur *in vitro*, suggesting either that PITPs' role in phosphoinositide production could rely uniquely on maintaining sufficient PI pools in the Golgi membrane or that additional protein partners may be required for the regulation of PI4K-IIIβ by PITPs.

Acknowledgements

They say that perhaps the most important qualities when looking for a mentor are being supportive, caring, and humane, and for that I would like to thank my supervisor, Dr. Jeffrey Atkinson. His wisdom, example-based leadership, the endless supply of interesting stories and ability to find the best words for any situation are unique and inspiring. A similar recognition is in order for Dr. Candace Panagabko, for her never-ending support and the altruism that permeates her actions. Her incessant curiosity and creativity are admirable and played a major role on the development of this project. I would like to also thank the members of my supervisory committee, Dr. Paul Zelisko and Dr. Stephen Glasgow, and to my external examiner, Dr. Roberto Botelho for their meaningful insights throughout my MSc path and defence.

Working in the Atkinson lab for the past five years would not have been the same without great colleagues with whom I shared my good and bad days, thoughts, experiments, asked for input when troubleshooting, and learned from. To Anneliese von Eicken, Vansh Metta, Sean Wilson, Jennifer Kujani, Alex Bernekier, Natalie Boccalon, Tayo Laleye, Morgan Robinson, Shannon Jewel, and Kailey Meehan: thank you. I am grateful too to members of Dr. Tony Yan's group, with whom we shared lab space, laughs, concerns, TA jokes and liquid nitrogen.

Special recognition is directed to my aunt, Dr. Muniz-Oliveira, who inspired me to pursue graduate studies by inviting me to attend her MA in Applied Linguistics defence when I was 11 years old. She has been a role model and fierce advocate for education within my family. Finally, to my close friends who became family in Canada, to my family back home who is always present, to my parents (who tirelessly taught me the value of education), and to my partner Felipe for being beside me rain or shine: muito obrigado! This MSc degree taught me so much, besides being fun, challenging, and intense. I would not have it any other way.

Table of Contents

List of Tables

List of Figures

List of Abbreviations

ACBD3: acyl-CoA-binding domain containing protein 3
ADP: adenosine diphosphate
Akt: protein kinase B
APS: ammonium persulfate
ARF1 and ARF1-GTP, Afr1: ADP-ribosylation factor 1
ATP: adenosine triphosphate
BME: 2-mercaptoethanol
BSA: bovine serum albumin
CR: cysteine-rich
CL: cardiolipin
CRAL-TRIO: protein structural domain named after cellular retinaldehyde-binding protein and TRIO guanine exchange factor
CDP: cytidine diphosphate
CDP-DAG: cytidine diphosphate diacylglycerol
COPI: coat protein, an ADP ribosylation factor (ARF)-dependent protein
DAG: diacylglycerol
DF: dilution factor
DMSO: dimethyl sulfoxide
DOPC: 1,2-dioleoyl-sn-glycero-3-phosphocholine
dNTP: deoxynucleotide triphosphate
DTT: dithiothreitol
EDTA: ethylenediaminetetraacetic acid
EGF: epidermal growth factor
EGTA: ethylene glycol-bis(β-aminoethyl ether)-N,N,N′,N′-tetraacetic acid
ENTH: Epsin N-terminal homology
ER: endoplasmic reticulum
FI: fluorescence intensity
Frq1: frequenin protein
FW: Forward primer
GFP: Green Fluorescent Protein
GTP: guanosine-5'-triphosphate
GST: glutathione S-transferase
GUV: giant unilamellar vesicle
HCV: Hepatitis C Virus
HDX-MS: Hydrogen-deuterium exchange – mass spectrometry
HEPES: 4-(2-hydroxyethyl)-1-piperazineethanesulfonic acid
HF: high-fidelity
HRV 3C: human Rhinovirus 3C protease
HSP: heat-shock protein
IMAC: Immobilized Metal Affinity Chromatography
Ins: *myo*-inositol
IP_3: inositol 1,4,5-trisphosphate
IPTG: isopropyl-1-thio-β-D-galactopyranoside
LB: lysogeny broth

LTPs: lipid transfer proteins
LKU: lipid kinase unique domain
Lsb6p: *Saccharomyces cerevisiae*'s orthologue of PI4K-II
LUVs: large (>100 nm), unilamellar (phospholipid) vesicles
Max FI: maximum fluorescence intensity of assay window
MES: 2-morpholin-4-ylethanesulfonic acid
Min FI: minimum fluorescence intensity of assay window
mTOR: mammalian target of rapamycin
mQH$_2$O: milli-Q H_2O
MW: molecular weight
NBD-PC: NBD C_{12}-HPC (2-(12-(7-Nitrobenz-2-Oxa-1,3-Diazol-4-yl)amino)Dodecanoyl-1-Hexadecanoyl-*sn*-Glycero-3-Phosphocholine)
NCS-1: neuronal calcium sensor-1
NLS: nuclear localization sequence
NMR: Nuclear magnetic resonance
OD: optical density
OSBP: oxysterol-binding protein 1
PA: phosphatidic acid
PAGE: polyacrylamide gel electrophoresis
PBS: phosphate buffered saline
PC: phosphatidylcholine
PCR: polymerase chain reaction
PDB: protein data bank
PE: phosphatidylethanolamine
PG: phosphatidylglycerol
PH: plekstrin homology
PI: phosphatidylinositol
Pik1: *Saccharomyces cerevisiae* type III β PI4K protein
PIK3C3: human phosphatidylinositol 3-kinase Class III protein
PIPK: phosphoinositide phosphate kinase
PIPs: phosphoinositides
PIPES: 1,4-Piperazinediethanesulfonic acid
PITPs: phosphatidylinositol/phosphatidylcholine transfer proteins
PI(3,4,5)P3: phosphatidylinositol 3,4,5-trisphosphate
PI(3,4)P2: phosphatidylinositol 3,4-bisphosphate
PI(3,5)P2: phosphatidylinositol 3,5-bisphosphate
PI(3)P: phosphatidylinositol 3-phosphate
PI(4,5)P2: phosphatidylinositol 4,5-bisphosphate
PI(4)P: phosphatidylinositol 4-phosphate
PI(5)P: phosphatidylinositol 5-phosphate
PI3K: phosphatidylinositol 3-kinase
PI4K: phosphatidylinositol 4-kinase
PI4K-IIIβ: phosphatidylinositol 4-kinase type III beta protein
PKD: protein kinase D
PLC: phospholipase C
PLD: phospholipase D

PMSF: phenylmethylsulfonyl fluoride
PtdIns: phosphatidylinositol
PTD: PI transfer domain
PTM: posttranslational modification
PR: proline-rich domain
PS: phosphatidylserine
PVDF: polyvinylidene fluoride
PX: Phox Homology domain
Rab11: Ras-related protein 11
RFU: relative fluorescence units
RO: reverse osmosis
RPM: rotations per minute
RT: room temperature (25ºC)
RV: reverse primer
SARS: severe acute respiratory syndrome
SD: standard deviation
SDS: sodium dodecyl sulfate
Sec14p: a *Saccharomyces cerevisiae* PITP
Ser: serine
Stt4: staurosporine and temperature sensitive, *Saccharomyces cerevisiae* type III α PI4K
SUVs: small (<100 nm), unilamellar (phospholipid) vesicles
Taq: *Thermus aquaticus*
TB: terrific broth
TBS: Tris-buffered saline
TBST: Tris-buffered saline, 0.1% Tween® 20 detergent
TEMED: *N,N,N',N'*-Tetramethylethylenediamine
TGN: trans-Golgi network
Thr: threonine
TMB: 3,3′,5,5′-Tetramethylbenzidine
Tris-HCl: Tris(hydroxymethyl)aminomethane-hydrochloride
Vps15: vacuolar protein sorting mutant 15 protein
Vps34: vacuolar protein sorting mutant 34 protein, *Saccharomyces cerevisiae* class III PI3K
WC: whole cell

1 INTRODUCTION

1.1 Phosphatidylinositol (PI) and Phosphoinositides (PIPs)

1.1.1 Biological membranes and phosphatidylinositol

Biological membranes, which include both the plasma and organelle membranes, are of primordial importance to the existence of living organisms as those barriers provide mechanical protection, compartmentalization, transport, and communication (Stillwell, 2016). Biological membranes are mostly composed of a phospholipid bilayer, but sugar-linked lipids, sterols, and proteins are also present. The polar headgroups of phospholipids are found on the two surfaces of the plasma membrane bilayer, affording a hydrophilic zone. Between the headgroups, fatty acyl chains form a highly hydrophobic barrier that separates the aqueous phases of the cytoplasm from either the extracellular matrix (when referring to the plasma membrane) or the interior compartment (when referring to an organelle) (Casares et al., 2019). The lipid composition of membranes varies according to the organism type (eukaryote, prokaryote), membrane type (cell membrane, organelles membranes), and the cell status (at rest or in response to stimuli/stress), which is key to membranes being recognized at the molecular level in many different biochemical pathways (Casares et al., 2019).

There are seven major classes of glycerophospholipids found in mammalian membranes: phosphatidic acid (PA), phosphatidylcholine (PC), phosphatidylethanolamine (PE), phosphatidylserine (PS), phosphatidylglycerol (PG), cardiolipin (CL), and phosphatidylinositol (PI) (Stillwell, 2016), the latter being the most relevant for the present study. PI represents about

5-7% of the total cellular phospholipid content in mammalian cellular membranes, and thus is a fairly minor constituent (Cockcroft & Raghu, 2016).

PI[1] is a glycerophospholipid whose glycerol is esterified at positions *sn*-1 and *sn*-2 by two fatty acid chains. Connected to the position *sn*-3 is a phosphate group, to which a *myo*-inositol ring is attached (**Figure 1**). The most prevalent fatty acid tails in budding yeast's (*Saccharomyces cerevisiae*) PI are palmitic acid (16:0) at the *sn*-1 position and oleic (18:1) or palmitoleic acid (16:1) at the *sn*-2 position (De Craene et al., 2017). In humans, the PI's acyl chains are enriched in stearic acid (18:0) and arachidonic acid (20:4) (Cockcroft & Raghu, 2016).

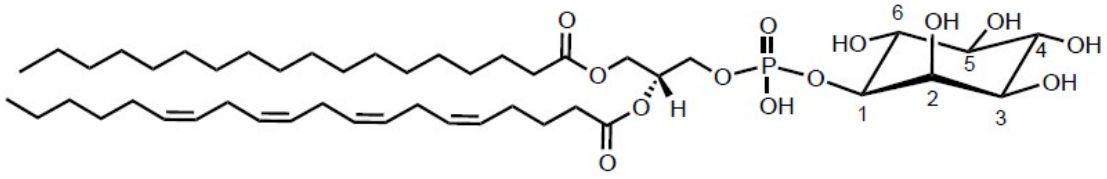

Figure 1: **Structure of the predominant form of phosphatidylinositol (PI) in mammalian cells.** The acyl chains shown in positions *sn*-1 and *sn*-2 are stearic acid (18:0) and arachidonic acid (20:4). Figure created with ChemDraw.

PI is biosynthesized in all mammalian cells. In humans, *de novo* synthesis of PI from PA is catalyzed by PI synthase on the cytoplasmic face of the endoplasmic reticulum (ER), Golgi complex, microsomes and mitochondria. PI can also be recycled from phosphatidylinositol-3 phosphate (PI(3)P), PI(4)P, and PI(5)P following the action of the respective lipid phosphatases

[1] Note: the abbreviations "PtdIns" and "PI" are both commonly used for phosphatidylinositol and its phosphorylated derivatives. It was previously suggested that "Ins" should be used when referring to *myo*-inositol as this is the biochemically relevant stereoisomer of inositol (Liébecq et al., 1992). Later, the International Lipid Classification and Nomenclature Committee established a Comprehensive Classification System for Lipids, in which the two-letter abbreviations for glycerophospholipids (*e.g.* "PC", "PS", "PI", etc.) were adopted (Fahy et al., 2009). In this work, and for simplicity, "PI" will be mostly used, but "PtdIns" may also appear in figures taken with authorization from other sources.

(De Craene et al., 2017). PA is formed by the phosphorylation of 1,2-diacylglycerol (DAG) by diacylglycerol kinases. In the presence of cytidine diphosphate (CDP), PA is converted to cytidine diphosphate diacylglycerol (CDP-DG) by CPD-DG synthase, which is followed by the condensation of the latter and *myo*-inositol by PI synthase. This reaction gives rise to PI, which is then transported to non-ER membranes via vesicular transport or by the action of phosphatidylinositol transfer proteins (PITP) (Cockcroft & Raghu, 2016). It has been shown that loss-of-function of the PI synthase gene is lethal in *Drosophila* and yeast, thus proving the importance of said lipid in normal functioning of eukaryotes, specifically signalling pathways (Cockcroft & Raghu, 2016). In fact, phosphorylated PI derivatives (phosphoinositides or PIPs) are the molecules that participate in different signaling pathways. Therefore, it is important to understand the details of PI-to-PIP conversions as well as their regulation.

1.1.2 PIPs and Lipids Signalling

PI's inositol ring is a polyol cyclohexane (or cyclitol) (**Figure 1**) whose hydroxyl groups linked to C-3, C-4, and C-5 can be phosphorylated by corresponding kinases, thus giving rise to seven possible phosphoinositides (PIPs) (Figure 2A):

- phosphatidylinositol 3-phosphate, PI(3)P;
- phosphatidylinositol 4-phosphate, PI(4)P;
- phosphatidylinositol 5-phosphate, PI(5)P;
- phosphatidylinositol 3,4-bisphosphate, PI(3,4)P_2;
- phosphatidylinositol 3,5-bisphosphate, PI(3,5)P_2;
- phosphatidylinositol 4,5-bisphosphate, PI(4,5)P_2;
- and phosphatidylinositol 3,4,5-triphosphate, PI(3,4,5)P_3.

Despite representing only 1% of the total cellular phospholipid content, PIPs play a crucial role in recruiting and/or activating effector proteins in a variety of intracellular pathways (De Craene et al., 2017), as well as aiding to define organelle identity and to regulate membrane trafficking, transport, and permeability (Grabon et al., 2019). For instance, $PI(4,5)P_2$ is known to be the main lipid determinant of the plasma membrane, whereas PI(3)P and $PI(3,5)P_2$ are the hallmarks of early and late endosomes (Boura & Nencka, 2015). Being so diverse in their structure and function, PIPs are continuously turned over and their concentrations in the cell are tightly regulated by the matching kinases/phosphatases (Fruman et al., 1998).

Perhaps the most studied PIP is $PI(4,5)P_2$, a substrate for phospholipase C (PLC). This enzyme turns $PI(4,5)P_2$ into inositol 1,4,5-triphosphate (IP_3) and diacylglycerol (DAG), both important intracellular second messengers (Gericke et al., 2013). IP_3, a soluble messenger, is able to diffuse across the cytoplasm and binds to IP_3-receptors on the ER surface, which in turn opens an ion channel that allows Ca^{2+} to be released from the ER (Payrastre et al., 2001) (Figure 2B). Maintaining the balance of intracellular Ca^{2+} levels by this pathway is important for the regulation of the excitation-contraction mechanism in smooth muscle (Somlyo & Somlyo, 1994).

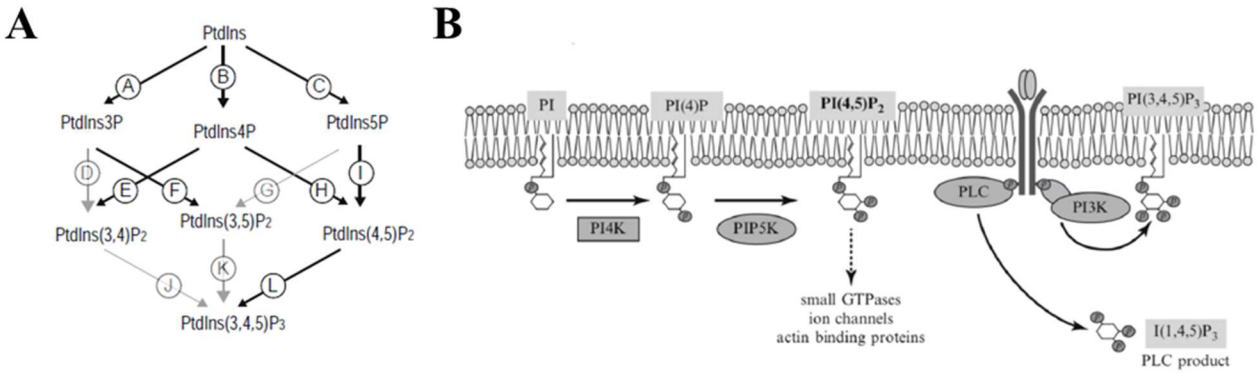

Figure 2: The fate of PI *in-vivo.* 2A: Different PIPs can be generated by phosphorylation of PI at different C-positions on the inositol headgroup. Phosphorylation is performed by many PI- and PIP-kinases, which are represented by letters A-L. Image used with permission from Sasaki *et al*., 2009. **2B:** In a classic example of PIP turnover, subsequent phosphorylation reactions of PI lead to the production of $PI(4,5)P_2$, which in turn is cleaved by PLC to give IP_3 and DAG (not shown), both known second messengers. Image used with permission from Gerike et al (2013).

Besides being a precursor to important intracellular second messengers, $PI(4,5)P_2$ can also act as a signalling molecule on its own. This PIP has been shown to affect cytoskeleton organization by interacting with actin-binding proteins like profilin and gelsolin. More specifically, $PI(4,5)P_2$ promotes profilin-actin dissociation thereby regulating the concentration of free actin monomers intracellularly (Hilpelä et al., 2004). Additionally, it has been suggested that $PI(4,5)P_2$ acts as a secondary messenger by controlling the local adhesion energy between the cytoskeleton and the plasma membrane. Raucher *et al*. (2000) documented a direct relationship between lower concentrations of $PI(4,5)P_2$ and smaller adhesion energy, thus leading to the formation of membrane blebs (Raucher et al., 2000).

Another member of this family, PI(4)P is now seen as more than a mere predecessor of other PIPs. Chiefly produced on the Golgi complex membrane though the phosphorylation of PI by PI(4)-kinases or through dephosphorylation of $PI(4,5)P_2$ and $PI(3,4)P_2$ by phosphatases, PI(4)P is the main lipid determinant of the Golgi and *trans*-Golgi network (TGN) (Boura & Nencka, 2015), which is also where this phospholipid executes some of its main functions. Being a central "station" in membrane trafficking, the Golgi complex relies on tightly regulated mechanisms to sort proteins and lipids between different intracellular compartments. In yeast, PI(4)P has been shown to be required for secretory vesicle formation, notably those formed at the Golgi and targeted to the plasma membrane (De Craene et al., 2017). More specifically, effector proteins involved in vesicle formation such as small GTPases of the Rab and Arf families bind to PI(4)P on the Golgi membrane surface and recruit the vesicle biogenesis machinery that triggers vesicle budding (Grabon et al., 2019). At the same locus, PI(4)P also attracts many lipid transfer proteins (LTPs) like OSBP (oxysterol-binding protein 1), CERT (ceramide transport protein), and FAPP2 (four-phosphate-adaptor protein), which facilitates cholesterol, ceramide and

sphingolipid transport, respectively (McPhail & Burke, 2023). Proteins that bind the headgroup of membrane resident PI(4)P contain domains such as the Pleckstrin Homology (PH), Phox Homology (PX), Epsin N-Terminal Homology (ENTH), among others (Boura & Nencka, 2015).

PI(4)P is also formed at the plasma membrane, where it contributes to the pool of polyanionic lipids characteristic of the inner leaflet. This is important as many proteins identify the plasma membrane through basic amino acid residues that interact with anionic lipid head groups (Hammond et al., 2012). In addition, PI(4)P at the plasma membrane also serves as substrate for the formation of $PI(4,5)P_2$, which in turn is detected by clathrin adaptors during endocytic vesicle budding (Posor et al., 2022). PI(4)P can also be found in the membrane of other organelles such as phagosomes, lysosomes, and endosomes (reviewed in (De Matteis et al., 2013)). In the present work, however, the regulation of PI(4)P at the Golgi membrane will be focused on due to the PITPs and PI-kinases employed herein. The pools of PI(4)P in cellular membranes are produced by PI4-kinases and fine tuned by the antagonizing action of phosphatases like Sac1 (in yeast and mammals) (De Matteis et al., 2013) and PI(4)P/sterol exchangers like oxysterol binding proteins (Mukherjee et al., 2018).

1.2 PI-Kinases

1.2.1 PI3-kinases and PI5-kinases

An important aspect to understanding the structure and function of PIPs is appreciating the enzymes that control their synthesis. PI-kinases are enzymes that phosphorylate the headgroup of inositol at different positions. These enzymes catalyze the transfer of the gamma-phosphate group from ATP to the hydroxyl groups connected to C-3, C-4, or C-5 of the inositol ring, and thus are divided into three general families: PI(3)-kinases (PI3K), PI(4)-kinases (PI4K), and PI(5)-kinases (PIPK) (Fruman et al., 1998). Other than differing as to which

phosphorylated products they give rise to, these enzymes have also been historically differentiated by their biochemical properties (*e.g.* sensitivity to adenosine and non-ionic detergents), physiochemical properties (*e.g.* apparent molecular weight), as well as by their cellular locations. More specifically, type I PI-kinases are sensitive to non-ionic detergents but not inhibited by adenosine. In contrast, PI-kinases type II are inhibited by adenosine but activated by non-ionic detergents. Lastly, type III PI-kinases are maximally active when their substrates are present in detergent micelles, and they show relative resistance to adenosine inhibition. Furthermore, type III PI-kinases have been reported to be resistant to a monoclonal antibody that effectively inhibited type-II kinases (Carpenter & Cantley, 1990). At least one divalent cation such as Mg^{2+} or Mn^{2+} is required to neutralize negative charges in the ATP binding site, thus enabling catalytic activity of all of these enzymes (Adams, 2001; Lo et al., 2022). Type III PI3Ks are maximally active with Mn^{2+} (Stack & Emr, 1994; Volinia et al., 1995), but assays with type III PI4Ks typically employ Mg^{2+} (Burke et al., 2014; Fowler et al., 2016; Schaaf et al., 2008; X.-H. Zhao et al., 2000).

PI3Ks have representative enzymes in classes I, II, and III. Class I PI3Ks consists of heterodimeric proteins whose catalytic subunits are 110-120 kDa in size. These kinases can phosphorylate PI, PI(4)P, and PI(4,5)P_2 at position C-3 of inositol (Fruman et al., 1998), and play important roles in tumorigenesis via dysregulation of the PI3K/Akt/mammalian target of rapamycin (mTOR) signaling pathway (He et al., 2021). Additionally, members of the class I PI3K sub-family are known to have intrinsic protein kinase activity (L. Zhao & Vogt, 2008). Class II PI3Ks are larger proteins, ranging from 170-210 kDa, and phosphorylate preferentially PI and PI(4)P. Members of this class of PI3Ks, like PIK3C2, have a C-terminal region homologous to C2 domains, which are critical for Ca^{2+}-mediated binding to lipid membranes

(Fruman et al., 1998). Finally, class III PI3Ks are the most substrate-specific, as they only phosphorylate PI. The sole representative of class III PI3Ks in *Saccharomyces cerevisiae* is termed Vps34, an essential enzyme for proper sorting of nascent proteins from the Golgi to the vacuole. Vps34 is known to associate with Vps15, a protein kinase that activates the yeast PI3K type III and recruits it to membranes, thereby enhancing Vps34's activity. Vps15 has been shown to also be essential for vesicle sorting (Fruman et al., 1998). The human orthologue of Vps15, p150, performs a similar function on the human homologue of Vps34, PIK3C3 (Panaretou et al., 1997).

Although PI5Ks are also important in maintaining PIP homeostasis in the cell, namely in the conversion of PI(4)P to PI(4,5)P_2 (Fruman et al., 1998), this family of PIP-kinases will not be further discussed here as this project is focused on one of the PI4K proteins.

1.2.2 PI4-kinases

PI4-kinases (PI4Ks) have been explored for approximately 50 years, but much is still unknown about these proteins. PI4Ks are mostly abundant in the plasma and organelle membranes such as those of the Golgi apparatus, lysosomes, plasma membrane and ER. Unlike most of the other PI-kinases discussed earlier, PI4Ks seem to only use PI as their substrate. This makes PI4Ks very unique for signalling pathways as they feed PI(4)P (Figure 3) to be further phosphorylated by PI3Ks and PIPKs (Fruman et al., 1998). There are two classes of PI4Ks, II and III, and these are ubiquitously expressed by all eukaryotes from yeast to humans. Notably, class III PI4Ks are more closely related to PI3Ks than to PI4K type II (Boura & Nencka, 2015).

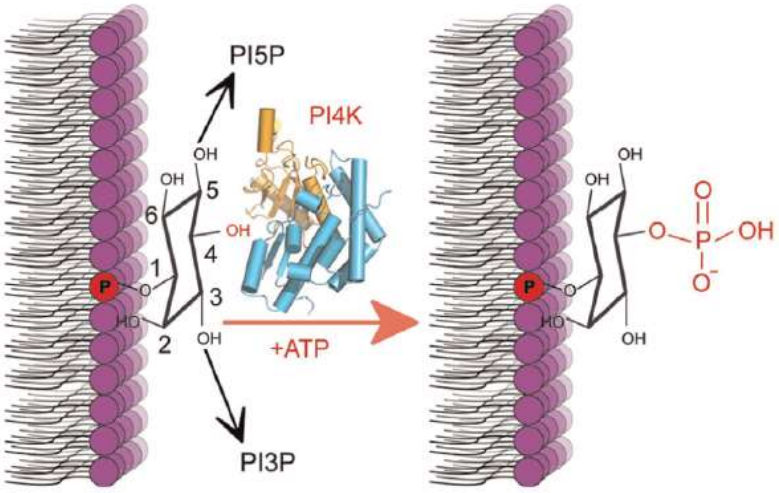

Figure 3: **Schematic of reaction catalyzed by PI4Ks**. The transfer of the γ-phosphate from ATP to the C-4 position of inositol on membrane-bound PI, giving rise to PI(4)P. PI(3)P and PI(5)P can also be formed by the action of respective PI-kinases. Image used with permission from from Boura & Nencka, 2015.

1.2.2.1 Class II PI4Ks

Class II PI4Ks have an apparent molecular weight of 45-55 kDa, are activated by non-ionic detergents such as Triton X-100 but inhibited by Ca^{2+} and have a considerably lower sensitivity than PI3Ks to the inhibitor wortmannin. Furthermore, this is the most plentiful subgroup of PI kinases in most animal cells and tissues (Strahl & Thorner, 2007). *S. cerevisiae*'s only PI4K-II, named Lsb6p, is involved in the regulation of actin polymerization and endosome mobility, though knockdown of the *Lsb6* gene was not lethal. In humans, there are two sub-types of class II PI4Ks, namely α and β. Both subtypes contain a cysteine-rich (CR) motif (**Figure 4**) in the kinase domain that can be palmitoylated, a process that is needed for stable membrane association and enzyme activation (Boura & Nencka, 2015). PI4K-IIα is highly expressed in the brain (Sasaki et al., 2009), mostly localises to the Golgi and endosomes, and has been reported to be the most active PI4K in humans accounting for the synthesis of ≈ 50% of all

PI(4)P in the cell (Boura & Nencka, 2015). Counterintuitively, mice lacking PI4K-IIα kinase activity developed progressive neurodegeneration only in the adulthood, appearing normal at first (Simons et al., 2009). The other isoform, PI4K-IIβ, was reported to be involved in early T cell activation mechanisms (Boura & Nencka, 2015).

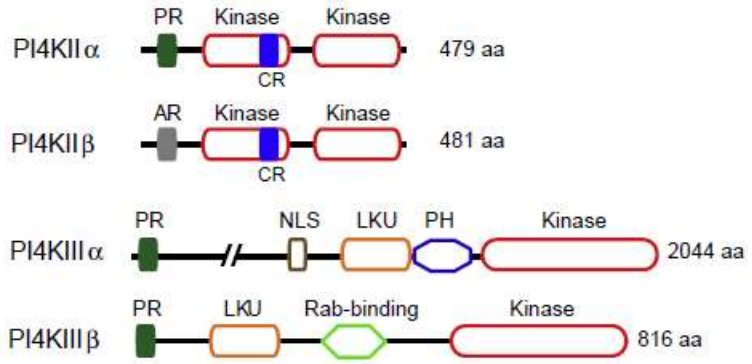

Figure 4: **Structural features of mammalian PI4Ks**. PI4K class II are smaller proteins than the class III members. All four proteins have a kinase domain towards the C-terminus, and all but PI4K-IIβ have a proline-rich (PR) motif at the N-terminus. Class II PI4Ks have a cysteine-rich (CR) motif within their central kinase domains, and class III PI4Ks have a lipid kinase unique (LKU) domain thought to be homologous to that of PI3Ks. PI4K-IIIα has a nuclear localization sequence (NLS) and a pleckstrin homology (PH) domain, both believed to be associated with membrane binding. PI4K-IIIβ has a Rab-binding domain between the LKU and kinase domains. Binding of Rab11 to this site has been reported to be necessary for Golgi localization. Figure used with permission from Sasaki et al., 2009.

1.2.2.2 Class III PI4Ks

Based on domain structure and sensitivity to inhibitors, type III PI4Ks are more closely related to PI3Ks (**Figure 5**) than to PI4K-II (**Figure 4**) (Sasaki et al., 2009). For instance, class III PI4Ks are activated by Triton X-100, show marginal inhibition by adenosine (if at all), and similarly to PI3Ks, are inhibited by wortmannin, which is explained by both sharing their C-terminal lipid kinase domain (Strahl & Thorner, 2007). In addition, PI4Ks class III are much larger proteins when compared to their class II counterparts, having apparent molecular weights

ranging from 92 to 230 kDa. As for their structures, PI4K-III proteins contain a proline-rich (PR) N-terminal domain, a lipid kinase unique (LKU) domain that is believed to be homologous to PI3K helical domain, and they do not contain a CR motif that is seen in type II PI4Ks (**Figure 4**). As with the class II PI-kinases, however, there are two isozymes of PI4Ks Class III, namely α (≈ 215-230 kDa) and β (≈ 92-120 kDa) (Sasaki et al., 2009). Importantly, class III PI4Ks are soluble cytosolic proteins that are directed to their target membranes via interactions with other proteins (Klima et al., 2016).

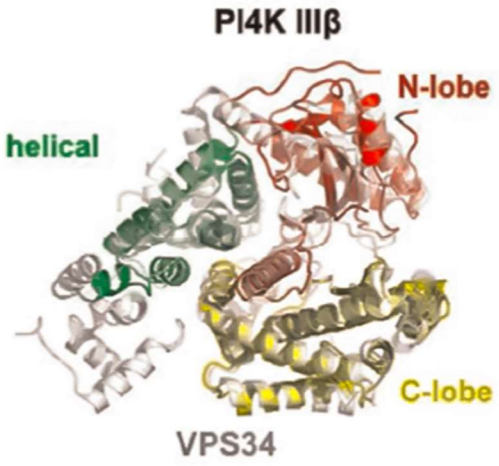

Figure 5: **Structural superposition of human PI4K-IIIβ on human PIK3C3.** Superposition of human PIK3C3, here denoted "VPS34" (in light grey), and human PI4K-IIIβ reveals that all subdomains (helical in green, N-lobe in red, and C-lobe in yellow) align quite well between the two paralogs. Reproduced from (Boura & Nencka, 2015) with permission.

S. cerevisiae PI4Ks were the first to be identified and characterized. Stt4, whose gene is essential in yeast, is the orthologue of human PI4K-IIIα. Stt4 localizes to the plasma membrane and is responsible for supplying PI(4)P to the yeast PIPK Mss4P for synthesis of $PI(4,5)P_2$ (Boura & Nencka, 2015). Mammalian PI4K-IIIα contains a bipartite nuclear localization sequence (NLS) and a Pleckstrin homology (PH) domain thought to be involved in membrane association (**Figure 4**). Although expressed in many organs, the mRNA of rat PI4K-IIIα has

been detected mostly in brain tissues. Immunocytochemical analyses revealed that membranes of the ER, mitochondria and nucleus harbour PI4K-IIIα (Sasaki et al., 2009), but it is at the plasma membrane that this protein plays the vital role of furnishing the substrate needed for $PI(4,5)P_2$ generation, which is the defining PIP of the plasma membrane (Nakatsu et al., 2012). PI4K-IIIα has also been shown to be indirectly indispensable for Ca^{2+} signalling and, mimicking its yeast counterpart, results in embryonic lethality in mice when its encoding gene was ablated (Sasaki et al., 2009). Lastly, activity of PI4K-IIIα has been reported as essential for Hepatitis C Virus (HCV) replication, which happens within ER-derived membranous web structures. By hijacking PI4K-IIIα activity, more PI(4)P is produced, thus leading to the nucleation of viral and host cellular proteins to the membrane web structures where HCV replicates intracellularly (Reiss et al., 2013).

1.2.3 Yeast Pik1 and its recruitment to the Golgi membrane by frequenin (Frq1)

Yeast's PI4K-IIIβ, conventionally named Pik1, is a 120 kDa enzyme shown to also be essential for *S. cerevisiae* survival. Pik1 is mostly localized in the Golgi and the nucleus, playing a central role in the regulation of vesicular trafficking in the late secretory pathway. Past studies have demonstrated that temperature-sensitive *pik1* mutants had exaggerated Golgi membranes with ring-shaped structures, fragmented vacuoles, and multinucleated cells suggesting a defect in cytokinesis (Balla & Balla, 2006). The function of Pik1 in the nucleus is not fully understood, but it has been suggested that this protein is needed to supply the precursor of $PI(4,5)P_2$, which in turn is a regulator of nuclear proteins like RNA polymerase (Boura & Nencka, 2015).

Localization of Pik1 to the Golgi membrane has been proposed to require frequenin (Frq1), a 22 kDa essential protein in yeast that strongly associates with two of Pik1's helices (residues 125-135, 156-169) (Dornan et al., 2016), which explains why the former co-purifies with the latter (Strahl et al., 2007). Frq1 binds three Ca^{2+} atoms in all but one of its EF-hand domains and is *N*-myristoylated *in vivo*. Despite enhancing Frq1-promoted activation of Pik1, neither calcium nor *N*-myristoylation are essential for binding of the two proteins nor for activation of the lipid kinase (Strahl et al., 2007). NMR-based structural studies demonstrated that upon binding of Ca^{2+}-loaded Frq1, the bound Pik1 region assumes a U-shaped format, which may bring Pik1's LKU domain into closer proximity with Pik1's catalytic domain. Such allosterically induced conformational change has been suggested to be responsible for Frq1-triggered activation of Pik1. Inserted into the Golgi membrane, Frq1's *N*-myristoyl group would aid the complex to target said membrane, thus bringing the enzyme closer to its substrate. A model has been proposed based on these observations (**Figure 6**) (Strahl et al., 2007).

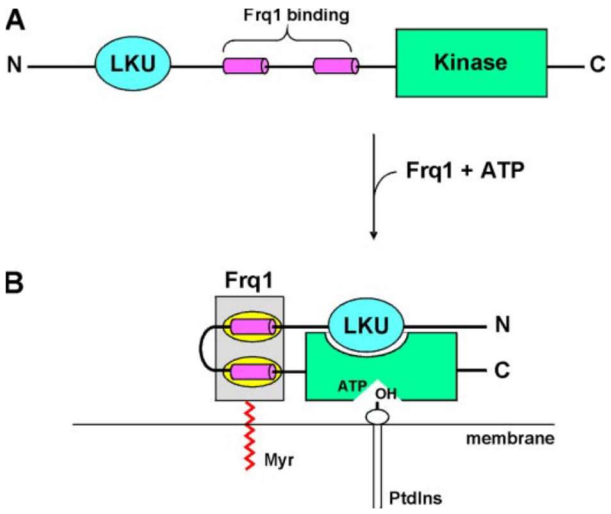

Figure 6: **Proposed model of Frq1-induced Pik1 activation**. **6A:** Mapped domains of Pik1 sequence. It contains a Lipid Kinase Unique (LKU, in blue) motif closer to the N-terminal (residues 35-110), followed downstream by two helices (in pink) which are the direct target of Frq1 (125-135, 156-169), and finally by a C-terminal catalytic kinase domain (in green). **6B:** Binding of Ca^{2+}-charged Frq1 leads to a U-shaped conformational change in Pik1's structure, thus bringing Pik1's LKU domain into closer proximity with the catalytic domain. The *N*-myristoyl group of Frq1anchors the complex to the membrane, which may facilitate the ATP-dependent conversion of PI to PI(4)P by Pik1. Figure reproduced with permission from (Strahl et al., 2007).

1.2.4 Human PI4K-IIIβ

There are two isoforms of mammalian PI4K-IIIβ produced by alternative splicing: isoform 1 (Uniprot ID: Q9UBF8-1), ~ 92 kDa, and isoform 2 (Uniprot ID: Q9UBF8-2), ~ 90 kDa, with no reported difference in enzymatic activity. PI4K-IIIβ is ubiquitously expressed in tissues and is present mostly in early Golgi compartments but also in the nucleus. This protein can be phosphorylated at eight sites, which appears to affect its cellular location: PI4K-IIIβ phosphorylated by members of the protein kinase D (PKD) family on Ser_{294} is targeted exclusively to the Golgi, whereas PI4K-IIIβ phosphorylated on Ser_{496} or Thr_{504} was detected in the nucleus (Szivak et al., 2006). Phosphorylation on Ser_{294} has been implicated with a 60%

increase in the lipid kinase activity of PI4K-IIIβ when compared to a non-phosphorylatable mutant (Hausser et al., 2005).

As for its biological role, PI4K-IIIβ plays a major role in producing PI(4)P in the *trans*-Golgi Network (TGN), thereby regulating the Golgi-to-plasma membrane trafficking, such as the intra-Golgi transport of influenza hemagglutinin and the basolateral transport of vesicular stomatitis virus (SVS) G protein in Madin-Darby canine kidney cells (Balla & Balla, 2006). Moreover, PI4K-IIIβ is needed in biological processes that entail a rapid delivery of membrane vesicles, such as the considerable membrane remodelling that takes place at the end of cell division. Differently from its yeast orthologue, the knockout of PI4K-IIIβ does not impair survival of progeny in flies, despite rendering the male flies infertile due to defects in spermatogenesis. Loss of PI4K-IIIβ in mice cells led to abnormal myelination of peripheral nerves (Burke et al., 2022). As is the case with the α-isozyme, intracellular PI4K-IIIβ's activity is enhanced upon infection by RNA viruses like HCV, SARS coronavirus and enteroviruses, which is essential for their replication (Burke et al., 2014). Significant effort is being made in the research of PI4K-IIIβ inhibitors for the development of antiviral medication (Burke et al., 2022).

1.2.4.1 PI4K-IIIβ regulation and recruitment to the Golgi membrane

As a soluble protein acting chiefly at the Golgi membrane, the recruitment of PI4K-IIIβ's to the Golgi, and also its regulation, are matters of continuing interest. Early studies demonstrated that the small GTP-binding protein Arf1 (ADP-ribosylation factor-1) attracted PI4K-IIIβ to Golgi membranes resulting in a twofold increase in PI(4)P production (Godi et al., 1999). Another protein that seems to regulate PI4K-IIIβ is the mammalian NCS-1 (neuronal

calcium sensor), a Frq1 homolog. Briefly, this Ca^{2+}-binding protein alone was reported to enhance the activity of PI4K-IIIβ by 70%, which was reduced to a 50% stimulation when Arf-1 was also present (Haynes et al., 2005). NCS-1 binds to the kinase in question at a binding site next to the LKU domain, and co-localized with PI4K-IIIβ to the Golgi in immunocytochemistry experiments (Bourne et al., 2001). Nevertheless, NCS-1 is only expressed by some cell types, suggesting that if it is needed for PI4K-IIIβ recruitment to the membrane, this occurs in a tissue-specific manner (Klima et al., 2016).

PI4K-IIIβ also has a site for binding of Rab11 (**Figure 7**), a GTP-bound protein. Nevertheless, such interaction is needed for Rab11 to associate with the Golgi membrane, rather than the opposite, this being an example of non-catalytic functions that the kinase can perform (Balla & Balla, 2006; Burke et al., 2014). In addition, the Golgi resident protein acyl-coA binding domain containing 3 (ACBD3), also named PAP7, GCP60, GOCAP1, and GOLPH1, can bind to PI4K-IIIβ and has been shown to suffice for recruitment of the latter to the Golgi. Experiments involving siRNA-mediated depletion of ACBD3 led to disperse cytoplasmic localization of PI4K-IIIβ (Boura & Nencka, 2015). Klima *et al.* showed that ACBD3 and the lipid kinase interact with a K_D value in the submicromolar range *in vitro*. Moreover, ACBD3 can recruit the kinase to model membranes *in vitro* and to COS-7 cells' mitochondria, a location where PI4K-IIIβ is never naturally found (Klima et al., 2016).

Lastly, the small, acidic regulator 14-3-3 has been shown to positively regulate PI4K-IIIβ activity in cells by protecting its phospho-Ser_{294} from phosphatases (Hausser et al., 2006). More recently, *in vitro* studies on biomimetic giant unilamellar vesicles (GUVs) detected comparable PI(4)P production both in the presence and absence of 14-3-3. Instead, this protein was shown to stabilize PI4K-IIIβ activity by protecting it from proteolytic degradation as 14-3-3's binding site

is a disordered region on the lipid kinase structure (Chalupska et al., 2017). A later study showed that 14-3-3 forms a compact complex with PI4K-IIIβ, which in turn promotes the recruitment of Rab11 to form a ternary complex. Furthermore, the association with 14-3-3 did not seem to affect PI4K-IIIβ's recruitment to the Golgi membrane, which in fact appears to rely on ACBD3. In this latter case, a ternary complex was also formed with Rab11 and ACBD3, confirming that PI4K-IIIβ may also play a role as an adaptor protein (Chalupska et al., 2019). Overall, many binding partners have been proposed as the regulators of both PI4K-IIIβ activity and its recruitment to the Golgi membrane. Tight regulation is expected for such a physiologically important enzyme, and investigations continue to progress in this field.

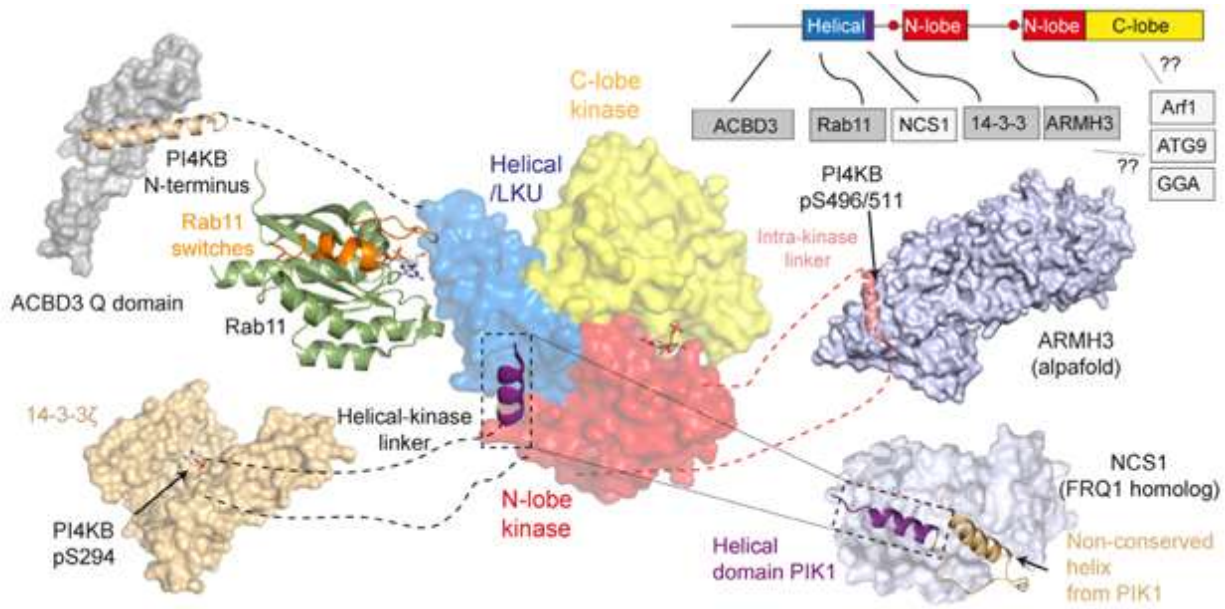

Figure 7: Structure of PI4K-IIIβ highlighting binding partners' recognition domains. Space-filling structure of human PI4K-IIIβ showing regions recognized by its binding partners: ACBD3 binds to an N-terminal region (golden helix) which involves an order-disorder transition; Rab11 recognizes the LKU domain (in blue, specific helices in green); NCS-1 binds to a helix at the C-terminal end of the LKU domain; 14-3-3 stabilizes phosphor-Ser_{294} in a disordered loop; and ARMH3 (also called c10orf76) binds to phosphor-Ser_{496} in a region just upstream of the catalytic domain (N-lobe in red, C-lobe in yellow). It is still unclear where exactly other binding partners such as Arf1 bind to on the lipid kinase. Image used with permission from (McPhail & Burke, 2023).

1.2.4.2 Recombinant expression and solved structures of PI4K-IIIβ

Early studies with PI4K-IIIβ homologues resorted to isolation of this kinase from tissues such as bovine brain (Downing et al., 1996). This was soon replaced by the molecular cloning and recombinant expression of PI4K-IIIβ, initially expressed in *Escherichia coli* (Meyers & Cantley, 1997; X.-H. Zhao et al., 2000), and later in baculovirus-infected insect cells (Suer et al., 2001). Producing recombinant forms of proteins of interest is generally more affordable and accessible than recovering these biomolecules from their native tissues (Structural Genomics Consortium et al., 2008). Cloning of bovine PI4K-IIIβ, which shares >99% sequence identity

with its human orthologue, was performed in the BL21 (DE3) *E. coli* cell line. Induction of expression was by the addition of 30 μM isopropyl-1-thio-β-D-galactopyranoside (IPTG) at 16-19 ºC for 6 hours, yielding 0.5 mg of purified GST-tagged protein per liter of bacterial culture. Autophosphorylation at the C-terminal catalytic domain was reported, and in this scenario the enzyme's PI kinase activity was negatively affected (X.-H. Zhao et al., 2000). Meyers and Cantley performed the cloning and characterization of human PI4K-IIIβ also in *E. coli* but inducing with 100 μM IPTG at 25 ºC overnight (Meyers & Cantley, 1997). Alternatively, Suer *et al.* achieved expression of recombinant human PI4K-IIIβ by infection of Sf9 cells (*Spodoptera frugiperda*) with baculovirus DNA. Phosphorylation of PI4K-IIIβ was also reported, but in this case suggested to be due to sample contamination by other kinases rather than by autophosphorylation. Importantly, phosphatase treatment of the phosphorylated PI4K-IIIβ only decreased its lipid kinase activity by 20% (Suer et al., 2001). In fact, these two expression systems (i.e. in *E. coli* BL21 and Sf9 cells) seem to be the methods of choice to obtain recombinant PI4K-IIIβ in recent studies (Burke et al., 2014; Klima et al., 2016; Reuberson et al., 2018; Chalupska et al., 2019;).

Although many solved structures of PI4K-IIIβ have been published in the last decade (PDB IDs: 4D0L, 4WAG, 4WAE, 6GL3, 2N73, 5EUQ, 5C46), none of them describes the full-length protein. The wild-type enzyme contains disordered loops that hamper proper crystal diffraction. Hydrogen-Deuterium Exchange – Mass Spectrometry (HDX-MS) experiments revealed rapid H/D exchange in three regions (*i.e.* 1-120, 408-510 and 785-801) of PI4K-IIIβ , which correlates with disordered regions in crystallographic analyses (Burke et al., 2014). Deletion of said regions, and the resulting decrease in the protein's MW, appears to render bacterial expression less burdensome and increases protein stability (Chalupska et al., 2019),

which has enabled sufficient recovery of the recombinant protein for crystallization studies. Activity studies, however, have been done in different constructs since the 785-801 segment falls within PI4K-IIIβ's catalytic domain. Deletion of this region has ablated the activity of the lipid kinase in *in vitro* studies (Burke et al., 2014). Despite not inactivating the lipid kinase, removal of other disordered loops did reduce production of PI(4)P by 60% (Klima et al., 2016) and 70% (Fowler et al., 2016) when compared to the full-length protein activity. Hence, many researchers resort to the wild-type protein for activity assays even when employing constructs with deleted regions for structural studies (Burke et al., 2014; Mejdrová et al., 2015; Rutaganira et al., 2016; Reuberson et al., 2018).

1.3 Lipid Transfer Proteins (LTPs)

It has been widely accepted for some time now that cells largely rely on LTPs to properly sort lipids between biomembranes. Lipids are mostly synthesized in the ER, which implies that rapid transfer mechanisms are needed to sustain lipid homeostasis and organelle identity. The first transfer mechanism is the vesicular pathway, whereby cargo vesicles deliver lipids from donor to acceptor vesicles via membrane fusion. This process is particularly relevant for exo- and endocytosis, but also for the secretory pathway (Srinivasan et al., 2023). Although efficient, the vesicular pathway may not deliver lipids at sufficient rates to ensure proper organelle biogenesis, and is negatively regulated during cellular stress (Reinisch & Prinz, 2021). An alternative transfer mechanism, termed the non-vesicular pathway, is mediated by LTPs. These proteins shield lipids from the largely hydrophilic cytosol and rapidly transport them between organelles (Srinivasan et al., 2023).

1.3.1 Sec14p

Among many LTPs, the yeast Sec14 protein (Sec14p) is a topic of extensive research efforts by Dr. Jeffrey Atkinson's group and deserves special attention. Sec14p, a cytosolic ≈ 35 kDa protein that is the prototypical member of the cellular retinaldehyde binding – triple functional (CRAL-TRIO) structural superfamily, is an eukaryotic, ancient, and non-enzymatic protein known to mediate the transport of PI and PC between membrane bilayers *in vitro* in an energy independent fashion (Holič et al., 2021). Deletion of *Sec14* was shown to be lethal in yeast, and a temperature sensitive Sec14p mutant led to accumulation of proteins in the Golgi due to insufficient vesicle budding from this organelle (Lipp et al., 2020).

The crystal structure of Sec14p has been solved (PDB ID 1AUA) (Sha et al., 1998) and shows that this protein has 12 α-helices, 6 β-strands, and 8 3_{10}-helices. Targeting to the Golgi membrane is done by the N-terminal A_1-A_4 α-helices, which form a tripod-like motif. The hydrophobic pocket where the lipid binds is formed by the β-strands combined with 3 of the α-helices and is gated by a A_{10}/T_4 helix gating module. Notably, this gating module is mobile, assuming different conformations when bound to lipid or to a membrane. A model has been proposed to explain lipid/membrane binding by Sec14p: when in its lipid-bound state, the gated module is closed. The A_{10}/T_4 module then transitions to the open state upon binding to the membrane, thus allowing for the bound lipid to be released and another lipid can enter the binding pocket (Ryan et al., 2007). Importantly, only one phospholipid at a time fits in Sec14p's hydrophobic cavity, and the presence of PI in acceptor vesicles stimulates the delivery of PC analogues by Sec14p in *in vitro* membranes (Panagabko et al., 2019). The helix gating module then closes and Sec14p dissociates from the membrane as it shuttles to another membrane to deliver the recently bound lipid (Ryan et al., 2007).

1.3.1.1 The heterotypic lipid exchange and the nanoreactor model

The heterotypic lipid exchange between lipid bilayers mediated by Sec14p, namely of PC and PI, has long been discussed. This model proposes that Sec14p delivers either PC or PI to a membrane, and in doing so retrieves the other phospholipid to be transported elsewhere in the cell (Schaaf et al., 2008). Therefore, the heterotypic exchange performed by Sec14p may fine tune pools of PI and PC at given membranes. For instance, removing PC from the Golgi membrane would alleviate the toxicity of this lipid on trafficking. When PC is not withdrawn from membranes, a surplus of DAG, otherwise consumed during PC biosynthesis, is created. Vesicle biogenesis relies on small amounts of DAG, as it induces negative curvature on membranes due to its conical shape. Excess DAG, however, results in vesicle fission due to exaggerated negatively-curved membranes (Shemesh et al., 2003). As for its other ligand, Sec14p is thought to maintain PI homeostasis on the Golgi membrane, thereby allowing Pik1 to produce PI(4)P at adequate levels. Lack of proper Sec14p activity results in reduced levels of PI(4)P at the Golgi surface and a 2-fold decrease of the aforementioned PIP in the cell (Schaaf et al., 2008).

Considering the previous correlations, a model has been proposed (Ile et al., 2006) to explain the presentation-phosphorylation of PI (**Figure 8A**). It is theorized by the nanoreactor model that, at the moment of the exchange, PC binding would cause the partial expulsion of PI from the Sec14p binding cavity so that a Sec14p-PI intermediate would be formed. In this intermediate, PI's head group would be presented to Pik1 so that phosphorylation of PI would be favoured. In this case, the activity of Pik1 would be boosted when in presence of Sec14p (Ile et al., 2006). An alternate, not-mutually exclusive scenario postulates that slow exit of bound PC would facilitate the presentation of PI to Pik1 (**Figure 8B**). More specifically, PI's inositol

headgroup binding site is situated proximally to Sec14p's surface, which favours fast loading into the protein cavity. On the other hand, bound PC is buried in Sec14p's interior, thus rendering its unloading rather slow. Such kinetic mismatch would create an overlap, whereby slowly egressing PC may delay PI ingress. In this transitory scenario, PI would assume a partially incorporated status where it becomes a superior substrate for Pik1 (Schaaf et al., 2008).

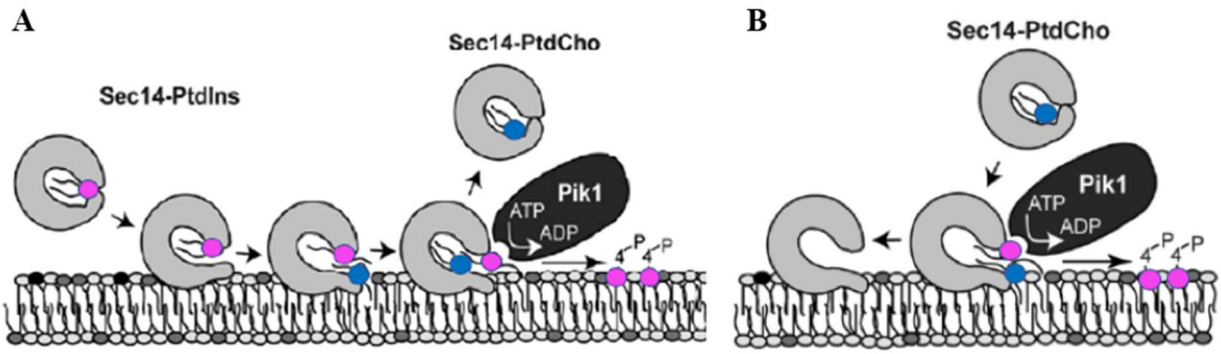

Figure 8: **Nanoreactor model of PI presentation to Pik1 by Sec14p**. **8A:** Sec14p brings PI (pink) to the membrane and entering PC (blue) forces PI out of the binding pocket. During this heterotypic exchange, a Sec14p-PI intermediate is formed so that the inositol head of PI is favourably exposed to Pik1 (black), which in turns produces PI(4)P. Sec14p then mediates transport of PC to another membrane. **8B:** Alternatively, slow egress of bound PC delays PI entry into the binding cavity of Sec14p. The momentaneous phospholipid overlap originated by this kinetic mismatch includes a partially incorporated PI, which render its headgroup a better substrate for Pik1. Images modified with permission from (Schaaf et al., 2008).

This model helps to explain that Pik1 would be needed to aid the displacement of PI by PC, considering that Sec14p has a range of 7-16 higher affinity for PI than for PC, such as shown by our group (Panagabko et al., 2003). Moreover, the necessity of Sec14p for yeast cell viability can be bypassed by further silencing the genes for Sac1p (the predominant PI(4)P phosphatase in yeast) (Rivas et al., 1999) or Kes1p (a sterol/PI(4)P exchanger) (X. Li et al., 2002). Removal of these proteins in Sec14p-null mutants restores normal levels of PI(4)P at the Golgi membrane, which corroborates the rationale of Sec14p's contribution to PIP homeostasis. The nanoreactor

model also posits a second role for Sec14p, that of a PC sensor. The pool of DAG, essential for TGN trafficking, can be depleted during intense PC biosynthesis. Large pools of PC on a given membrane would stimulate the heterotypic exchange, which in turn may enhance PI(4)P production. Elevated levels of this PIP bypasses abnormally low DAG levels, thus sustaining vesicular trafficking (Lipp et al., 2020).

Notwithstanding the described parallels, there is no clear evidence yet that the nanoreactor model is true. For instance, a Sec14p mutant devoid of PC binding still evoked PI(4)P production by PI4K-IIIβ, Pik1's orthologue in humans, when offered PI-rich membranes (Schaaf et al., 2008). Furthermore, there is no indication that a physical interaction between Pik1 and Sec14p occurs (Lipp et al., 2020). Altogether, these observations suggest that this model needs further investigations.

1.3.2 Human PI Transfer Proteins

In humans, the proteins responsible for mediating PI transport are simply termed PI Transfer Proteins (PITPs), all containing a PI Transfer Domain (PTD). In fact, there are 5 of these proteins: PITP class I, sub-divided in isoforms α and β, known to transfer PC and PI *in vitro* between membranes and possibly performing the same PC/PI exchange seen in Sec14p (De Vries et al., 1995); and class II, represented by Nir2, Nir 3, and Rdgbβ, known to mediate PA/PI exchange. Although the latter class of proteins has been implied to be involved in the important PLC-based signalling pathways (Lipp et al., 2020) , only class I PITPs will be further discussed here due to relevance to the present project.

Expression of PITPα occurs largely in the brain and localizes to the axons, nucleus, and cytosol, whereas its counterpart PITPβ is more abundant in the liver, localizing to the Golgi complex and the ER. These two proteins are 77% identical at the sequence level and share 94% sequence similarity (Baptist et al., 2016). Crystal structures of murine PITPα and human PITPβ have been solved, showing that the PTD has an eight-stranded β-sheet that is flanked by two long α-helices, forming a pocket that houses either PC or PI. Similar to what is seen with Sec14p, there is an α-helix (G-helix) that functions as a gate to the binding pocket, alongside 11 C-terminal amino acids (**Figure 9**). The polar head group of PI makes contacts with four amino acids that are conserved in the PTD of many proteins. However, atomic details of how PC's headgroup interacts in the binding pocket of these proteins has not yet been determined. Also, in a similar fashion to Sec14p, both PITP class I isoforms bind and transfer PI with higher affinity than PC (Tilley et al., 2004). Docking onto membranes is enabled by exposure of hydrophobic residues when the G-helix swings out, mimicking the mechanism used by Sec14p (Lipp et al., 2020). Lastly, our group has demonstrated that PITPβ has a higher affinity for membranes and a higher ligand transfer rate when compared to PITPα. Also, both isoforms preferred membranes that were highly curved when transferring lipids (Baptist et al., 2016).

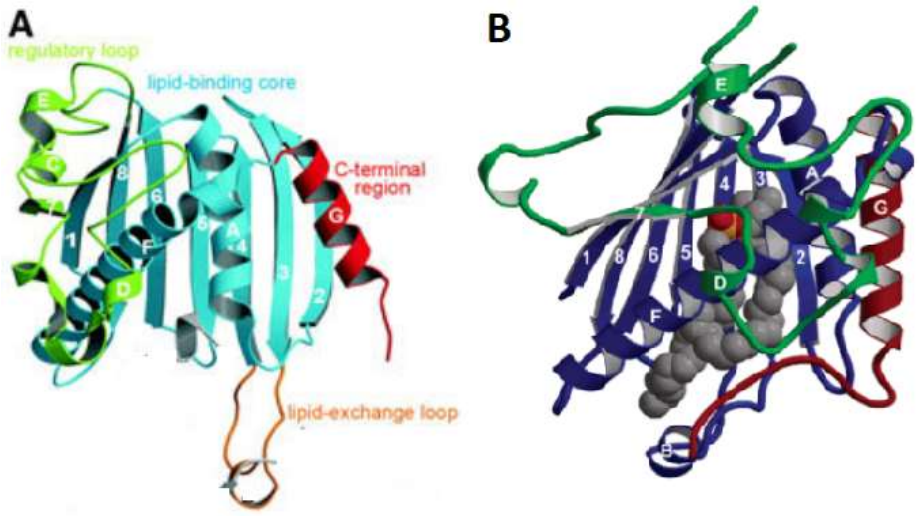

Figure 9: Crystal structure of human apo-PITPα (9A) and PITPβ (9B). **9A**: The G-helix (red) is open in the absence of ligand in the binding pocket of PITPα. Once in the lipid-binding core (cyan), ligands are shielded from the cytosolic environment. Image used with permission from (Schouten et al., 2002). **9B**: The G-helix (burgundy) is closed when PC is present in the protein's binding pocket (navy-blue). Image reprinted with permission from (Vordtriede et al., 2005). Copyright 2005 American Chemical Society.

Although facilitating the same transfers, PITPα and PITPβ have different physiological roles. The α isoform is thought to be recruited by Epidermal Growth Factor-, or EFG-receptors to supply PI that can be phosphorylated by PI4Ks. Following action of PLC-γ, a robust signal of $PI(4,5)P_2$ and consequently of related second messengers is produced. Despite not being essential for viability, knock-out of the *PITPA* gene in mice led to premature death due to defects in ER function of multiple cell types leading to cerebellar diseases, hypoglycemia, and intestinal and hepatic steatosis (Alb et al., 2003). The β-isoform of PITP, encoded by the essential *PITPB* gene (Alb et al., 2002), has been shown to perform PC/PI exchange between ER and the Golgi in RNAi knockdown experiments. This study revealed that PITPβ may be fundamental for Golgi-to-ER retrograde trafficking, in which it would transport PI from the ER to the Golgi to maintain a PI(4)P pool, thus allowing the formation of COPI-coated vesicles (Carvou et al., 2010)(Nile et

al., 2010). Importantly, a degree of functional interchangeability between the human PITPs and Sec14p has been demonstrated by the heterologous expression of PITPβ in yeast, which rescued the defects caused by ablation of Sec14p activity (Skinner et al., 1993), and by *in vitro* experiments whereby PITPβ and Sec14p replaced the activity of PITPα (Alb et al., 2002).

As is the case with Sec14p and Pik1, it is still unclear if and how PITPs would present bound PI to PI4K-IIIβ, which could presumably enhance the activity of the lipid kinase. Importantly, heterologous expression of PITPβ in yeast rescued the defects caused by ablation of Sec14p activity (Skinner et al., 1993), altogether demonstrating a degree of functional interchangeability between the human and the yeast PITP. As mentioned previously, stimulation in PI-kinase activity was observed *in vitro* when PIK3C3 was tested with PITPα, PITPβ and Sec14p, where an enhancement of more than 250% in the kinase activity was reported (Panaretou et al., 1997). Due to the homology and domain conservation between class III of PI3Ks and PI4Ks (**Figure 5**) (Boura & Nencka, 2015), we hypothesized that the activity of PI4K-IIIβ would also be enhanced in the presence of PITPs *in vitro*, thus suggesting that the latter would present PI to be phosphorylated by PI4K-IIIβ *in vivo* in a nanoreactor model (**Figure 8**) fashion.

1.4 Lipid Kinase Assays

Lipid kinase activity can be measured by methods based on different principles, namely radioactivity (Panaretou et al., 1997; Meyers & Cantley, 1997; Suer et al., 2001), bioluminescence (Klima et al., 2016), and electrochemical signals (Gao et al., 2017). Radioactive assays are reliable, sensitive and have been the classical approach to monitor the kinase activity of enzymes, but the harmful nature of these compounds and the labor needed for such assays are

a pitfall (Zwier et al., 2010). Moreover, the existing assays mostly offer endpoint readouts, *i.e.* incubation of a reaction's components, termination of reaction, readout. The endpoint format does not allow time-specific interventions on the assayed reaction, such as additions of inhibitors/enhancers, nor the determination of kinetic parameters like initial rates and time required for reaction completion. These limitations led our group to develop a time-resolved assay (Meehan, K., 2019). Importantly, this assay uses lipid vesicles (*i.e.* liposomes) instead of detergent-solubilized lipids. This is advantageous as vesicles better mimic features of *in vivo* biological membranes such as lipid packing and membrane curvature (Matos et al., 2012) .

The assay used in this project is fluorescence-based and is a modification of the Bellbrook Labs Transcreener® ADP^2 FI Assay. This assay detects the production of adenosine diphosphate (ADP) as a by-product of the phosphorylation of PI by PIKs, which enables one to follow the kinase catalyzed reaction. Initially, an ADP^2 monoclonal antibody conjugated to an IRDye® QC-1 quencher is allowed to complex with an ADP Alexa Fluor® 594 Tracer dye. In the absence of kinase reaction, no fluorescence signal is detected as the Alexa Fluor® 594 fluorophore is quenched. When the kinase is introduced to the system and allowed to phosphorylate its substrate, ADP is produced. The latter displaces the Alexa Fluor® 594 Tracer from the antibody-quencher conjugate, ceasing quenching of the fluorophore (**Figure 10**). The increase in fluorescence signal is proportional to the ADP production by the enzyme (Lowery & Kleman-Leyer, 2006). Although presently used for lipid kinase activity assessment (Klink et al., 2008; Demian et al., 2009; Zhang et al., 2011; Rathinaswamy et al., 2022), this method traditionally provides an endpoint reading, and was the basis for the development of a time-resolved assay (Meehan, K., 2019).

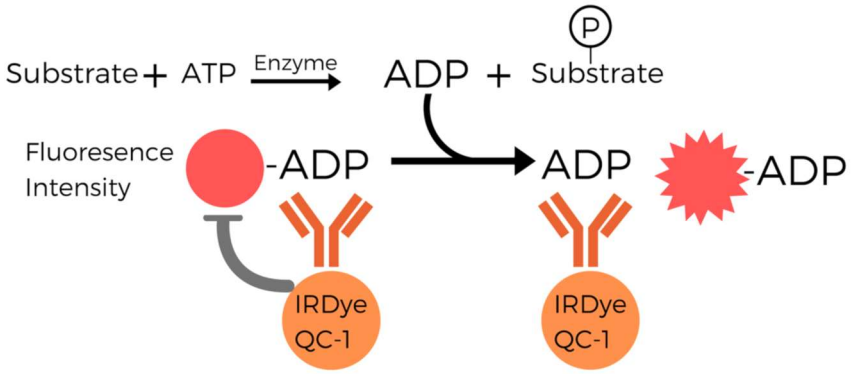

Figure 10: **Diagram of the Bellbrook Labs Transcreener® ADP² FI Assay**. The phosphorylation of substrate by protein kinase generates ADP, which in turn displaces the Alexa Flour® 594 Tracer from the antibody-quencher conjugate. No longer quenched, the fluorophore produces a fluorescent signal that is proportional to the kinase reaction. Retrieved from (Meehan, K., 2019).

Dr. Atkinson's group adapted the assay described above to a time-resolved assay (**Figure 10**) by incorporating three key changes: 1) increasing the reaction volume from 25 µL to 50 µL, and thus adapting the concentration of all components in the reaction to account for such increase in the reaction volume; 2) removal of ethylenediamineedtatetraacetic acid (EDTA) from the reaction, as this chelator strips Mg^{2+} from the enzyme active site thus stopping the reaction; 3) increasing the number of fluorescence intensity (FI) measurements (Meehan, K., 2019). It is noteworthy that the change in the reaction volume was to account for removing EDTA from the mixture, as 25 µL of the buffer that contained this chelator is added to the endpoint format of this assay. Despite some inconsistencies with some controls, the new assay format was shown to be successful in measuring kinetic parameters of PI kinases activity (Meehan, K., 2019), hence it was the chosen method for the present study.

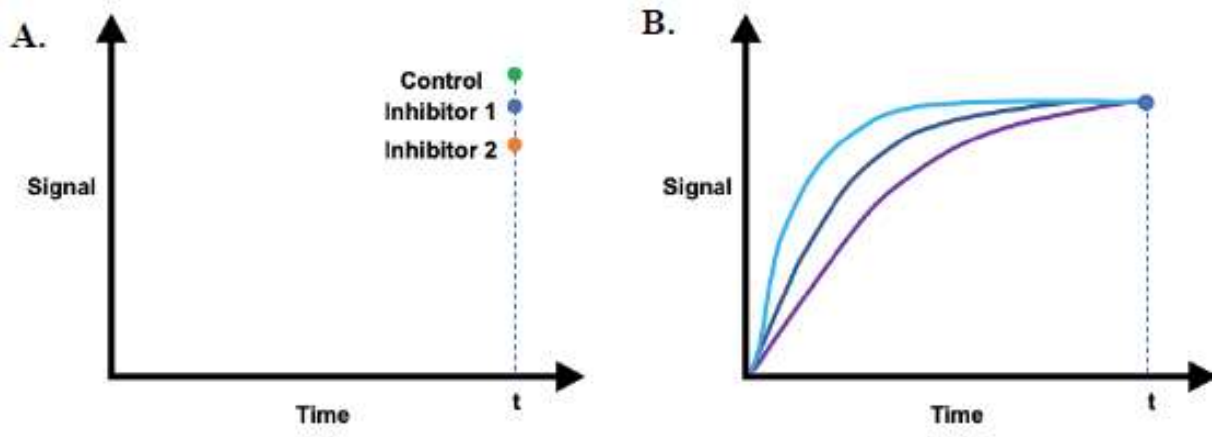

Figure 11: **Illustrative graphs representing the Bellbrook Labs Transcreener® ADP^2 FI Assay readings in endpoint mode (11A), and in time-resolved mode (11B) as developed by the Atkinson group.** Retrieved from (Meehan, K., 2019)**.**

1.5 Purpose of the Project

This project aimed at testing the nanoreactor model (Ile et al., 2006) by assessing the activity of PI4K-IIIβ in the presence of LTPs such as PITPα, PITPβ and Sec14p. PI4Ks binding partners such as Frq1 were also included in our *in vitro* assays for recruitment of PI4K-IIIβ to liposomes. We hypothesized that the production of PI(4)P would be enhanced in the presence of the aforementioned LTPs, thus corroborating the nanoreactor model. For this, the recombinant expression and purification of human PI4K-IIIβ in *E. coli* was optimized, as was the time-resolved, vesicle-based PI-kinase assay protocol developed by our group (Meehan, K., 2019) to then monitor the activity of PI4K-IIIβ alone and with LTPs.

2 MATERIALS

2.1 DNA and Bacterial Strains

NEB® 10-beta Competent *E. coli* (High Efficiency) from New England Biolabs (catalogue #3019H) was used for plasmid preparations.

PI4K-IIIβ

Bacterial strains Rosetta™ 2(DE3) Singles™ Competent Cells (EMD Millipore-Sigma catalogue 71400) were transformed, separately, with all vectors in **Table 1**. These vectors were cloned to contain the gene for PI4K-IIIβ isoform 2 (Uniprot Q9UBF8-2) alone or with a co-expressing protein.

Table 1: Features of plasmids used in the present study for the expression of recombinant human PI4K-IIIβ in *E. coli*.

Plasmid	Selectable Marker	Addgene#	Promoter	Tag(s)	Gene
pGEX-6P1-FLAG	Ampicillin	119759	tac	N-FLAG and N-GST	PI4K-IIIβ and PI4K-IIIβ + Frq1 (Uniprot Q06389)
p7XNH3	Chloramphenicol and Kanamycin	47064	T7	N-His_{10}; N-terminal 3C protease site (PreScission site)	PI4K-IIIβ
pBXNH3	Chloramphenicol and Ampicillin	47067	araBAD	N-His_{10}; N-terminal 3C protease site (PreScission site)	PI4K-IIIβ
pBXC3H	Chloramphenicol and Ampicillin	47068	araBAD	C-His_{10}; C-terminal 3C protease site	PI4K-IIIβ
pBXNH3CA	Chloramphenicol and Ampicillin	47069	araBAD	N-His_{10} and C-AVI-tag; C-terminal 3C protease site (PreScission site)	PI4K-IIIβ
pBXNAC3H	Chloramphenicol and Ampicillin	47074	araBAD	N-AVI-tag and C-His_{10}; C-terminal 3C protease site (PreScission site)	PI4K-IIIβ + cdc37 (Uniprot P06101)

p7XNH3, pBXNH3, pBXC3H and pBXNH3CA were a gift from Raimund Dutzler & Eric Geertsma.

<u>PITPα and PITPβ</u>

BL21(DE3) pLysS-T1 Competent Cells were transformed with the pRSET-C plasmid vector the gene for human PITPα (Uniprot Q00169) and PITPβ (Uniprot P48739-2). This plasmid was kindly gifted by Dr. Shamshad Cockcroft (University College London).

Sec14

BL21(DE3) pLysS-T1 Competent Cells were transformed with the pGEX-4T1 plasmid vector cloned to contain the gene for *Saccharomyces cerevisiae* Sec14 (Uniprot P24280). This plasmid was kindly provided by Dr. Christopher McMaster (Dalhousie University).

Frequenin

BL21(DE3) Competent Cells (New England Biolabs catalogue C2527H) were transformed by Dr. Candace Panagabko (Brock University) with the pGEX-6P1-FLAG vector cloned to contain the gene for *Saccharomyces cerevisiae* frequenin (Uniprot Q06389).

2.2 Buffers, Solutions, and Media

2.2.1 Media for bacterial growth

All media for bacterial growth were made with either reverse osmosis (RO) or MilliQ (mQ) H_2O and autoclaved (Panasonic MLS-3751L) using the liquid sterilization program (121°C, 15 min)

Lysogeny Broth (LB) agar plates – 4.0 g agar, 1.0 g yeast extract, 2.0 g tryptone, 2.0 g NaCl, dissolved in 200 mL mQ H_2O, autoclaved, poured plates. Antibiotics were added as selection markers to final concentrations of 100 μg/mL (ampicillin and carbenicillin), 50 μg/mL (kanamycin), and 34 μg/mL (chloramphenicol) just prior to pouring the plates

LB broth – 5.0 g NaCl, 5.0 g yeast extract, 10 g tryptone, dissolved in 1L RO H_2O, autoclaved

Terrific Broth (TB) – 6.0 g yeast extract, 5.0 g tryptone, 1.25 mL glycerol, dissolved in 225 mL RO H_2O, autoclaved. **TB buffer** – 0.72 M K_2HPO_4, 0.17 M KH_2PO_4, dissolved in 25 mL mQ H_2O, autoclaved and added to 225 mL of TB prior to inoculation

TB auto-induction – 1.2 g tryptone, 2.4 g yeast extract, 15 mg $MgSO_4$, 330 mg $(NH_4)_2SO_4$, 650 mg KH_2PO_4, 710 mg Na_2HPO_4 were dissolved in 100 mL mQ H_2O, pH adjusted to 7.0 ± 0.2, autoclaved for 15 min (program 2-3). Prior to inoculation, glucose and α-lactose were dissolved in water, filter-sterilized (0.4 μm pore filter) and added to final concentrations of 0.05% and 0.2%, respectively

2.2.2 Buffers

mQ H_2O was used to bring buffers to volume, unless otherwise noted. When needed, pH adjustments were done using NaOH or HCl. All buffers were autoclaved unless otherwise noted

2.2.2.1 Buffers used for protein extraction/purification

Human Rhinovirus 3C Protease (HRV 3C) Cleavage Buffer - 25 mM 4-(2-hydroxyethyl)-1-piperazineethanesulfonic acid (HEPES) pH 7.5, 150 mM NaCl, 1 mM dithiothreitol (DTT), filter-sterilized (0.4 μm pore filter)

<u>PI4K-IIIβ, Sec14 and Frequenin</u>

Buffer "A" – 150 mM tris(hydroxymethyl)aminomethane (Tris) pH 7.4, 150 mM NaCl, 1 mM Ethylenediaminetetraacetic acid (EDTA), 10% glycerol, 10 mM 2-mercaptoethanol (BME), 0.2 mM Phenylmethylsulfonyl fluoride (PMSF). Made just prior to using, kept on ice

Buffer "B" – 30 mL Buffer A, 0.5% Triton X-100, 10 mM $MgCl_2$. Made just prior to using, kept on ice

Buffer "C" – 50 mM Tris pH 7.4, 150 mM NaCl, 10 mM $MgCl_2$, 10 mM 2-mercaptoethanol. Made just prior to using, kept on ice

1X Phosphate-buffered saline (PBS) – 137 mM NaCl, 2.7 mM KCl, 4.3 mM $Na_2HPO_4 \cdot 7H_2O$, 1.4 mM KH_2PO_4, pH adjusted to 7.4, stored at RT

Elution Buffer – 20 mg glutathione, 4 mL 1X PBS, 1 mL mQ H_2O, pH adjusted to 9.0, made just prior to using

Cleansing Buffer 1 – 0.1 M borate acid, 0.5 M NaCl, pH adjusted to 8.5, stored at RT

Cleansing Buffer 2 - 0.1 M sodium acetate, 0.5 M NaCl, pH adjusted to 4.5 with acetic acid, stored at RT

3X PI4K Storage Buffer – 150 mM HEPES pH 7.5, 450 mM NaCl, 0.75 mM DTT, 0.3 mM PMSF, 75 % glycerol. Sterile filtered (0.4 μm pore filter), stored at 4 ºC

PITPα and PITPβ

Resuspension Buffer - 50 mM KH_2PO_4, 300 mM NaCl, 10 % glycerol, pH 7.5

Wash Buffer - 50 mM KH_2PO_4, 300 mM NaCl, 20 mM imidazole, 10 % glycerol, pH 7.5

PITP Elution Buffer - 50 mM KH_2PO_4, 300 mM NaCl, 150 mM imidazole, 10 % glycerol, pH 7.5

Resin Regeneration Buffer - 20 mM MES (2-morpholin-4-ylethanesulfonic acid), 100 mM NaCl, pH 5

Storage Buffer - 20 % ethanol

PIPES Buffer - 20 mM PIPES (1,4-Piperazinediethanesulfonic acid), 137 mM NaCl, 2.7 mM KCl, pH 6.8

2.2.2.2 Buffers used in gel electrophoresis

Stacking Gel Buffer – 0.5 M Tris-HCl, pH adjusted to 6.8, stored at RT

5X SDS Sample Buffer – 0.25 M Tris-HCl pH 6.8, 50% glycerol, 0.02% bromophenol blue, 1% sodium dodecyl sulfate (SDS), 0.5 M DTT, stored at -20°C and thawed prior to using

10 X SDS-PAGE (Polyacrylamide Gel Electrophoresis) Running Buffer – 0.25 M Tris, 1.92 M glycine, 1% SDS, pH 8.3. Working 1X running buffer was prepared by diluting 100 mL 10X running buffer to 1 L. Both stock and working solutions were stored at room temperature (RT)

10 X TBE (Tris/Borate/EDTA) Buffer – 108 g/L Tris base, 55 g/L boric acid, 20 mM EDTA, pH 8.3

2.2.2.3 Buffers used for lipids, the Bellbrook Transcreener® ADP^2 FI Assay, and binding assays

Autoclaved mQ H_2O was used to bring the buffers to desired volume.

2.5x Lipid Dilution Buffer - 62.5 mM HEPES (pH 7.5), 1.25 mM ethylene glycol-bis(β-aminoethyl ether)-*N*, *N*, *N'*, *N'*-tetraacetic acid (EGTA), sterile filtered then stored at -20°C

10X PI4K-IIIβ Assay Buffer - 250 mM HEPES (pH 7.5), 500 mM NaCl, 30 mM $MgCl_2$, 0.25 mg/mL BSA (Bovine Serum Albumin), 0.02% brij-35, filter-sterilized (0.4 μm pore size), stored at 4 ºC protected from light. Working 1X PI4K-IIIβ Assay Buffer was prepared by dissolving 10 mL 10X stock into 90 mL mQ H_2O

1X TKE Buffer: 50 mM Tris, 100 mM KCl, 1 mM EDTA, pH 7.4

2.2.2.4 Buffers used in PCR / Mutagenesis

10X T4 Ligase Buffer – 10 mM ATP, 10 mM $MgSO_4$, 50 mM potassium phosphate (69.8% KH_2PO_4: 30.14% K_2HPO_4) , adjusted to pH 7.5

3X Long-term Bacterial Stock Buffer - 65% glycerol, 25 mM Tris-HCl pH 8.0, 0.1 M $MgSO_4$

2.2.3 Solutions

2.2.3.1 Solutions used in bacterial growth

100 mg/mL ampicillin – 500 mg ampicillin (BioShop, catalogue AMP201) was dissolved in 5 mL mQ H_2O, then aliquoted in Eppendorf® tubes and stored at -20°C

100 mg/mL kanamycin - 500 mg kanamycin (Bioshop, catalogue KAN201) was dissolved in 5 mL mQ H_2O, then aliquoted in Eppendorf® tubes and stored at -20°C

100 mg/mL carbenicillin - 500 mg carbenicillin (BioShop, catalogue CAR544) was dissolved in 5 mL mQ H_2O, then aliquoted in Eppendorf® tubes and stored at -20°C

34 mg/mL chloramphenicol – 34 mg chloramphenicol (Bioshop, catalogue CLR201) was dissolved in 1 mL ethanol and stored at -20°C

1 M Isopropyl β-D-thiogalactopyranoside (IPTG) – 238 mg IPTG (Bioshop, catalog IPT001) was dissolved in 1 mL mQ H_2O and stored at -20°C

2.2.3.2 Solutions used in protein extraction

10 mg/mL RNAse solution – 10 mg RNAse (BioShop, catalogue RNA675) was dissolved in 1 mL mQ H_2O, stored at -20°C

100 mg/mL Lysozyme – 100 mg lysozyme (BioShop, catalogue LYS702) was dissolved in 1 mL mQ H_2O, stored at -20°C

100 mM PMSF – 174 mg PMSF (Millipore Signa, catalogue 10837091001) was dissolved in 10 mL isopropanol, stored at -20°C

1 M DTT – 154 mg DTT (Bioshop, catalogue DTT001) was dissolved in 1 mL mQ H_2O, stored at -20°C

5 M BME – 350 µL 14.3 M BME (Sigma, catalogue M6250-10ML) was dissolved in 1 mL mQ H_2O, stored at -20°C

2.2.3.3 Solutions used for SDS-PAGE

10% Ammonium Persulfate (APS) – 0.5 g $(NH_4)_2S_2O_8$ was dissolved in 5 mL RO H_2O, stored at -20°C

4% Stacking Gel: 18.8 mL RO H_2O, 7.5 mL Stacking gel buffer, 3 mL Acrylamide/

Bis-Acrylamide (37.5:1) 40% solution, 300 µL 10% SDS, 74 µL 50% glycerol, were all mixed followed by addition of 300 µL of 10% ammonium persulfate (APS) and 30 µL of *N*,*N*,*N*',*N*'-tetramethylethane-1,2-diamine (TEMED) immediately before casting. This recipe makes 6, 1 mm-thick gels.

10% Resolving Gel: 11.4 mL RO H_2O, 6 mL 1.5M Tris-HCl pH 8.8, 6 mL Acrylamide/Bis-Acrylamide (37.5:1) 40% solution, 240 µL 10% SDS, 180 µL 50% glycerol, were all mixed followed by addition of 240 µL of 10% APS and 24 µL of TEMED immediately before casting. This recipe makes 6, 1 mm-thick gels.

Colloidal Coomassie Blue Gel Stain – 0.12% Coomassie Brilliant Blue G-250 (BioRad, catalogue 1610406)**,** 10% $(NH_4)_2SO_4$, 10% H_3PO_4, 20% methanol in mQ H_2O (Candiano et al., 2004). Stored at RT for up to 6 months

Gel De-staining Solution – 25% methanol in mQ H_2O

2.2.4 Commercial chemicals and materials used

2.2.4.1 Lipid Substrates

L-α-Phosphatidylinositol (PI) - Liver PI (10 mg/mL in chloroform) purchased from Avanti Polar Lipids (catalogue 840042C)

L-α-Phosphatidylserine (PS) - Brain PS (10 mg/mL in chloroform) purchased from Avanti Polar Lipids (catalogue 840032C)

1,2-Dioleoyl-*sn*-glycero-3-phosphocholine (DOPC) – (25 mg/mL in chloroform) purchased from Avanti Polar Lipids (catalogue 850375P)

1,2-Dioleoyl-sn-glycero-3-phosphoethanolamine (DOPE) – (10 mg/ mL in chloroform) purchased from Avanti Polar Lipids (catalogue 850725)

Cholesterol – Synthetic plant-derived cholesterol purchased from Avanti Polar Lipids (catalogue 700100)

NBD C_{12}-HPC (2-(12-(7-Nitrobenz-2-Oxa-1,3-Diazol-4-yl)amino)Dodecanoyl-1-Hexadecanoyl-*sn*-Glycero-3-Phosphocholine) (NBD-PC) – Purchased from Life Technologies, Burlington, ON, Canada)

2.2.4.2 Mutagenesis / Polymerase Chain Reaction (PCR)

Q5 Reaction Buffer – purchased from New England Biolabs (catalogue #B9027S)

Deoxynucleotides triphosphate s (dNTP) – purchased from New England Biolabs (catalogue #N0447S)

Agarose – purchased from Fisher Scientific (catalogue #PI17850)

Ethidium Bromide – purchased from Millipore Sigma (catalogue #E7637)

Dimethyl sulfoxide (DMSO) – purchased from Millipore Sigma (catalogue #D8418)

Monarch® PCR & DNA Cleanup Kit – purchased from New England Biolabs (catalogue #T1030S)

NEBuffer™ Set (r1.1, r2.1, r3.1 and rCutSmart™) – purchased from New England Biolabs (catalogue #B7030S)

SOC Outgrowth Medium – purchased from New England Biolabs (catalogue #B9020S)

NEB® 10-beta/Stable Outgrowth Medium – purchased from New England Biolabs (catalogue B9035S).

QIAprep Spin Miniprep Kit – purchased from Qiagen (catalogue #27104)

Gel Loading Dye, Purple (6X) – purchased from New England Biolabs (catalogue #B7024S)

HighRanger 1 kb and CloneSizer 100 bp DNA Ladders – purchased from Norgen Biotek Corp. (catalogue #11900 and #11600, respectively)

2.2.4.3 Enzymes, antibodies and other proteins

Q5 High Fidelity (HF) DNA Polymerase – purchased from New England Biolabs (catalogue #M0491S)

DpnI – purchased from New England Biolabs (catalogue #R0176S)

KpnI HF – purchased from New England Biolabs (catalogue #R3142S)

HpaI – purchased from New England Biolabs (catalogue #R0105S)

SapI – purchased from New England Biolabs (catalogue #R0569S)

T4 DNA Ligase – purchased from New England Biolabs (catalogue #M0202S)

Bovine Serum Albumin (BSA) – Purchased from Sigma (catalogue A7906)

HRV 3C Precision Protease – Purchased from Millipore Sigma (catalogue 71493)

Thrombin Protease – Purchased from GE Healthcare Life Sciences (catalogue GE27-0846-01)

DNAse – Purchased from BioShop (catalogue DRB003)

Standard Molecular Weight Protein Ladder – FroggaBio BLUelf Prestained Protein Ladder (catalogue PM008-0500)

Goat Anti-mouse IgG antibody – Purchased from ThermoFisher (catalogue 31430)

2.2.4.4 Other materials

Bellbrook Labs Transcreener® ADP² FI Assay (Bellbrook Labs, catalogue 3013)

Corning® 384-well plates (catalogue 4514)

12% and 4-15% Mini-PROTEAN® TGX™ Precast Protein Gels, 10-well – Purchased from Bio-rad (catalogue numbers 4561043 and 4561084, respectively)

Glutathione-Agarose – Purchased from Sigma Aldrich (catalogue G4510)

Glutathione Sepharose 4B – Purchased from Cytiva Life Sciences (catalogue 17075601)

TALON® Metal Affinity Resin – Purchased from Takara Bio USA, Inc. (catalogue 635501)

PD-10 Desalting Columns containing Sephadex G-25 – purchased from Cytiva Life Sciences (catalogue 17085101)

Polycarbonate Membranes (50, 100, 200 nm) – Purchased from Avanti Polar Lipids (catalogue 610003, 610005, 610006)

Extrusion filter – Purchased from Millipore Sigma (catalogue 610014)

Phospholipid Vesicle Extruder – Purchased from Avanti Polar Lipids (catalogue 610000)

Bradford Reagent – Purchased from Millipore Sigma (catalogue B6916)

cOmplete™, Mini, EDTA-free Protease Inhibitor Cocktail – Purchased from Millipore Sigma (catalogue 11836170001)

3 METHODS

3.1 Production of PI4K-IIIβ mutants

3.1.1 Site-directed mutagenesis (deletion)

PI4K-IIIβ mutants were created following the QuikChange protocol (Agilent Technologies). The human PI4K-IIIβ gene isoform 2 (UniProt entry Q9UBF8-2) cloned into the pGEX-6P1-FLAG plasmid vector was used for site-directed mutagenesis. Two truncated PI4K-IIIβ mutants were developed: "C" (Δ453-511) and "L" (Δ408-507). The primers (**Table 1**) were manufactured by Millipore-Sigma and designed using NEBaseChanger® so that both the forward and the reverse primers would flank the PI4K-IIIβ gene region to be deleted. Additionally, KpnI restriction sites (bolded and underlined sequences in **Table 2**) were included on both forward (FW) and reverse (RV) primers (example on **Figure 12**) for the creation of cohesive ends, which would be needed for the ligation reaction in subsequent steps.

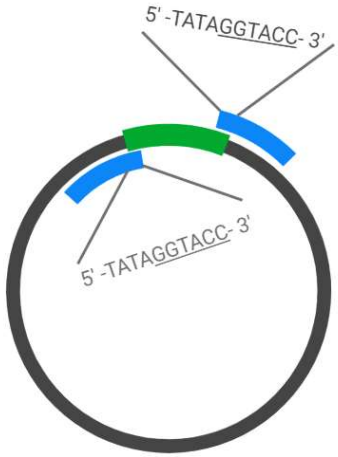

Figure 12: Primer design for the creation of truncated mutants of PI4K-IIIβ. A pGEX-6P1-FLAG plasmid vector containing the gene for PI4K-IIIβ is represented by the black circle, and the gene region to be deleted is depicted in green. Primers (in blue) were designed so that they would flank the gene region to be deleted. Primers also included in their 5'-end restriction sites for KpnI (sequence underlined), thus allowing the creation of sticky ends necessary for an eventual ligation reaction. Figure created with BioRender.com.

The PCR amplification reaction was carried in 1X Q5 Reaction Buffer and contained 2.5% DMSO, 200 μM dNTPs, 0.5 μM of each forward and reverse primers, 50 ng DNA template and 0.02 U Q5 High-Fidelity (HF) DNA polymerase per μL of reaction.

Table 2: Oligonucleotide primers used for the creation of PI4K-IIIβ truncated mutants. Underlined, bolded sequences represent KpnI-HF recognition sequences.

Primer	Sequence (5'-3')	Melting Temperature (T_m), in °C
"C" - FW	TATA**GGTACC**GATCCTTCTGCAGTTGCTC	63
"C" - RV	ATAA**GGTACC**CAGCTCGCCTATGTCATC	63
"L" - FW	TATA**GGTACC**CGAGACCCAGAAGATCCTTCTG	67
"L" - RV	TATA**GGTACC**TCGGTTCTCGGGGATCCG	70

The cycling parameters employed to generate the PI4K-IIIβ mutants are listed in **Table 3**:

Table 3: Thermocycler settings for the creation of PI4K-IIIβ truncated mutants.

Program	Number of Cycles	Temperature (°C)	Time	Activity
1	1	98	30 s	Initial Denaturation
2	15	98	30 s	Denaturation
		69	15 s	Annealing
		72	3 min 30 s	Extension
3	20	98	30 s	Denaturation
		64	15 s	Annealing
		72	3 min 30 s	Extension
4	1	72	5 min	Final Extension
5	1	4	hold	End

The PCR products were visually assessed by DNA agarose gel electrophoresis (**Section 3.1.2**).

3.1.2 DNA agarose gel electrophoresis

1% Agarose gels were prepared by mixing 0.5 g of agarose in 50 mL 1X TBE. The mixture was heated, typically under a flame, while gently swirling the flask. Once completely homogeneous, the solution was allowed to cool down until its flask was safe to touch. Next, 1.5 µL of a 500 µg/mL ethidium bromide stock solution was added to the dissolved agarose (final ethidium bromide concentration: 0.015 µg/mL) to allow for visualization of DNA later. The mixture was swirled until homogeneous, poured into a DNA agarose gel casting unit (which

contained combs for the creation of wells) and allowed to solidify while protected from ambient light. Once the gel had polymerized, it was placed in the running unit and covered with 1 X TBE buffer. Next, 5 µL of sample + 2 µL of loading buffer dye were mixed and transferred to the gel wells. DNA molecular weight markers were loaded alongside DNA samples. The gel was run at 100 V until the dye front had reached the bottom of the gel, and visualized using the software Image Lab 6.1 from Bio-Rad (Missisauga, ON, Canada).

3.1.3 PCR and DNA clean-up

PCR products were cleaned up using the Monarch® PCR & DNA Cleanup Kit, aiming at concentrating the products and removing minor, non-specific products. The protocol was carried out following manufacturer instructions.

3.1.4 DNA quantification

0.5 µL of the purified plasmid DNA was diluted in 350 µL of mQ H_2O in a quartz cuvette, mixed by pipetting and placed in a spectrophotometer cell. Absorbance readings at 260 nm were taken in triplicates and converted to DNA concentration by using the formula:

$$[DNA] = Abs_{260} * 50\ \mu g/mL * Dilution\ Factor$$

Protein contamination on purified plasmid DNA samples was assessed by repeating the procedure above but performing absorbance readings at 280 nm. Low protein contamination levels were obtained when the $Abs_{260}/Abs_{280} \geq 1.8$.

3.1.5 Restriction enzyme digestion and DNA ligation

Enzymatic digestion of plasmid DNA was performed concomitantly with DpnI (for removal of methylated, parent plasmid DNA) and KpnI-HF (for the creation of cohesive ends

needed for the ligation reaction). 50 µL reactions were carried out for 1 hour at 37 °C in 1 X NEB r1.1 Buffer, and contained 1 µg of purified plasmid DNA alongside 10 units each of DpnI and KpnI-HF. Once completed, the reaction was subjected to clean-up following the same protocol referred to in **Section 3.1.3**. This procedure removed digested DNA from the restriction enzymes.

Ligation of the purified plasmid DNA was carried out overnight at RT in 1 X T4 Ligase Buffer and contained 400 units of T4 DNA Ligase alongside ~ 300 µg DNA. Once completed, the reaction was stopped by incubating the reaction mixture for 20 minutes at 80 °C.

3.1.6 DNA transformation

Transformation of plasmid DNA into competent cells was performed using the heat shock approach (Panja *et al.*, 2008). For plasmid DNA propagation, 4 µL of each DNA products from the ligation reaction were mixed with 40 µL of ice-thawed NEB® 10-beta Competent *E. coli* (High Efficiency) cells in an Eppendorf® tube. After 30 minutes incubation on ice, the tubes were subjected to heat shock by immersion in a 42 °C water bath for 30-60 seconds, followed by a 2-minute ice incubation. Next, 500 µL of NEB® 10-beta/Stable Outgrowth Medium were added to the tube and incubated at 37 °C for 3 hours with gentle spinning. At the ends of this period, 200 µL of the transformation mixture were plated on a LB agar plate containing ampicillin for selection and incubated at 37 °C in a static incubator overnight.

For recombinant protein expression, purified plasmid DNA (obtained at the end of the procedure outlined in **Section 3.1.7**) was transformed in BL21 Rosetta 2(DE3) competent cells. The procedure followed manufacturer instructions. After transformation, cultures were plated on

LB plates containing both ampicillin and chloramphenicol for selection of pGEX and pRARE2 plasmid vectors, respectively. The plates were incubated overnight at 37 °C in a static incubator.

3.1.7 DNA extraction

Single colonies from plated, transformed NEB® 10-beta Competent *E. coli* (High Efficiency) cells were selected and used to inoculate 5 mL LB-ampicillin culture tubes. The cultures were incubated overnight at 37 °C, 266 RPM in an incubator.

The next day, cells from the bacterial cultures were pelleted by centrifugation at 7,000 *g* for 3 minutes at RT. Plasmid DNA extraction was performed using QIAprep Spin Miniprep Kit following manufacturer instructions. The extracted DNA was assessed by DNA agarose electrophoresis and restriction enzyme digestion with KpnI-HF and HpaI in NEB 1 X rCut Smart Buffer.

3.1.8 Bacterial freeze culture stocks

Long-term storage BL21 Rosetta 2(DE3) cells containing the plasmids for wild-type PI4K-IIIβ, as well as the "C" and "L" truncated mutants, were made by growing cells in LB-ampicillin-chloramphenicol overnight at 30 °C, 266 RPM in a shaking incubator. The next day, the cultures were aliquoted in cryogenic vials, diluted in 3 X Long-term Bacterial Stock Buffer, and stored at -80 °C.

3.2 Protein expression

3.2.1 Expression of recombinant PI4K-IIIβ in *E. coli*

LB agar plates supplemented with the appropriate antibiotic(s) (ampicillin, 100 μg/mL; kanamycin, 50 μg/mL; chloramphenicol, 34 μg/mL) were inoculated with a frozen culture of PI4K-IIIβ construct (see **Table 1** for constructs and respective selectable markers) in Rosetta™

2(DE3) (prepared by Dr. Candace Panagabko, Brock University). The plates were incubated overnight at 37 °C in a static incubator. Colonies were picked the next day and used to inoculate baffled flasks with 100-250 mL of autoclaved media (TB or TB auto-induction) containing the appropriate antibiotics. The flasks were placed in a shaking incubator at 37°C and 266 RPM.

Bacterial growth was monitored by optical density (OD) measurements (at λ = 600 nm) using the spectrophotometer Thermo Scientific GENESYS 10S UV-Vis blanked with virgin media. When a culture OD_{600} of 0.8-1.0 was obtained: 1) if TB media: 100 µM IPTG were added to the culture for induction of protein expression. Upon addition of IPTG, the culture was incubated for approximately 5 hours at 19°C, 266 RPM; or 2) if TB auto-induction media, no IPTG was added and the culture was incubated for 48-72 hours at 266 RPM, at 19°C.

3.2.2 Expression of recombinant Frequenin, PITPα, PITPβ and Sec14 in *E. coli*

The procedure described on **Section 3.2.1** was followed closely, except for the following: (1) LB plates containing ampicillin and chloramphenicol were incubated with the respective frozen cultures of PITPα, PITPβ and Sec14p, all in BL21(DE3)pLysS cells. Frequenin was expressed in BL21 (DE3) cells; and (2) post-induction, the cultures were incubated overnight at 28 °C, 266 RPM.

3.2.3 Sample harvesting and optical density measurement

A sample from the harvested cultures were transferred to cuvette tubes (pathlength (l) = 1 cm) when OD_{600} measurements were performed to monitor cell growth and/or to obtain whole cell samples for analysis via gel electrophoresis. The spectrophotometer was blanked with virgin medium. If the sample OD_{600} was above 1.0, the sample was diluted usually with a DF of 10 (*e.g.*, 100 µL sample (or blank media) + 900 µL RO H_2O). The volume of whole cell samples retrieved to be screened by gel electrophoresis was normalized to OD_{600} = 0.8. After pelleting by

centrifugation at 10,000 RPM for 5 minutes (ThermoIEC Micromax), whole cell samples were stored at -20°C for future analysis by gel electrophoresis.

3.3 Protein Extraction and Purification

3.3.1 Preparation of HSP Removal Wash for removal of heat-shock protein (HSP) contaminants

The protocol employed herein was adapted from Rial & Ceccarelli, 2002. Non-transformed BL21 (DE3) cells were grown in 100 mL TB media overnight at 37°C, 266 RPM. The cells were harvested by centrifugation, and a soluble fraction was prepared as described on section **3.3.2**. The proteins in the lysate were denatured by incubation at 65°C for 10 minutes, followed by centrifugation for 10 minutes at 12,000 x *g*. After removal of the pellet, the supernatant ("HSP Removal Wash stock") was stored at -20°C for future use. The working HSP Removal Wash was made by diluting the respective stock to ≈ 0.1 mg/mL protein with Buffer A that contained 20 mM ATP and 20 mM $MgCl_2$.

3.3.2 Purification of GST-tagged recombinant proteins

The following procedure was adapted from the protocol for purification of GST-tagged α-tocopherol transfer protein (α-TTP), developed by Dr. Atkinson's group. It was applied for the purification of PI4K-IIIβ, Sec14p, and Frequenin.

The bacterial cultures were pelleted by centrifugation at 10,000 RPM for 25 minutes at 4°C, using a Thermo Scientific Sorvall RC 6 Plus Centrifuge. The cell pellets were weighed and stored at -80°C when not used immediately. The cell pellet was resuspended in Buffer A (enough to achieve sufficient resuspension, but approximately 3.5 mL of buffer A per gram of cell mass) along with one tablet of protease inhibitor cocktail, followed by addition of 40 mg lysozyme/3 g cell pellet. The cells were then incubated on ice for 30 minutes, followed by sonication (using a

Qsonica sonicator, Model CL-334) on ice for 3 cycles of 30 seconds (1 sec on / 1 sec off), with 30 seconds intervals in between the cycles. Next, the lysate was passed 5 times through an 18 ½ gauge needle attached to a 10 mL syringe. Then, 10 mM $MgCl_2$, 0.1% Triton X-100, 2 units DNAse/mL cell lysate, and 50 µg/mL RNAse were added to the cell lysate followed by another 30-min incubation. At the end of the incubation period, the lysate was again passed through the 18 ½ gauge needle as described above. The cell lysate was then centrifuged for 25 min at 4°C, 18,000 RPM. The supernatant, now called "soluble fraction", was poured into a column containing 1 mL of glutathione agarose/Sepharose resin that had been washed with 10 mL 1X PBS and washed/equilibrated with 15 mL buffer B. The column was attached to a spinning wheel or shaking platform, which was then turned on, and incubated at 4°C overnight (note: the overnight incubation at 4°C could be replaced by 30 minutes at RT + 90 minutes at 4°C).

The flow-through was collected from the column, followed by a 5 mL wash with Buffer B. 5 mL HSP Removal Wash was added to the column, which was then incubated for 10 minutes at 37°C. After elution of the aforementioned wash, the column was further rinsed with 15 mL buffer B, followed by 10 mL buffer C. Enough buffer C was left in the column to cover the resin.

3-3.5 units of HRV 3C protease[2] (if PI4K-IIIβ or Frequenin, roughly 1U/150 µg protein) or 50 µL of thrombin (if Sec14p) were diluted to 1 mL in HRV 3C cleavage buffer (25 mM HEPES, 150 mM NaCl, 1 mM DTT, pH 7.5) and added to the column. The column was incubated at 4°C overnight. On the following day, the flow through was collected (containing the native protein of interest) alongside 5 x 1 mL fractions of buffer C wash.

[2] The amount of protease was based on the approximate yield of fusion protein obtained in pilot trials and on pilot protease reactions performed in Eppendorf® tubes. The reaction was performed in 25 mM HEPES, 150 mM NaCl, 1 mM DTT, pH 7.5, overnight at 4°C and assessed by gel electrophoresis.

Following the steps above, 5 mL of glutathione elution buffer was added to the column and allowed to equilibrate. The flow-through was collected in 5 x 1 mL fractions and kept on ice. Finally, the column was regenerated by washing it with 5 mL Cleansing Buffer 1, followed by 10 mL mQ H_2O, 5 mL Cleansing Buffer 2, and 5 mL mQ H_2O. The column was then stored at 4°C in a 2.5 M NaCl solution containing trace amounts of NaN_3 (for agarose-based resin) or 20% ethanol in mQ H_2O (for Sepharose-based resin).

3.3.3 Purification of His-tagged proteins by IMAC (Immobilized Metal Affinity Chromatography)

The following procedure was adapted from (Baptist, 2016). It was applied for the purification of PITPα and PITPβ.

The bacterial cultures were pelleted by centrifugation at 10,000 RPM for 25 minutes at 4°C. The cell pellets were weighed and stored at -80°C when not used immediately. Cell pellets were re-suspended in approximately 8 mL Resuspension Buffer / g of cell pellet and quickly frozen in liquid nitrogen. Once thawed, one tablet of the protease inhibitor cocktail was added to the cell lysate, followed by 2 units of DNAse per mL of cell lysate and 10 mM $MgCl_2$. The mixture was incubated on ice for 20 minutes and then passed 10 times through an 18 ½ gauge needle. The soluble fraction was obtained by centrifugation of the cell lysate for 25 min at 4°C, 18,000 RPM.

A column containing 1 mL of TALON Metal Affinity Resin pre-loaded with cobalt was washed twice with 10 mL of Resuspension Buffer followed by 10 mL Wash Buffer. The supernatant was slowly poured into the column and incubated overnight at 4°C with gentle shaking. On the next day, the flow-through was eluted, followed by a 10 mL wash with the Wash Buffer. 5 mL of the HSP Removal Wash (section **3.3.1**) was added to the column, which was

incubated at 37°C for 10 minutes. At the end of this period, the column was washed with 5 mL Wash Buffer followed by 10 mL Wash Buffer containing 40 mM imidazole. PITPα and PITPβ were eluted with 5 mL Elution Buffer. The TALON resin was regenerated with 8 mL Regeneration Buffer and stored at 4°C in 20% ethanol. The three first 1 mL fractions eluted from the TALON resin were buffer exchanged to PIPES Buffer using a PD-10 desalting column. 8, 1 mL fractions were collected from the PD-10 column, which was regenerated with 20 mL 1X PBS and stored with trace amounts of NaN_3.

Note: although 8 fractions were collected from the PD-10 column, preference was given to the first or second fraction that had appreciable amounts of protein in it (as determined by the Bradford Assay, **Section 3.4**) when choosing which fraction would be used for the activity assays.

3.4 Protein Quantification by Bradford Assay

Protein quantification was performed by the Bradford Assay (Bradford, 1976). Briefly, 50 μL of purified protein was mixed with 1 mL Bradford reagent by pipetting. After 5 minutes, the absorbance (λ = 595 nm) of protein samples was recorded. The protein concentration was interpolated from a standard curve of BSA, whose standards ranged from 0.1 to 0.8 mg/mL.

3.5 Protein Expression and Purification Analysis by SDS-PAGE

3.5.1 Casting gels

Six sets of glass plates were cleaned, clipped together, and assembled into the casting stand. RO H_2O was used to check for leaks, and then poured out. The plates were patted dry with Kimwipe®. APS and TEMED were added to the remaining components of 10% resolving gel buffer, immediately followed by transfer of this mixture to the plates, filling to ¾ of their height.

The resolving gel was levelled by addition of small amounts of *n*-butanol, which also eliminated bubbles. The gels were allowed to polymerize at room temperature for approximately 40 minutes. *n*-Butanol was then removed by patting with Kimwipe®, followed by addition of a 4% stacking gel. A comb was inserted to allow formation of wells in the stacking gel, ensuring that no bubbles were below the comb's teeth. The gels were left on the benchtop for 30-40 minutes to polymerize. The clips were removed, the gels were wrapped in damp paper towel, placed in a sealed plastic bag, and stored at 4°C until use.

Note: the recipe above can be adjusted accordingly to prepare 12% or 15% acrylamide gels, and/or 1.5 mm-thick gels.

3.5.2 Running samples on SDS-PAGE gels

To normalize sample concentrations and avoid smearing, gel samples were prepared as described on **Table 4**:

Table 4: Normalization of SDS-PAGE gel samples. Different volumes of different protein samples were used to avoid protein overloading in the gel. Note: 50% glycerol was added last to allow better mixing of other components.

Sample Type	Sample volume (µL)	5X SDS Sample Buffer volume (µL)	Stacking Gel Buffer volume (µL)	50% Glycerol Volume (µL)
Whole cell	Varied, enough to ensure a cell density matching OD_{600} = 0.8 (explanation on section 3.1)	40	20	40
Soluble Fraction	5	5	20	-
Flow-Through	5	5	20	-
Elution Fractions	25	5	-	-

The samples were boiled for 5 min in water bath (~ 100 ºC), and then loaded in the gel (28 µL of sample mixture and 6 µL protein ladder were loaded in 1.0 mm-thick gels, or 45 µL of sample mixture and 7 µL protein ladder for 1.5 mm-thick gels). The gel was run using a Bio-Rad Mini-PROTEAN® Tetra System at 125 V until samples entered the resolving gel and then at 150 V until the dye front reached the bottom of the gel. The gel was stained overnight with the gel staining solution under gentle rocking. De-staining was performed with 25% methanol in mQ H_2O (5 x 20 minutes), followed by imaging using a Bio-Rad Gel Doc® EZ Imager (white tray).

3.6 Preparation of lipid vesicles

Generally, 0.5 mg/mL stock vesicles were prepared. First, the appropriate volume of each lipid stock was transferred to a glass vial. Chloroform was evaporated with a stream of N_2 (g), then the vials were placed under high vacuum for 1 hour. The lipid mixture was resuspended in the desired volume of 2.5X Lipid Dilution Buffer and stored at 4°C overnight. If preparing small unilamellar vesicles (SUVs), the lipids were sonicated on ice using the 35% duty cycle (amp), 20 minutes, pulse 1 second on 1 second off on the following day. The vial contents were transferred to Eppendorf® tubes and centrifuged at 15,000 RPM for 5 minutes to remove metal particulates that resulted from the sonicator probe. The lipid mixtures were then immediately transferred to new glass vials, and the glass vials were placed in a water bath at ≈ 40°C for ≈ 10 minutes. If large, unilamellar vesicles (LUVs, 100-1000 nm in diameter) were desired, the lipid sonication step was skipped (Szoka & Papahadjopoulos, 1980).

A small amount of 2.5X Lipid Dilution Buffer was passed through the Phospholipid Vesicle Mini-Extruder Apparatus (Avanti Polar Lipids) that had been assembled as per manufacturer instructions, using a 50 nm polycarbonate membrane for SUVs or 200nm for LUVs. The buffer was then discarded, and enough of the warm lipid mixture was passed through

the extruder at least 5 times forward and back. The extruded lipids were then transferred to new vials and stored at 4°C until use.

3.7 Binding assays

The binding of PITPα, PITPβ and Sec14p to the fluorescent PC analogue, NBD-PC, was tested in a QuantaMaster-QM-2001-4 fluorometer. 150 nM NBD-PC (from an ethanol stock) was added to a 1 mL quartz cuvette containing 1X TKE buffer. Fluorescence readings (λ_{EX} = 469 nm, λ_{EM} = 527 nm) were taken before and after adding 220 nM PITPs to the cuvette until a plateau was reached or for ~ 350 seconds. The data was fitted to an exponential, two phase association curve using GraphPad Prism, Version 9.5.1 (GraphPad Software Inc., La Jolla, CA, USA).

3.8 Tryptophan intrinsic fluorescence spectrum

Intrinsic tryptophan fluorescence spectra were monitored in a Molecular Devices SpectraMax i3 microplate reader. The fluorescence emission of 13 μM Frq1, alone and with 100 μM Ca^{2+}, was measured between 315 and 370 nm with λ_{EX} = 295 nm in 25 mM HEPES, 150 mM NaCl, pH 7.5. Buffer controls (with and without calcium) were also run.

3.9 Activity assay

3.9.1 Determining the optimal ADP^2 Antibody-IRDye® QC-1

The concentration of ADP^2 Antibody-IRDye® QC-1 in an assay is proportional to the chosen concentration of ATP. Manufacturer instructions (*Transcreener® ADP FI Assay Technical Manual*, 2023) suggest that the ADP^2 Antibody-IRDye® QC-1 concentration should be calculated from the linear relationship below:

$$y = 0.93x + 0.7 \qquad \textbf{Equation 1}$$

where y = the concentration of ADP[2] Antibody-IRDye® QC-1 at 1 X (note: running assay conditions require a final antibody concentration at 0.5 X) and x = [ATP] (in µM) in the reaction.

For better results, it is recommended that the antibody concentration for a given ATP concentration is titrated in the buffer system employed. First, the reaction buffer was prepared omitting the enzyme, but including ATP and the lipid substrate. **Table 5** below shows an example of an antibody titration for assays run with 10 µM ATP.

Table 5: Components of the reaction buffer for the antibody titration.

Component	[Stock]	Concentration in 20 µL Assay Mix	Volume per assay (µL)	Number of Assays (x)	Volume for x assays (uL)
ATP (uM)	500 µM	10 µM	0.4	36	14.4
Lipid Substrate	0.5 mg/mL	0.2 mg/mL	8.0	36	288
PI4K-IIIβ Assay Buffer	10 X	0.5 X	1.0	36	36.0
mQ H_2O			0.6	36	21.6
		Total =	10	36	360

Next, it was necessary to determine the range of antibody concentrations used in the titration. For 10 µM ATP, **Equation 1** estimates that 5 µg/mL of antibody should be used in an assay.

$$y = 0.93x + 0.7$$

$$y = 0.93(10) + 0.7$$

$$y = 10\ \mu M\ ATP\ (at\ 1\ X)$$

$$y = 5\ \mu M\ ATP\ (at\ 0.5\ X)$$

This calculated amount was used as a guiding parameter to determine the range of antibody concentrations to be employed. Since the antibody is diluted serially by a factor of 2 during the titration experiment, it was thought that choosing 5 antibody concentrations above 5 µg/mL and 5 antibody concentration below 5 µg/mL should provide a satisfactory window. Hence, the starting highest antibody concentration was set to 100 µg/mL. The solution with the highest antibody concentration to be used in the titration was made in the same buffer as above.

3.9.2 Determining the FI assay window

As per manufacturer instructions (*Transcreener® ADP FI Assay Technical Manual*, 2023), minimum and maximum fluorescence values were determined to obtain the detection window for The Bellbrook Labs Transcreener® ADP^2 FI Assay. The Fluorescence Intensity (FI) was achieved by measuring the lowest and highest signals at the conditions and antibody concentrations used for the assay, *i.e.*, "low" = tracer with antibody + quencher, "high" = tracer without antibody + quencher. The components, described on **Tables 6** and **7**, were transferred to microcentrifuge tubes, gently shaken for approximately 10 minutes at RT, and aliquoted into the assay microplate 20 µL/well). The fluorescence was measured with the Endpoint FI Assay Window protocol (see **Section 3.9.4.2**).

Table 6: Low Relative Fluorescence Units (RFUs) mixture for the PI4K-IIIβ assay conditions. Autoclaved mQ H_2O was used to fill to desired volume.

Component	[Final]
ADP^2 Antibody-IRDye® QC-1	8.80 µg/mL
10X PI4K-IIIβ Assay Buffer	1X
ADP Alexa Fluor® 594 Tracer	4 nM

Table 7: High RFUs mixture for the PI4K-IIIβ assay conditions. Autoclaved mQ H_2O was used to fill to desired volume.

Component	[Final]
10X PI4K-IIIβ Assay Buffer	1X
ADP Alexa Fluor® 594 Tracer	4 nM

3.9.3 ATP/ADP standard curves

First, the Detection Mix was made following the components and volumes listed in **Table 8**. Enough of each component for 48 wells (with ≈ 10% excess to account for losses during pipetting) was transferred to a microcentrifuge tube, which was shaken for approximately 15 minutes at RT protected from light.

Table 8: Detection Mix for the ATP/ADP standard curve.

Component	[Stock]	Concentration in 20 µL Assay Mix	Volume per well (µL)	Number of assays	Volume for x assays (µL)
ADP[2] Antibody-IR Dye® QC-1	1690 µg/mL	8.80 µg/mL	0.104	53.00	5.512
ADP Alexa Fluor® 594 Tracer	800.0 nM	4.00 nM	0.100	53.00	5.300
PI4K-IIIβ Assay Buffer	10.0 X	0.20 X	0.400	53.00	21.20
mQ H_2O	-		1.396	53.00	73.98
Total	-		2.000	53.00	106.0

Next, the Assay Mix was made following the components and volumes listed in **Table 9**. Enough of each component for 48 wells (+ ≈ 10% excess) was transferred to a labelled microcentrifuge tube, which was equilibrated at 15 minutes at RT with gentle shaking.

Table 9: Assay Mix for the ATP/ADP Standard Curve.

Component	[Stock]	Concentration in 20 µL Assay Mix	Volume per well (µL)	Number of assays	Volume for x assays (µL)
Lipid Substrate (mg/mL)	0.5 mg/mL	0.2 mg/mL	8.0	53.0	424.0
PI4K-IIIβ Assay Buffer (X)	10.0 X	0.8 X	1.6	53.0	84.8
mQ H_2O	-		5.4	53.0	286.2
Total	-		15.0	53.0	795.0

Finally, mQ H_2O, ATP, and ADP from stock solutions were pipetted into twelve autoclaved microcentrifuge tubes, labelled 0-60%, following the volumes on Table 9. A 10% excess for each conversion point to be run in quadruplicates was prepared to account for volume loss during pipetting. The solutions were kept on ice until used.

Table 10: Volumes required to make >4 times each %ATP/ADP conversion solution. 10 µM ADP stock was used for conversion points 1-8%, and 100 µM ADP stock was used for the other ones. 100 µM ATP stock was used.

% ATP conversion	[ATP] (µM)	[ADP] (µM)	Vol. ATP stock per assay (µL)	Vol. ADP stock per assay (µL)	Vol. mQH_2O per assay	Number of replicates	Vol. ATP stock (µL) for x replicates	Vol. ADP stock for x replicates (µL)	Vol. mQH_2O for x assays	Total Volume (uL)
0	10.00	0.00	2.00	0.00	1.00	4.40	8.80	0.00	4.40	13.20
1	9.90	0.10	1.98	0.20	0.82	4.40	8.71	0.88	3.61	13.20
2	9.80	0.20	1.96	0.40	0.64	4.40	8.62	1.76	2.82	13.20
4	9.60	0.40	1.92	0.80	0.28	4.40	8.45	3.52	1.23	13.20
6	9.40	0.60	1.88	0.12	1.00	4.40	8.27	0.53	4.40	13.20
8	9.20	0.80	1.84	0.16	1.00	4.40	8.10	0.70	4.40	13.20
10	9.00	1.00	1.80	0.20	1.00	4.40	7.92	0.88	4.40	13.20
15	8.50	1.50	1.70	0.30	1.00	4.40	7.48	1.32	4.40	13.20
20	8.00	2.00	1.60	0.40	1.00	4.40	7.04	1.76	4.40	13.20
30	7.00	3.00	1.40	0.60	1.00	4.40	6.16	2.64	4.40	13.20
40	6.00	4.00	1.20	0.80	1.00	4.40	5.28	3.52	4.40	13.20
60	4.00	6.00	0.80	1.20	1.00	4.40	3.52	5.28	4.40	13.20

When all the solutions had been made, 106 µL of the Detection Mix was transferred to the microcentrifuge tube containing the Assay Mix (final volume: 901 µL). 17 µL of this mixture

(*i.e.*, Assay Mix + Detection Mix) was transferred to wells of a Corning® 384-well plate. Finally, 3 µL of each %ATP conversion was transferred to the respective wells on the plate and the FI was monitored using the Endpoint Assay Window (settings listed on **Section 3.9.4.2**).

3.9.4 Running the Bellbrook Labs Transcreener® ADP² FI Assay

3.9.4.1 Preparing reagents

Assay components were divided in three main groups for the order of preparation:

1) the Detection Mix (containing ADP Alexa Fluor® 594 Tracer, ADP² Antibody-IRDye® QC-1 and 20% of the total Assay Buffer) to a final volume of 2 µL in a 20 µL assay;
2) the Assay Mix (containing proteins, lipid substrate and 80% of the Assay Buffer) to a final volume of 16.4 µL in a 20 µL assay;
3) ATP (the desired dilution of ATP in autoclaved mQ H_2O) to a final volume of 1.6 µL in a 20 µL assay.

The Detection Mix was prepared first to ensure that antibody and tracer had equilibrated prior to being exposed to other reaction components. The appropriate volume of autoclaved mQ H_2O, ADP Alexa Fluor® 594 Tracer, ADP² Antibody-IRDye® QC-1 and Assay Buffer were transferred to an microcentrifuge tube. The tube was covered in aluminum foil and mixed at RT for approximately 15 minutes. **Table 11** below displays an example of volumes used to make up the Detection Mix for 9 assays in quadruplicates. An excess of approximately 15% was used to account for losses due to pipetting.

Table 11: Detection Mix Components.

Component	[Stock]	Concentration in 20 µL Assay Mix	Volume per assay (µL)	Number of Assays (x)	Volume for x assays (µL)
ADP[2] Antibody-IRDye® QC-1	1690 µg/mL	8.80 µg/mL	0.104	42	4.368
ADP Alexa Fluor® 594 Tracer	800 nM	4.00 nM	0.100	42	4.200
PI4K-IIIβ Assay Buffer	10 X	0.20 X	0.400	42	16.80
mQ H_2O			1.39	42	58.63
		Total =	2.00	42	84.00

While the Detection Mix was equilibrating, the Assay Mix was prepared in different microcentrifuge tubes. **Tables 12-14** below display examples of reagents and volumes used to make up the Assay Mix for 3 assay conditions in quadruplicates. An excess of 12.5% was used to account for losses due to pipetting.

Table 12: Assay Mix for the No Protein control

Component	[Stock]	Concentration in 20 µL Assay Mix	Volume per assay (µL)	Number of Assays (x)	Volume for x assays (µL)
PIK3C3 Assay Buffer	10 X	0.8 X	1.60	4.5	7.20
Lipid Substrate 200 nm LUVs	0.5 mg/mL	0.2 mg/mL	8.00	4.5	36.0
mQ H_2O			6.80	4.5	30.6
		Total =	16.4	4.5	73.8

Table 13: Assay Mix for the No Lipid control

Component	[Stock]	Concentration in 20 µL Assay Mix	Volume per Assay (µL)	Number of Assays (x)	Volume for x assays (µL)
PI4K-IIIβ Assay Buffer	10 X	0.8 X	1.60	4.5	7.20
PI4K-IIIb	1535 nM	22 nM	0.29	4.5	1.30
mQ H_2O			14.51	4.5	65.3
		Total =	16.4	4.5	73.8

Table 14: Assay Mix for the PI4K-IIIβ + Frq1 + Sec14p assay

Component	[Stock]	Concentration in 20 µL Assay Mix	Volume per Assay (µL)	Number of Assays (x)	Volume for x assays (uL)
PI4K-IIIβ Assay Buffer	10X	0.2X	1.60	4.5	7.20
Lipid Substrate 200 nm LUVs	0.5 mg/mL	0.2 mg/mL	8.00	4.5	36.0
PI4K-IIIb	1535 nM	22 nM	0.29	4.5	1.30
Sec14	8910 nM	220 nM	0.49	4.5	2.22
Frq	1000 nM	22 nM	0.44	4.5	1.98
mQ H_2O			5.57	4.5	25.1
		Total =	16.4	4.5	73.8

Notes: 1) Whenever a Lipid Transport Protein was present in the Assay Mix, this protein was added to the tube right after the lipid substrate and incubated at 37 ºC for 5 min to equilibrate; 2) PI4K-IIIβ was always added last to the Assay Mix tubes.

Once the Assay Mixes were prepared, they were incubated for approximately 10 minutes at room temperature with gentle shaking. Then, 9 µL of the Detection Mix was added to each Assay Mix tube and mixed by pipetting. The tubes were then kept on ice and protected from ambient light until the tube's contents were transferred to the plate wells.

Once the plate reader had been set up (settings on **Section 3.9.4.2**), 18.4 µL of the contents in the microcentrifuge tubes containing Assay Mix + Detection Mix were transferred to the appropriate wells in the 384 well plate. Once all wells had been loaded as described above, 1.6 µL of a 125 µM ATP stock (final ATP concentration in the assay = 10 µM) were transferred to the plate wells in as short of a time as possible. The plate was then inserted into the plate reader and read for 3 hours.

3.9.4.2 Running the assay

Molecular Devices SpectraMax i3

Software: SoftMax pro 7.03

Settings:

Endpoint or Kinetic - Time: 3 h, Interval: 2 min, Reads: 91

Fluorescence

Excitation Wavelength: 584 nm, Emission Wavelength: 618 nm

Auto cut-off: 610 nm

Reading Height: 5.74 mm

PMT and Optics: Auto, 6 flashes/read

More Settings: a) endpoint - shake once before 1st read (3 s, orbital, low intensity); or b) kinetic - shake for 3 s before first read and for 3 s between reads (both orbital, low intensity); calibrate OFF, carriage speed normal

Temperature: room temperature (~ 25 °C)

3.10 Statistical tests

All statistical tests were performed with GraphPad Prism 9.5.1 software. Unpaired, two-tailed t-tests were employed for graphs shown in Figures 19, 21, 28B, 35B-C, 36B. Ordinary one-way ANOVA was used for graphs shown in Figures 23B, 24F, 31D and 35D.

4 RESULTS AND DISCUSSION

4.1 Expression and purification of recombinant human PI4K-IIIβ in *E. coli*

Initial attempts of producing recombinant, GST (Glutathione-S-Transferase) -tagged PI4K-IIIβ resorted to expression in the routinely used T7-based *E. coli* expression host BL21 (DE3). This strain incorporates a chromosomal copy of the T7 RNA polymerase gene under the control of the T7 promoter, which presumes high yields of recombinant protein (Jia & Jeon, 2016). Nevertheless, only modest yields of GST tag-free (*i.e.*, native) PI4K-IIIβ were obtained when expressing in BL21(DE3), *i.e.*, 48.8 ± 19.8 μg of protein per gram of bacterial cell pellet (**Figure 19**). These yields were likely due to the large size of the expressed construct, ~ 116 kDa, which usually hinders sufficient expression and/or recovery of soluble product, even though our expression trials involved low inducer concentrations (*i.e.*, ≤ 100 μM IPTG) and low post-induction temperatures (*i.e.*, 16-20 ºC). These conditions are typically employed when expressing large and/or insoluble proteins in *E. coli* (Structural Genomics Consortium et al., 2008).

4.1.1 Impact of different culture media in the expression of recombinant PI4K-IIIβ

With the goal to improve the yields, a few strategies were employed: 1) addition of trace metals (50 μM Fe^{3+}, 20 μM Ca^{2+}, 10 μM Mn^{2+}, 2 μM of each Co^{2+}, Ni^{2+}, Mo^{2+} and borate) to LB medium as this was reported to increase the cell density 13-fold and enabled high levels of target protein expression (Studier, 2005); 2) addition of one of PI4K-IIIβ's natural ligand (*i.e.* 11 μM PI) at induction to LB medium, as binding to a ligand can stabilize protein structure (Mazal et al., 2018), which could aid in expression levels; 3) bacterial growth in LBTP, an auto-inducing, buffered, tryptone-enriched LB medium containing Mg^{2+} and phosphate, reported to enhance bacterial growth and consequently recombinant protein expression (Studier, 2005). Although

GST-tagged PI4K-IIIβ was in fact expressed, as per analysis of a whole-cell screening SDS-PAGE gel (**Figure 13**), the yield of the purified, native protein was at best not significantly higher than what was obtained in previous attempts. Difficulty in obtaining sufficient yields of our target protein could be explained by the widely known difficulty of over-expressing proteins > 60 kDa in soluble form in bacteria (Structural Genomics Consortium et al., 2008). Transcription and translation occur simultaneously in prokaryotes, but eukaryotic proteins (especially larger ones) often necessitate longer times and/or the help of chaperones for proper folding. Thus, the fast pace at which proteins are translated in bacteria often leads to unfolded, partially unfolded or fully unfolded species (Francis & Page, 2010).

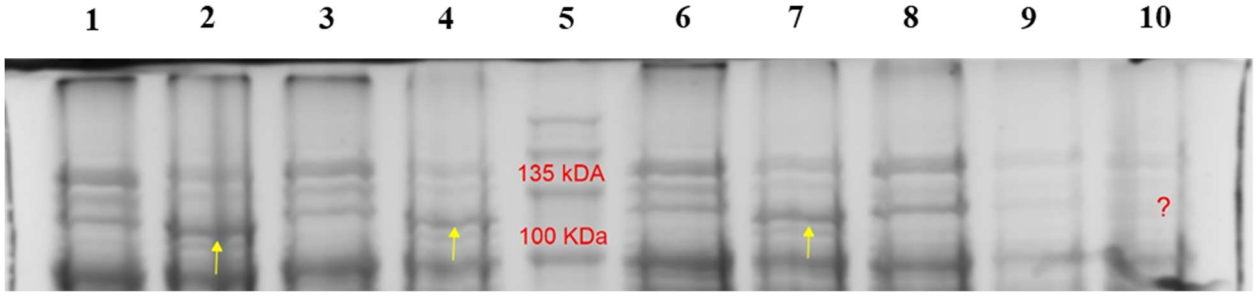

Figure 13: Whole-cell screening of GST-tagged PI4K-IIIβ expression in different bacterial culture media. Three difference conditions for bacterial growth and recombinant protein expression were tried and compared to growth in LB (lanes 1 and 2, uninduced and induced controls, respectively): addition of PI at induction to LB medium (lane 3, pre-induction; lane 4, 16 h post-induction), addition of trace metals to LB medium (lane 6, uninduced; lane 7, 16 h post-induction), and growth in LBTP medium (lane 8, uninduced; lane 9, 16 h post-induction; lane 10, 40 h post-induction). Induction was done with 0.1 mM IPTG to the medium at OD_{600} 0.8-1.0, except for LBTP as it is an auto-induction medium. The temperature was lowered from 37 ºC to 18 ºC upon induction (or at OD_{600} 0.8-1.0 for the culture in LBTP) and further grew for 16 h (unless otherwise specified) with shaking set to 266 RPM. No significant differences are seen in the GST-PI4K-IIIβ band intensity (yellow arrows) when comparing the modified media (lanes 4 and 7) to the control (lane 2). No visible band matching the MW of GST-PI4K-IIIβ was detected in the LBTP culture at 16 h nor at 40 h. PI was added add 11 µM at induction; the trace metals included addition of 50 µM Fe^{3+}, 20 µM Ca^{2+}, 10 µM Mn^{2+}, 2 µM of each Co^{2+}, Ni^{2+}, Mo^{2+} and borate. Lane 5, protein ladder.

4.1.2 Switching to His_{10}-tagged constructs and co-expressing PI4K-IIIβ with binding partners

In light of the results and rationale above, we hypothesized that replacing the 26 kDa GST tag by the 1.6 kDa deca-histidine (His_{10}) tag could improve yields due to the significant reduction (*i.e.,* 27%) in MW of the fusion protein (*i.e.,* ∼116 kDa to ∼ 91 kDa). His_{10} tags are also advantageous in comparison to GST tags as the former do not tend to interfere with the target protein structure, while the latter tag is itself a dimer thus potentially promoting dimerization of the fusion protein. Both N- and C-terminally His_{10}-tagged constructs of our protein of interest were made, to account for the fact that C-terminal affinity tags can sometimes rescue the solubility of recombinant proteins that form inclusion bodies when N-terminally tagged (Structural Genomics Consortium et al., 2008) such as our GST-PI4K-IIIβ. To overcome potential problems in correct protein folding, and an additional aid, constructs in which PI4K-IIIβ was co-expressed with 1) Frq1 or 2) the kinase co-chaperone cdc37 (cell division cycle 37) were made. Co-expression of binding partners may aid in co-folding and has been shown to be advantageous in the production of some recombinant proteins that otherwise were insoluble (Romier et al., 2006). Frq1 may bind to PI4K-IIIβ at the semi-conserved NCS-1 recognition domain (Strahl et al., 2007; McPhail & Burke, 2023), and cdc37 is a yeast molecular chaperone shown to recruit HSPs to maturing kinases (Wandinger et al., 2008). Lastly, expression in arabinose-based systems were investigated, as this tightly controlled system has been shown to increase protein solubility in *E. coli* and aid in the heterologous expression of toxic proteins (Guzman et al., 1995). All constructs mentioned in this paragraph were kindly made by Dr. Candace Panagabko, Brock University.

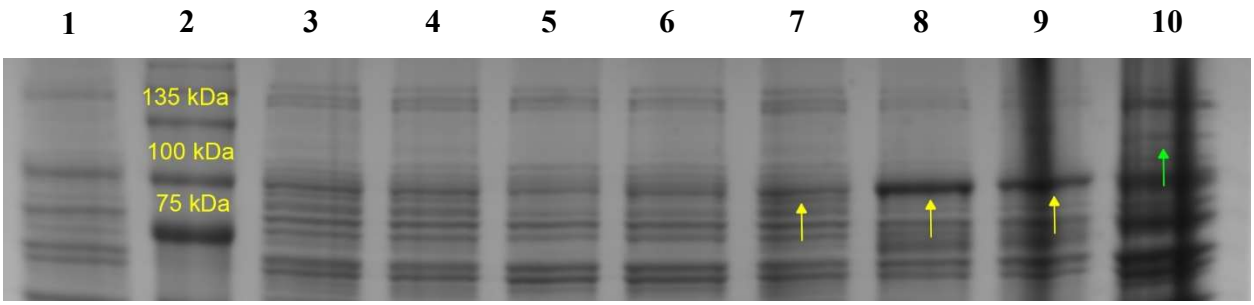

Figure 14: Whole-cell screening of His_{10}-tagged PI4K-IIIβ constructs. Different PI4K-IIIβ (here termed "PI4K", for simplicity) constructs were expressed in BL21(DE3) cells. Constructs with an N-terminal His_{10} tag ("His-PI4K") and C-terminal His_{10} tag ("PI4K-His") were prepared by Dr. Candace Panagabko. Samples were loaded as follows: lane 1 - uninduced; 2 - protein ladder; 3 - His-PI4K, arabinose-inducible; 4 - PI4K-His, arabinose-inducible; 5 - PI4K-His; 6 - GFP-PI4K-His; 7 - His-PI4K + cdc37; 8 - His-PI4K; 9 - His-PI4K + Frq1; 10 - GST-PI4K. Unless otherwise stated, the constructs were expressed from IPTG-inducible vectors. A Green Fluorescent Protein (GFP)-tagged construct was also made for fluorescent-based identification during the purification protocol. Evident overexpression of fusion PI4K-IIIβ is apparent on lanes 8, 9 and 7 (to a lesser extent) when compared to an uninduced sample (lane 1). Intense bands corresponding to the theoretical MW of His_{10}-PI4KIIIβ, *i.e.* 91 kDa, are indicated by yellow arrows. A GST-tagged construct was also run for comparison (lane 10), and it shows a faint band corresponding to the fusion PI4K-IIIβ's MW, 116 kDa.

Initial whole-cell screening of 7 different constructs indicated 3 with apparent high-expression levels of PI4K-IIIβ: 1) IPTG-induced, 2) co-expression with Frq1, and 3) co-expression with cdc37, all with N-terminal His_{10} tags (**Figure 14**). IMAC-based purification of the 3 chosen constructs yielded concentrated yet highly impure fractions as seen on **Figure 15**. This could be a result of endogenous proteins that possess surface exposed histidine residues, thus allowing them to co-purify with the fusion protein of interest even when a gradient of imidazole-containing washes is performed. Additionally, His_{10} tags are often ineffective in supporting proper folding of proteins with solubility issues (Wood, 2014). In fact, IMAC-based purifications generally require further downstream processing like size-exclusion chromatography to eliminate contaminants (Structural Genomics Consortium et al., 2008). Ergo, optimization of the purification of our His_{10} constructs was possible, but labour and time

intensive. (Note: work with the purification of His-tagged PI4K-IIIβ constructs involved collaboration with Dr. Candace Panagabko and Morgan Robinson).

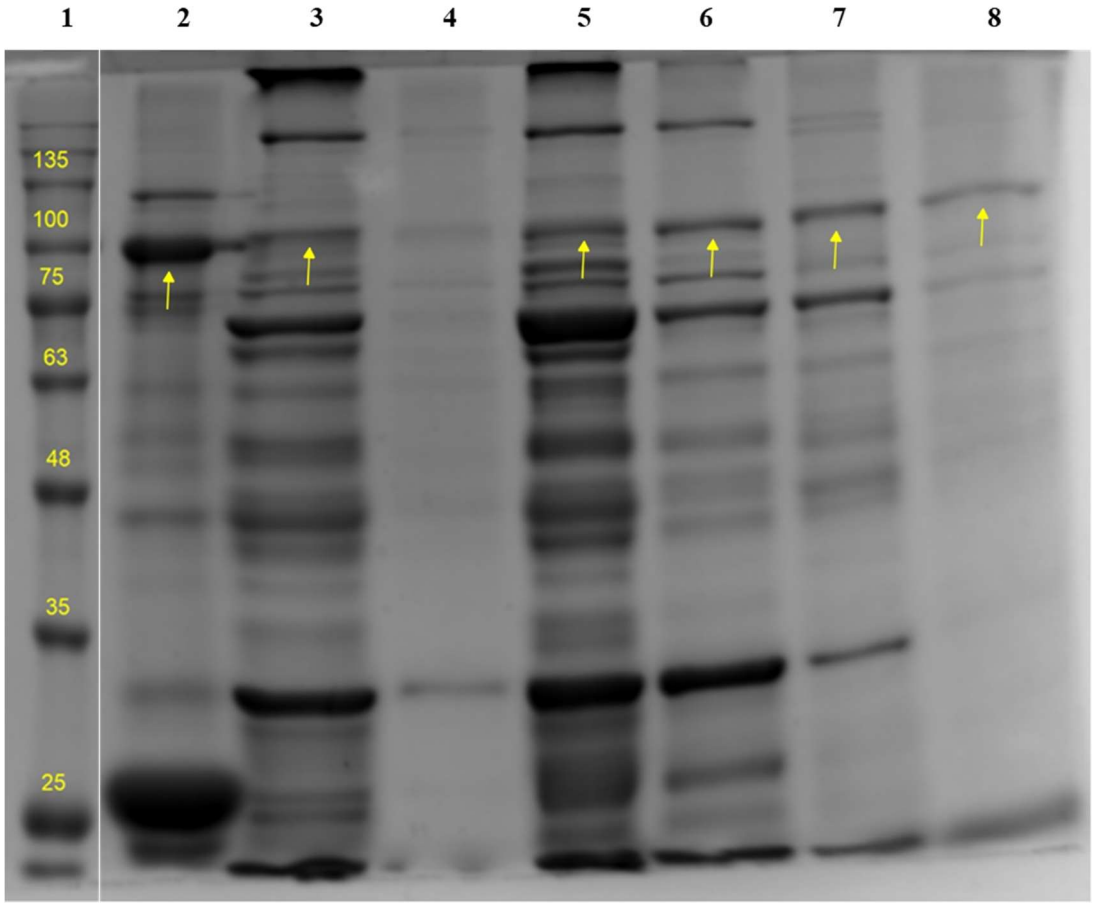

Figure 15: Purification of different His_{10}-tagged PI4K-IIIβ constructs. Different PI4K-IIIβ (here termed "PI4K", for simplicity) constructs were expressed, alone or co-expressed with the binding partners cdc37 and Frq1, in BL21(DE3) cells and purified by IMAC. A gradient of imidazole (ImH) washes was performed on the resin-bound soluble fractions to remove unbound and weakly-bound proteins. Neither washes containing 0.2 nor 0.5 M imidazole were sufficient for selectively eluting the fusion protein of interest (indicated by yellow arrows). A glutathione elution buffer eluate from the purification of GST-PI4K-IIIβ was loaded (lane 2) for comparison, and also contained remanescents of native PI4K-IIIβ (yellow arrow). Samples were loaded as follows: lane 1 – protein ladder; 2 – glutathione elution buffer wash; 3 - 0.2 M ImH His-PI4K; 4 - 0.5 M ImH His-PI4K; 5 - 0.2 M ImH His-PI4K + cdc37; 6 - 0.5 M ImH His-PI4K + cdc37; 7 - 0.2 M ImH His-PI4K + Frq1; 8 - 0.5 M ImH His-PI4K + Frq1

4.1.3 Expressing recombinant PI4K-IIIβ in Rosetta 2(DE3) cells

Alongside processing of the His_{10}-tagged constructs, experiments with GST-tagged, Rosetta 2 (DE3)-expressed PI4K-IIIβ suggested a shorter path to securing sufficient yields of our target protein. The Rosetta 2(DE3) strain is a BL21 derivative that contains a chloramphenicol-selectable plasmid encoding tRNAs for 7 codons rarely used in *E. coli* (AGA, AGG, AUA, CUA, GGA, CCC, and CGG). Providing the host with this additional support lessens the effect of the codon usage bias (Plotkin & Kudla, 2011) and has been shown to enhance the production of eukaryotic proteins in bacteria, particularly for helping with folding and stability of recombinant proteins during translation (Structural Genomics Consortium et al., 2008). To predict whether expressing in Rosetta 2(DE3) cells might be beneficial, we analyzed the coding sequence of PI4K-IIIβ's on the freely available Sequence Manipulation Suite http://www.ualberta.ca/~stothard/javascrip (Stothard, 2000). This algorithm inspects a given coding sequence and returns the number and frequency of each codon type based on the genetic code of an organism of choice. The obtained report (**Figure 16 in Appendix**) suggested that, for expression in bacteria, the rare tRNAs supplied in Rosetta 2(DE3) cells might be the most impactful for codons like CCC (Pro), CGG and AGG (Arg), each appearing 19, 14 and 8 times in PI4K-IIIβ's sequence.

As expected, expression of wild-type PI4K-IIIβ in Rosetta 2(DE3) cells was successful. The average yield of purified, native protein increased from 43.88 to 125.28 ± 41.97 μg of protein per gram of bacterial cell pellet, an approximate 2.5-fold increase when compared to results obtained in BL21 (DE3) cells (see beginning of **Section 4.1**), as seen in **Figure 19**.

4.1.4 Deleting disordered loops from PI4K-IIIβ sequence

Concomitantly to switching the expressing *E. coli* strain, it was also thought that creating mutants of our protein of interest where disordered loop regions were removed might also augment recombinant protein yields. Previous HDX-MS experiments indicated the existence of 3 unstructured regions in PI4K-IIIβ's sequence, namely 1-120, 408-510 and 785-801 (Burke et al., 2014). Many groups since have resorted to eliminating these regions when expressing PI4K-IIIβ to improve yields and protein stability, (Burke et al., 2014; Mejdrová et al., 2015; Rutaganira et al., 2016; Reuberson et al., 2018). Thus, we thought of creating two mutants of PI4K-IIIβ, each with a deleted disordered loop: mutant "L" with deletion of 408-507 (Δ408-507) and mutant "C" with deletion of 453-511 (Δ453-511). The rationale to selecting these specific regions, and not others was 3-fold:

1- Deletion of 785-801 rendered a previous construct inactive as this region falls within the catalytic domain of PI4K-IIIβ (Burke et al., 2014);
2- While the deleted segment in "L" (*i.e.* Δ408-507) closely agreed with one of the HDX-MS-suggested unstructured regions (*i.e.* 408-510), secondary structure prediction of PI4K-IIIβ by the widely used server Jpred4 ((Drozdetskiy et al., 2015), data not shown) suggested that there might be some defined secondary structure between residues 408-453; considering that PI4K-IIIβ constructs with removed disordered loops (other than 785-801) were 60% (Klima et al., 2016) and 70% (Fowler et al., 2016) as active as the full-length protein, we thought of a more conservative approach (hence "C") where a shorter unstructured region, 453-511, was deleted;

3- The N-terminal region of Pik1 is essential for Frq1 binding (Strahl et al., 2007). To ensure that the recognition site for Frq1 in PI4K-IIIβ was intact, the 1-120 segment was preserved in our constructs.

Creation of both "C" and "L" mutants following the QuikChange protocol (Agilent Technologies) was successful and verified at the DNA (**Figure 17**) and protein (**Figure 18**) levels. Restriction enzyme digests by KpnI and SapI were set up with the plasmids of both "C" (expected fragments 3142 bp, 2137 bp, 1104 bp, 861 bp) and "L" mutants (expected fragments 3155 bp, 2137 bp, 1104 bp, 725 bp). A second reaction was also set up with the "C"-containing plasmid, which was cleaved by HpaI and KpnI. The expected fragments were 3,097 bp and 4147 bp. Those fragments can be seen in lanes 4, 6 and 3 below (**Figure 17**).

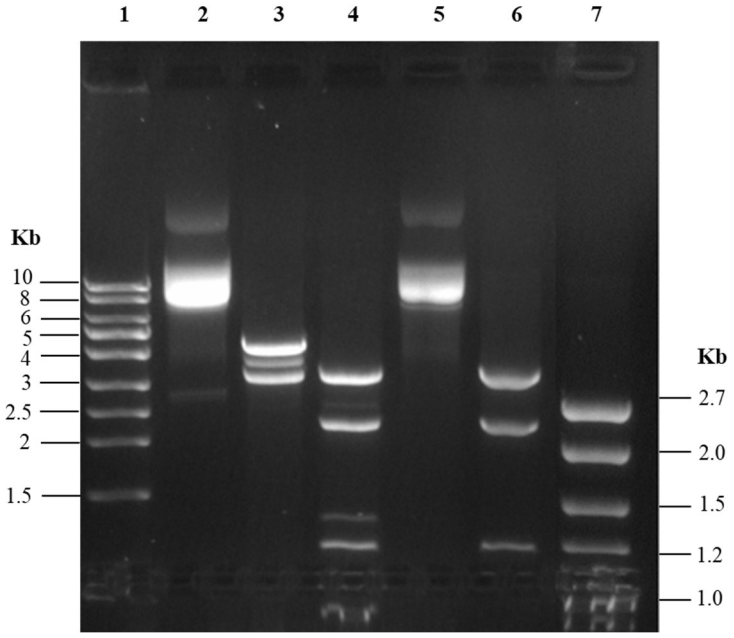

Figure 17: Restriction enzyme digestion of "C" and "L" plasmid DNA. "C" plasmid DNA was subject to Hpa + KpnI digestion (lane 3) and SapI + KpnI digestion (lane 4). The expected bands are 3097 bp and 4147 bp (lane 3) and 3142 bp, 2137 bp, 1104 bp, 861 bp (lane 4). "L" plasmid DNA was subject to SapI + KpnI digestion (lane 6). The expected bands include 3155 bp, 2137 bp, 1104 bp, and 725 bp (not visible). The undigested "C" and "L" plasmid DNAs were also loaded (lanes 2 and 5, respectively). DNA ladders were loaded on lanes 1 (Norgen's High Ranger) and 7 (Norgen's Clone Sizer), respectively.

Once expressed in Rosetta 2(DE3) cells and purified, analysis of SDS-PAGE gels confirmed the existence of protein constructs with MW lower than that for native, wt PI4K-IIIβ (89.8 kDa). Prominent bands for the "C" and "L" constructs could be seen around 83.2 kDa and 78.7 kDa respectively (**Figure 18**). By visual estimation of the SDS-PAGE gel, both constructs were ~70% pure. The gain in yield expected by the decrease in MW (Structural Genomics Consortium et al., 2008) was only seen with the "L" construct (**Figure 19**), which was the highest yielding construct obtained throughout this project.

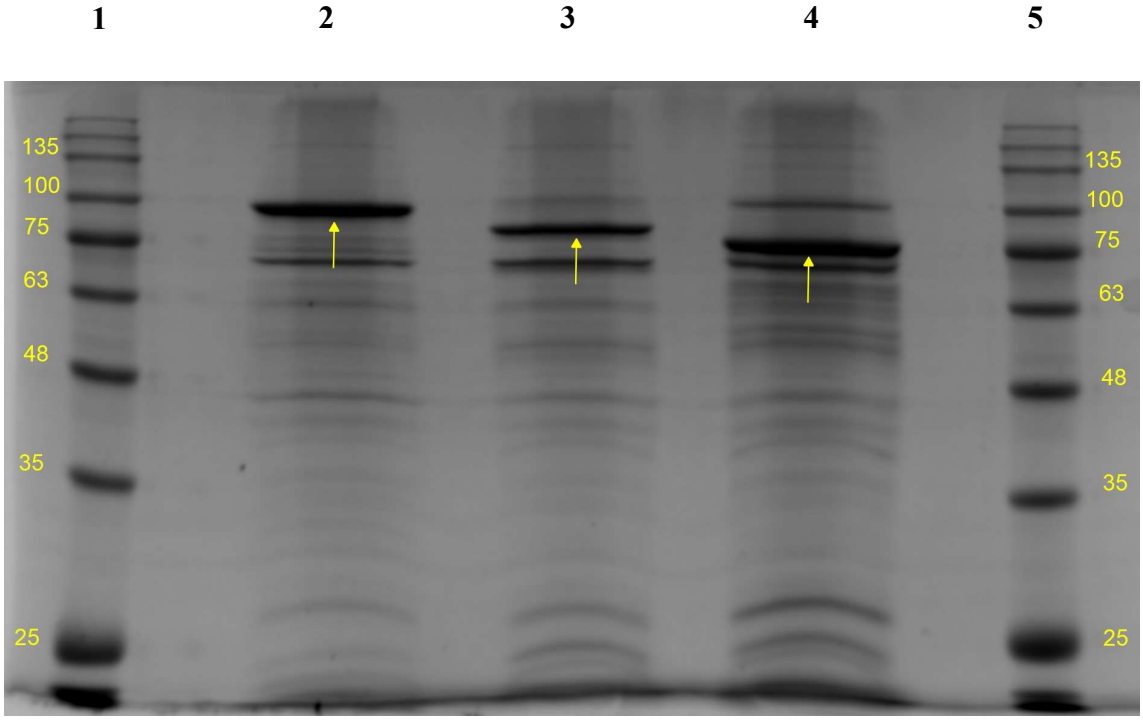

Figure 18: SDS-PAGE analysis of native wt PI4K-IIIβ alongside "C" (Δ453-511) and "L" constructs (Δ408-507). Expression was carried in Rosetta 2(DE3) cells as GST-tagged fusion proteins, and purification was achieved via glutathione affinity chromatography. Native PI4K-IIIβ fractions were eluted following cleavage of the GST affinity tag by HRV 3C protease. Prominent bands of expected MW are seen for all constructs and are indicated by yellow arrows: wt (lane 2, ~ 89.8 kDa), "C" (lane 3, ~ 83.2 kDa), "L" (lane 4, ~ 78.7 kDa). Lanes 1 and 5 contain protein ladders for MW determination of samples.

In general, expression of GST-PI4K-IIIβ was significantly improved in Rosetta 2(DE3) cells (**Figure 19**). Based on four independent expression and purification trials, 42.9 μg of purified PI4K-IIIβ was recovered per gram of bacterial cell pellet, versus 125.3 μg protein / g cell pellet obtained with Rosetta 2(DE3) cells (3 trials), overall representing almost 3-fold enhancement. Thus, Rosetta 2(DE3) was the selected *E. coli* strain to proceed with for the remainder of the project. Continuing to use the GST fusion system was overall beneficial due to the enhanced selectivity as well as the solubility-promoting feature of this affinity tag compared to polyhistidine tagged constructs, agreeing to previously reported trends (Structural Genomics Consortium et al., 2008). Furthermore, wild-type PI4K-IIIβ was chosen as the construct to continue further based on its superior performance on lipid kinase assays (discussed in **Section 4.3.5**). Additionally, the deletion mutants "C" and "L" did not appear to offer advantages in terms of recovered protein based on one expression and purification trial (data not shown).

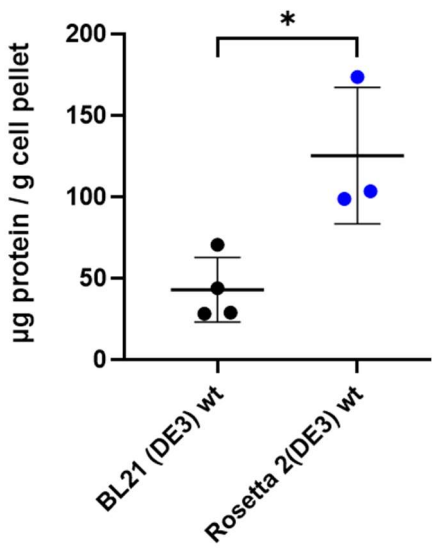

Figure 19: Yield comparison of purified native PI4K-IIIβ constructs expressed in BL21 (DE3) and Rosetta 2(DE3) *E. coli* cells. GST-tagged PI4K-IIIβ expressed in two different cell lines of *E. coli*, BL21 (DE3) and Rosetta 2(DE3) was purified by glutathione affinity chromatography. The native protein was obtained following HRV 3C proteolysis of the affinity tag, and protein concentration was determined by the Bradford Assay. The yield of purified, native, wild-type ("wt") PI4K-IIIβ was almost 3-fold higher when expressed in Rosetta 2(DE3) cells ($N = 3$, blue circles) than if expressed in BL21 (DE3) ($N = 4$, black circles). Error bars represent standard deviation.

4.2 Removal of contaminant HSPs from target proteins

The expression of recombinant proteins in bacteria is extensively employed as it is generally high yielding, faster and less expensive than eukaryotic expression hosts, particularly insect cells. Despite their robustness, bacteria cells do not possess the cellular machinery to perform post-translation modifications often needed in eukaryotic proteins. Additionally, producing large recombinant proteins (*i.e.*, > 60 kDa) that remain soluble is remarkably challenging in *E. coli* than when expressing smaller constructs (Structural Genomics Consortium et al., 2008). Another notorious difficulty when purifying recombinant proteins is contamination by host molecular chaperones, which are helper proteins that normally bind with high affinity to specific polypeptide sequences on a nascent protein thereby supporting its proper folding. Such

interaction may persist even beyond a complete protein purification workflow, thus potentially making the purified target protein impure, heterogeneously folded, or immunogenic. Furthermore, Hsp70 chaperones have ATPase activity (Morales et al., 2019), which is particularly problematic for assays that are sensitive to variations in the concentration of this nucleotide, such as the one employed herein (principles of the Bellbrook Labs Transcreener® ADP^2 FI Assay are detailed in **Section 1.4**). Hence, removing these contaminants from the proteins used in this study was essential to enable monitoring of true lipid kinase activity.

There are many published strategies for removal of chaperones from recombinant proteins. Those methods include washing the resin-bound target protein with: 1) denatured proteins from *E. coli* lysate + MgATP (Rial & Ceccarelli, 2002); 2) sub-denaturing concentrations of urea (Belval et al., 2015); and 3) a "cleanser protein" containing free functional binding sites for DnaK, *E. coli*'s homologue of Hsp70 (Morales et al., 2019). Moreover, some freely-available algorithms predict the binding propensity of DnaK to specific polypeptide sequences (Rudiger, 1997; Van Durme et al., 2009), which offers valuable *a priori* insight on whether or not this HSP might be a concern when expressing heterologous proteins in bacteria. Altogether, the plethora of methods developed to remove contaminant molecular chaperones reflect their prevalence when producing recombinant proteins in *E. coli*.

4.2.1 Removal of contaminant HSPs from PI4K-IIIβ and the problem of non-productive ATP hydrolysis

Early activity assays in the present investigation indicated high levels of non-productive ATPase hydrolysis, *i.e.*, when ATP is hydrolysed by the enzyme in the absence of a native acceptor substrate. In this study, this is assessed by the no-lipid control (NL), which contains the lipid kinase and ATP without lipid substrate. Since those early assays employed in-house

produced, bacteria expressed PI4K-IIIβ, futile ATP hydrolysis could be caused by 2 factors: 1) contaminating protein chaperones or other ATP-consuming proteins from the host expressing bacteria (described above), and/or 2) the inherent ATPase activity of PI-kinases (discussed further in **section 4.3.1**).

To remove unwanted, co-purifying chaperones from PI4K-IIIβ, we employed the approach described in (Rial & Ceccarelli, 2002). Briefly, the fusion protein bound to the glutathione-agarose resin was incubated at 37 ºC for 10 minutes with a diluted bacterial cell lysate, which also contained Mg^{2+} and ATP (the detailed procedure is found in **Sections 3.3.1** and **3.3.2**). SDS-PAGE analysis (**Figure 20A**) of native PI4K-IIIβ (yellow arrows) purified without the HSP Removal Wash (lane 2) and with the HSP Removal Wash (lane 3) confirms the disappearance of a prominent band at ~ 70 kDa (green arrow). This band, which corresponds to the MW of DnaK (*E.* coli's HSP70 homologue), is seen in a sample of the HSP Removal Wash eluate (lane 4, green arrow) suggesting that the wash successfully captured the majority of the contaminating chaperone. In fact, the HSP Removal Wash alone reduced the undesired background ATPase from 65% of the "true" lipid kinase signal (*i.e.*, the fluorescence produced by PI4K-IIIβ in the presence of PI) to below 30% of the same, representing a > 2-fold decrease (**Figure 20B**).

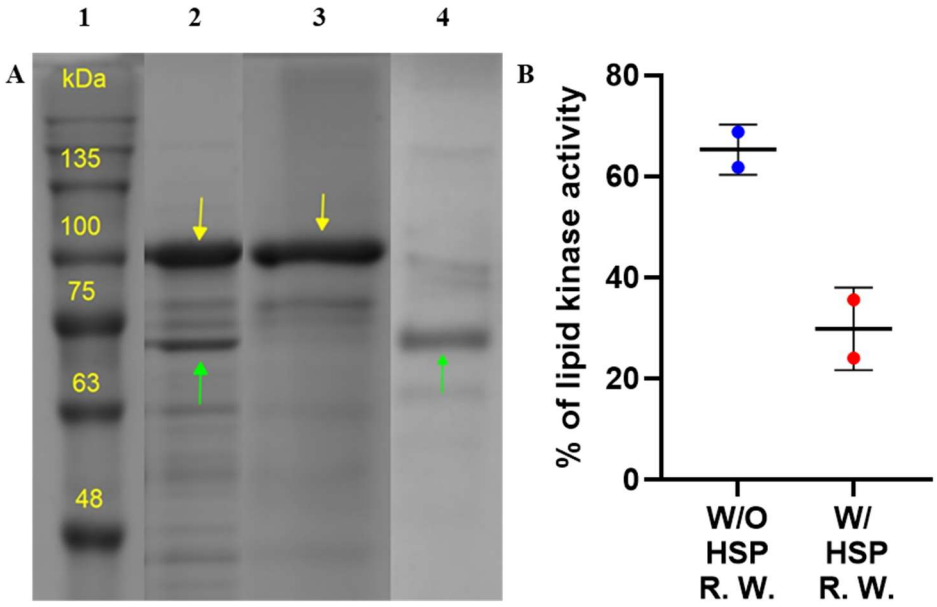

Figure 20: Effect of HSP Removal Wash in the purified recombinant PI4K-IIIβ. 20A: SDS-PAGE analysis of native PI4K-IIIβ (yellow arrows) produced in *E. coli* not including the HSP Removal Wash in the purification scheme (lane 2) shows a prominent band just below 75 kDa (green arrow). This band is assumed to be a contaminating HSP70 by MW comparison, which is visible as the major protein in the HSP Removal Wash eluate (lane 4, green arrow), but not seen in a fraction of native PI4K-IIIβ whose purification included the HSP Removal Wash (lane 3). Lane 1 contains a protein ladder. **20B:** PI4K-IIIβ purified with the HSP Removal Wash ("W/ HSP R. W.", red circles) displayed ~2-fold less non-productive ATP hydrolysis than PI4K-IIIβ purified without this step ("W/O HSP R. W.", blue circles). This was measured by an activity assay control whereby the lipid kinase was exposed to ATP and compared to the fluorescence counts generated by the same kinase when in presence of PI + ATP. $N = 2$.

4.2.2 Removal of contaminant HSPs from PITPα and PITPβ

Human PITPα and PITPβ were produced in bacterial cells, and could also contain ATP-consuming HSPs which co-purify with the target proteins. As such, it was necessary to test whether the PITPs alone might contribute to signal development in the activity assay before introducing them into assays with PI4K-IIIβ. Early assays with PITPα and PITPβ controls (*i.e.*, each PITP with lipid substrate and ATP, but without lipid kinase) revealed that PITPβ alone generated a fluorescence signal greater than that for the standard PI4K-IIIβ reaction. On the other hand, the PITPα control only displayed a negligible signal (**Figure 21B**, black bars). Since

neither PITPα nor PITPβ possess ATP-binding domains (Tilley et al., 2004; Vordtriede et al., 2005), we suspected that the observed background ATPase activity could only be generated by contaminating HSPs.

Considering the above, a second purification of both PITPα and PITPβ was pursued, and this time included the HSP Removal Wash as described previously (**Sections 3.3.1 and 3.3.2**). As seen in **Figure 21**, the prominent band at ~ 70 kDa detected in the HSP Removal Wash eluate (lanes 2 and 4, green arrows) is not as evident in the purified PITP fractions (lane 3 for PITPα, lane 5 for PITPβ), suggesting a substantial removal of the contaminating chaperone. Alone, this wash dramatically reduced the background ATPase activity generated by HSP contaminated PITPβ in the activity assay (**Figure 21B**), thus confirming our early predictions. Specifically, the contribution of PITPβ to the fluorescence signal in the activity assay decreased by 14-fold (from 229% to 15% of the lipid kinase signal produced by PI4K-IIIβ), while for PITPα the wash did not appear to offer a significant advantage (from 19.8% to 10.5% of the same parameter). Overall, this approach ensured that both human PITPs could be safely introduced in the activity assay with PI4K-IIIβ so that any eventual increase in fluorescence signal would be due to a true enhancement in the activity of the lipid kinase elicited by the PITPs rather than by ATP-depleting contaminants.

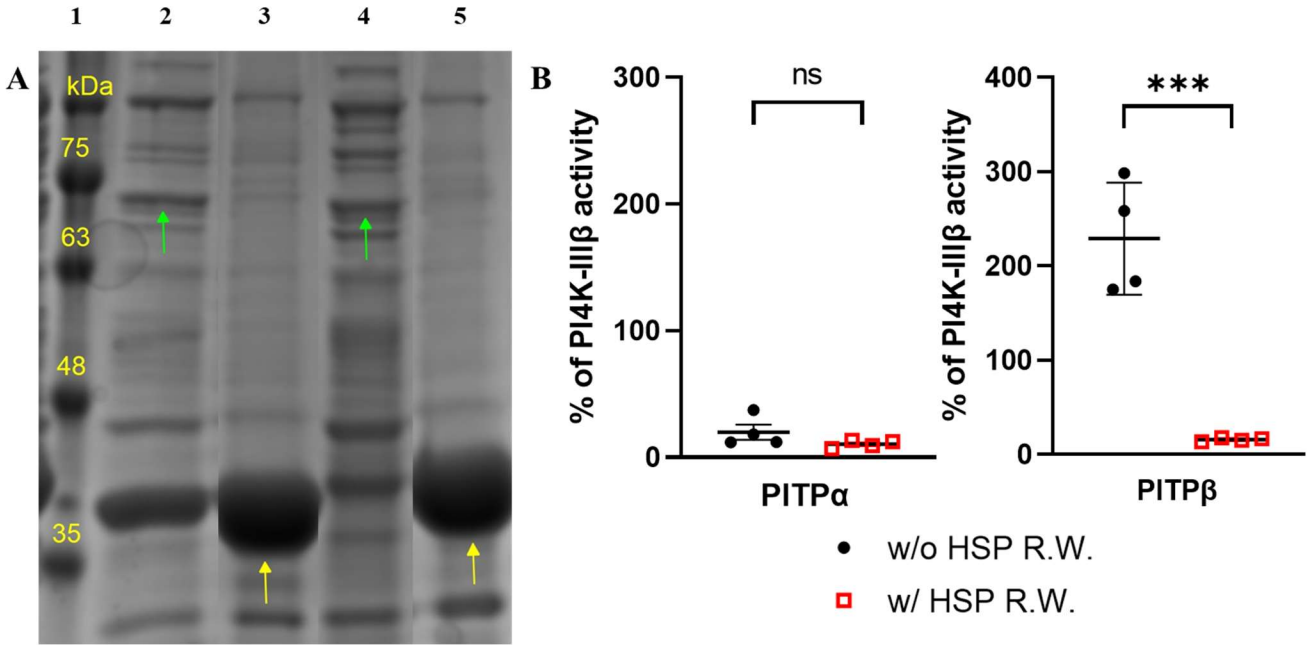

Figure 21: The effect of the HSP Removal Wash in the purified PITPα and PITPβ. 21A: A prominent band is seen at approximately 70 kDa in the HSP Removal Wash eluate (green arrows) for both PITPα (lane 2) and PITPβ (lane 4). A band at the matching MW is almost invisible in the elution fractions of purified PITPα (lane 3) and PITPβ (lane 5), suggesting successful elimination of the chaperone. Yellow arrows indicate the PITPs' bands. Lane 1 contains a protein MW ladder. **21B**: PITPβ purified with the HSP Removal Wash (red squares) displayed a drastic reduction in the background ATPase signal produced by contaminating HSPs when compared to PITPβ purified without the HSP Removal Wash (black circles). The same wash did not produce as pronounced a differenced when PITPα was considered. This was assessed by activity assay controls in four technical replicates ($n = 4$) whereby PITPs were exposed to PI-containing vesicles + ATP and compared to the fluorescence counts generated by PI4K-IIIβ when in the presence of PI-containing vesicles + ATP. Error bars = SD.

Considering that these PITPs are 77% identical at the sequence level and share 94% sequence similarity (Baptist et al., 2016), it was surprising to note the initial difference in the degree of HSP contamination between PITPα and PITPβ (**Figure 21B**, black bars). To investigate that, we analyzed their amino acid sequences in the DnaK-peptide binding prediction algorithm (Van Durme et al., 2009), which revealed that the propensity for DnaK to bind PITPβ was slightly higher than that for PITPα (**Figure 22**). Therefore, the disparities in the amount of co-purifying HSP would likely be caused by the minimal differences between the amino acid

sequences of PITPα and PITPβ. Perhaps the 53% greater yield of expressed PITPβ (1.59 mg purified PITPβ / g cell pellet) in comparison to the α isoform (1.04 mg purified PITPα / g cell pellet) could also contribute to the higher degrees of chaperone involvement during protein expression and thus contamination of the purified protein, as initial expression of DnaK has been shown to rely on translation rates of heterologous proteins in *E. coli* (Christensen et al., 2022).

Figure 22 below represents a summary of the reports produced by the algorithm that predicts DnaK binding to peptides (Van Durme et al., 2009), and includes all proteins analyzed by this method during our study. The full reports can be found in the Appendix. The relevance of BSA, lysozyme, carbonic anhydrase, RNAse, Sec14p, and PI4K-IIIβ analyses will be discussed in **section 4.2.3**.

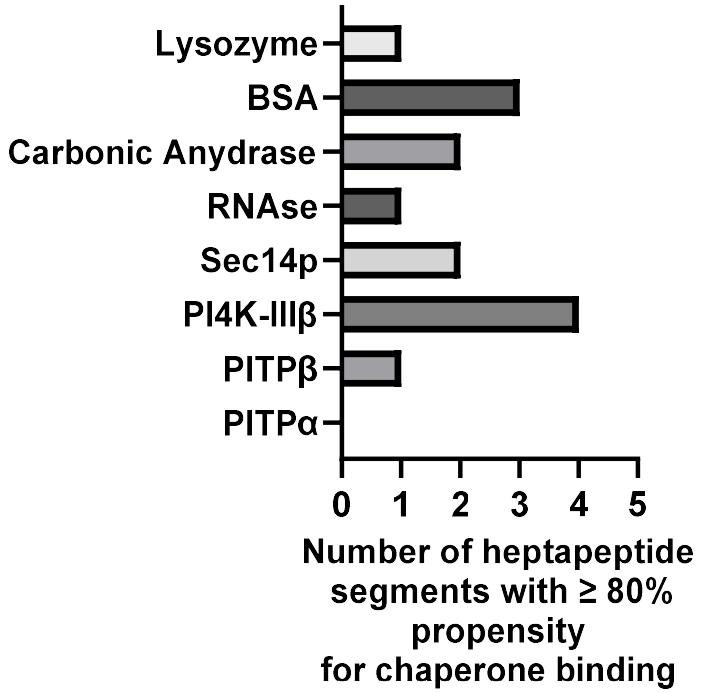

Figure 22: Propensity of DnaK binding for different proteins. The amino acid sequences of various proteins were analyzed by the DnaK-peptide binding prediction algorithm (Van Durme et al., 2009). Reports for each protein were summarized as a graph for easy comparison. The graph displays the number of heptapeptide segments contained in each protein sequence that have ≥ 80% propensity to bind DnaK, as calculated by the prediction algorithm.

4.2.3 Removal of contaminant HSPs from Sec14p and Frq1

With the experience gained in purifying PI4K-IIIβ and the human PITPs, the HSP Removal Wash was included in the purification scheme of Sec14p already in the first trial (**Figure 23A**, lane 2). Unexpectedly, the Sec14p control in the activity assay (*i.e.*, Sec14p + PI-containing vesicles + ATP) revealed that the traditional HSP Removal Wash did not eliminate the ATPase activity generated by contaminating bacterial chaperones (**Figure 23B**, black bar). Like human PITPs, Sec14p does not possess an ATPase binding domain (Sha et al., 1998), strongly suggesting that the unwanted ATP hydrolysis observed in the activity assay was caused by persistent bacterial HSPs or other ATPases that co-purified with Sec14p.

Analysis of the amino acid sequence of Sec14p by the DnaK-peptide binding prediction algorithm (Van Durme et al., 2009) indicated a greater propensity of said HSP to bind the yeast PITP than the human PITPβ (**Figure 22**). Inspired by the work of (Morales et al., 2019)), whereby a "cleanser" protein was designed to strongly attract DnaK during the purification of recombinant proteins expressed in bacteria, we thought of modifying the HSP Removal Wash by adding proteins for which DnaK might have a high propensity of binding, thus outcompeting its interaction with Sec14p. To make this a quick and inexpensive approach, we analyzed the amino acid sequences of non-ATP consuming proteins easily available in our lab (BSA, lysozyme, carbonic anhydrase and RNAse) in the DnaK-peptide binding prediction algorithm (Van Durme et al., 2009). PI4K-IIIβ was also examined and used as a positive control, since our experience had shown that appreciable amounts of DnaK co-purified with the lipid kinase (**section 4.2.1**). The reports (available in the Appendix and summarized in **Figure 22**) indicated that, among the sequences analyzed, BSA and carbonic anhydrase were the proteins for which DnaK might have a greater likelihood of binding to. Thus, BSA and carbonic anhydrase were added to the HSP

Removal Wash so that the final protein concentration in the new "Fortified HSP Removal Wash" remained ~ 0.1 mg/mL.

A new purification of Sec14p was attempted, including the incubation with the Fortified HSP Removal Wash (**Figure 23A**, lane 4). Notwithstanding the 150% decrease in chaperone contamination in the recovered Sec14p, the activity assay indicated that appreciable amounts of ATP hydrolysis were still generated by contaminants in the Sec14p control (**Figure 23B**, blue circles). To overcome that, we further purified Sec14p by size-exclusion chromatography using a resin at hand, Sephadex® G-100 (**Figure 23A**, lanes 6-9). This extra step was fruitful in lowering the fluorescence signal generated by the Sec14p control to baseline levels (**Figure 23B**, purple circles), indicating an overall 6-fold reduction of ATP-consuming contaminants from Sec14p. Like the human PITPs, the yeast counterpart obtained in this study was made sufficiently pure and concentrated for incorporation in the activity assay with PI4K-IIIβ.

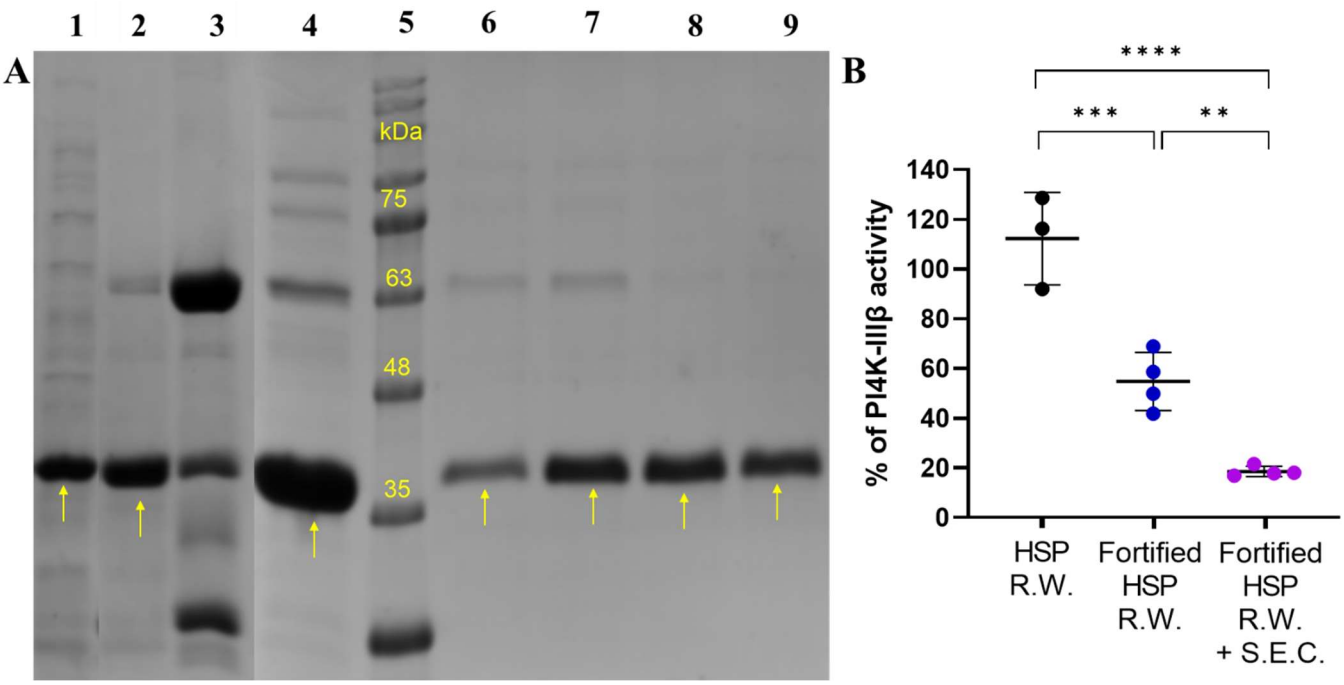

Figure 23: Strategies to eliminate contaminating chaperones from Sec14p. 23A: SDS-PAGE analysis shows a visual cleaning of Sec14p (yellow arrows) elution fractions purified by affinity chromatography by the addition of the HSP Removal Wash (lane 1 – without the HSP Removal Wash, purified by Alex Bernekier, Brock University; lane 2 – with the HSP Removal Wash). Sec14p purified with the Fortified HSP Removal Wash still exhibited some contaminants (lane 4), the most prominent at ~ 63 kDa. Comparison with a sample of glutathione elution buffer eluate (lane 3) suggests that this band is likely lingering GST-tagged Sec14p. The Sec14p elution fraction represented in lane 4 was further purified by size-exclusion chromatography (lanes 6-9), which yielded virtually pure Sec14p, specially at later elution fractions (lanes 8-9). Lane 5 – protein MW ladder **23B**: Sec14p that underwent incubation with the Fortified HSP Removal Wash ("Fortified HSP R. W.", blue circles, $n = 4$) displayed a 2.6-fold reduction in ATPase activity caused by contaminating chaperones when compared to Sec14p that had been incubated with normal HSP Removal Wash ("HSP R. W.", black circles, $n = 3$). Polishing by size-exclusion chromatography (S.E.C.) further diminished the degree of HSP contamination in Sec14p as assessed by the Sec14p control in comparison to the signal generated by PI4K-IIIβ in the activity assay under the same conditions ("Fortified HSP R. W. + S.E.C", purple circle, $n = 4$). Error bars = SD.

As for yeast Frequenin (Frq1), purification was carried out by Dr. Candace Panagabko (Brock University) based on glutathione-agarose affinity chromatography. It also included incubation with the traditional HSP Removal Wash, which was sufficient to ensure that Frq1 was free from ATP consuming contaminants. This was assessed by the Frq1 control in the activity assay, following the same approaches employed for the human PITPs and Sec14p.

4.3 Lipid kinase assays

After securing satisfactory amounts of all proteins to be examined in the PI4K activity assays and ensuring that all proteins were as free of contaminants as we could achieve, efforts were directed to monitoring lipid kinase activity *in vitro* elaborating on previous members of the Atkinson group's foundational work (Meehan, 2019). Our goal was to obtain a reliable assay whereby the activity of PI4K-IIIβ could be tested, alone or with protein partners, to gain insight into the lipid kinase proposed regulation by PITPs (Ile et al., 2006). For that, we needed to find the optimal ATP and Antibody-conjugated IRDye® QC-1 concentrations to be used in the assay, obtain a reliable standard curve and FI window, refine the protocol, and show a PI4K-IIIβ dose-dependent response. Next, we introduced active protein partners in the activity assay to investigate any possible effect on lipid kinase activity, while also testing different lipid substrates. Finally, we contrasted the behaviour of PI4K-IIIβ with that of PIK3C3 in the assay, as PIK3C3's activity has been shown to be affected by PITPs (Panaretou et al., 1997).

4.3.1 ATP titration

Several kinases display non-productive ATP hydrolysis, which has been extensively documented (Chen et al., 2000; Jencks, 2006; Wang et al., 2022; Ward & O'Brian, 1992), including for PI-kinases (Klink et al., 2008). Futile ATP hydrolysis can occur when the nucleotide's γ-phosphoryl group is transferred onto water molecules that may occupy the enzyme's active site (Ward & O'Brian, 1992; Jencks, 2006). Rates of ATP hydrolysis in the absence of a "true" acceptor substrate are typically much smaller than when the native substrate is present, but this varies between kinases (Wang et al., 2022). In *in vitro* assays, a way to minimize the signal produced by futile ATP hydrolysis is using high ratios of acceptor substrate to the nucleotide (Chen et al., 2000). Hence, early steps in the assay development required an

ATP titration with fixed amounts of enzyme and PI-containing vesicles (**Figure 24**) for determination of the optimal nucleotide supply to minimize substrate-independent ATP hydrolysis.

The ATP titration employed 0.2 mg/mL PI:PS vesicles, 111 nM PI4K-IIIβ, concentrations of ATP ranging from 10 to 100 μM and amounts of ADP2 Antibody–IRDye® QC-1 calculated by **Equation 1** (**Section 3.8.1**). The choice of this range of ATP concentrations was guided by the following: 1) early work with PI4K-IIIβ reported that its K_M for ATP varies from 0.4 to 1 mM (Suer et al., 2001; X.-H. Zhao et al., 2000), suggesting that ATP concentrations within this range might allow us to follow sufficiently fast reaction rates; 2) nonetheless, the Transcreener® ADP^2 FI Assay was developed to reliably monitor enzymatic activity at low substrate conversion, *i.e.*, up to 10% (preferably ≤ 2.5%), and only accommodates total ATP concentrations between 0.1 and 100 μM (*Transcreener® ADP FI Assay Technical Manual*, 2023); 3) the apparent ATP K_M for PI4K-IIIβ determined by a similar assay is 90 μM (*ADP-Glo™ Lipid Kinase Systems - Technical Manual*, 2022), thus suggesting that testing [ATP] lower than 100 μM in our assay would be a reasonable choice.

The FI signal window between lipid containing and the no-lipid (NL) control assays was widest at the lowest tested ATP concentration, 10 μM (**Figure 24F**). This trend follows those seen in previous works (Chen et al., 2000; Klink et al., 2008), whereby higher cognate substrate-to-ATP ratios decreased the contribution of the inherent, futile ATP hydrolysis by kinases. Our results also agree with observations that the Transcreener® ADP^2 FI might not perform optimally at high ATP concentrations as the ADP antibody displays a significant affinity for ATP (Hong et al., 2009; H. Li et al., 2009). Based on these results, 10 μM ATP was chosen as

the concentration used in activity assays henceforth for allowing the most reliable monitoring of true lipid kinase activity.

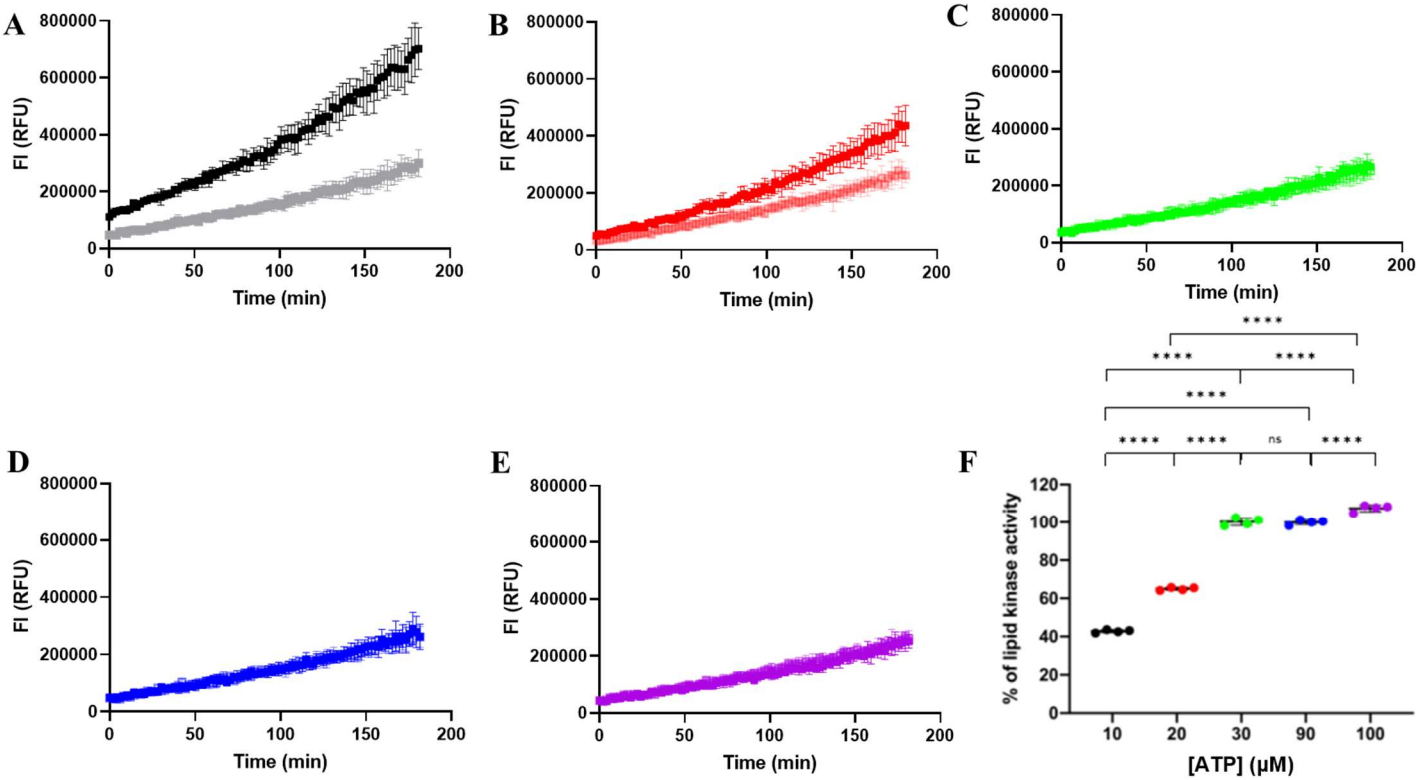

Figure 24: ATP Titration. At [ATP] ranging from 10 to 100 μM, the activity of 111 nM of PI4K-IIIβ was assayed in the presence of 0.2 mg/mL PI:PS SUVs and contrasted with signal produced by the NL control. The biggest signal difference between lipid containing (solid coloured square) and the NL control (faded coloured square) was seen in the assays with 10 μM ATP (**24A**, black curves). In comparison, assays with 20 μM ATP (**24B**, red curves) also displayed a difference, despite smaller. The signals produced by the lipid containing and NL control the presence of 30 (**24C**, green curves), 90 (**24D**, blue curves), and 100 μM ATP (**24E**, purple curves) overlap. **24F**: Summary of the ratio between the NL control and the lipid-containing assays with the titrated [ATP]. Circles represent technical replicates (n = 4) of the signal produced by the NL control at each time point normalized to the signal produced by PI4K-IIIβ in the presence of lipid substrate.

4.3.2 Optimizing the concentration of ADP[2] Antibody–IRDye® QC-1

It is suggested by the Transcreener® ADP FI Assay supplier that the amount of ADP[2] Antibody–IRDye® QC-1 for a given [ATP] calculated from **Equation 1** (**Section 3.8.1**) should

produce satisfactory results in terms of sensitivity and signal robustness, but our initial assay attempts suggested otherwise. When this is the case, a titration of the antibody in the buffer system of choice (for this study, lipid substrate, 10 μM ATP, 1X assay buffer) is needed for best results. The assay manufacturer recommends using the EC_{20} concentration of ADP[2] Antibody–IRDye® QC-1 for "a good compromise between sensitivity and maximal assay window" (*Transcreener® ADP FI Assay Technical Manual*, 2023). EC_{20} can be calculated from **Equation 2** below.

From **Equation 1** (**Section 3.8.1**), 5 μg/mL should be the final ADP[2] Antibody–IRDye® QC-1 concentration in assays with 10 μM ATP. Therefore, 5 μg/mL was selected as the approximate midpoint of antibody concentrations to be titrated, also considering that a series of 2-fold dilutions should be performed for this experiment according to the manufacturer protocol (*Transcreener® ADP FI Assay Technical Manual*, 2023). Following this rationale, ADP[2] Antibody–IRDye® QC-1 concentrations raging from 0.195 to 100 μg/mL were titrated for 10 μM ATP. The fluorescence signal produced was plotted against the log ([ADP[2] Antibody–IRDye® QC-1]) and fitted to an asymmetrical (5 parameter) dose-response curve using GraphPad Prism's model:

$$\text{Log}\,(X_b) = \text{Log}\,(EC_{50}) + \left[\left(\frac{1}{Hill\ Slope}\right) * \text{Log}\,\left(\left(2^{\frac{1}{S}}\right) - 1\right)\right] \qquad \textbf{Equation 2}$$

where X_b is the concentration of agonist that produces a response different than half-maximal effects (EC_{50}), and S is the unitless parameter that quantifies curve symmetry. The curve generated is seen in **Figure 25**:

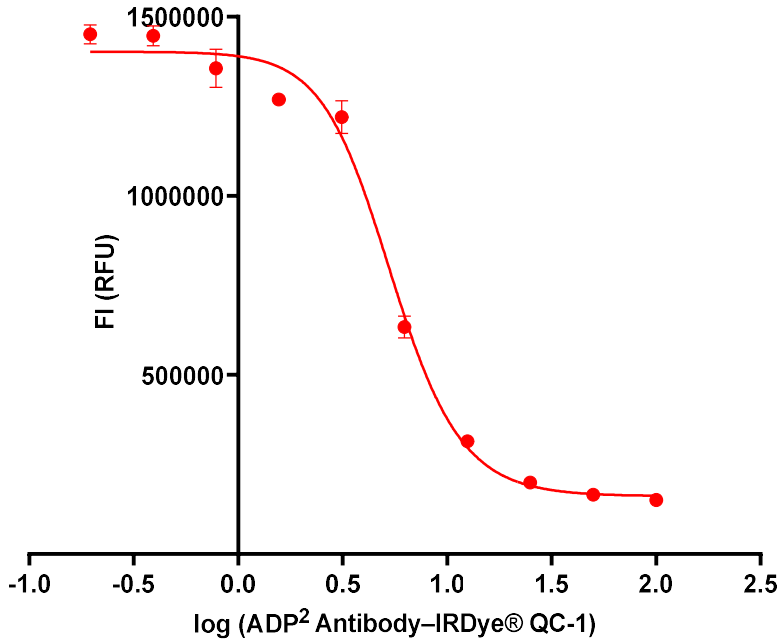

Figure 25: Titration of Antibody-conjugated IRDye® QC-1 for 10 µM ATP. Concentration of ADP^2 Antibody–IRDye® QC-1 ranging from 100 to 0.195 µg/mL were titrated in 1X Assay Buffer also containing 10 µM ATP and 0.2 mg/mL PI:PS SUVs. The curve obtained was fitted to an asymmetrical (5 parameter) dose-response curve employing the GraphPad Prism software. Parameters like Hill Slope and EC_{50}, derived from this curve, were used to calculate EC_{20}, thus used as the optimal antibody concentration for the present study's buffer system. Error bars = SD based on 4 technical repeats.

The Hill Slope and EC_{50} calculated from this curve (*i.e.*, -2.762 and 5.380, respectively) were plugged into **Equation 2** to obtain EC_{20}:

$$EC_{20} = 0.25^{\left(\frac{1}{Hill\ Slope}\right)} * EC_{50}$$

$$EC_{20} = 8.88\ \mu g/mL$$

The EC_{20} concentration of ADP^2 Antibody–IRDye® QC-1 determined by the antibody titration for 10 µM ATP was 8.88 µg/mL, suggesting that our assay system required 77% more antibody than that calculated by **Equation 1**, *i.e.*, 5 µg/mL. Antibody optimization has been reported elsewhere when using the Transcreener® ADP technology for PI3-kinases (Klink et al., 2008). Hereafter, 8.88 µg/mL was selected as the ADP^2 Antibody–IRDye® QC-1 concentration

to be used in the assays, which improved the quality of crucial parameters like the ATP/ADP conversion standard curve and FI Assay Window (**Section 4.3.3**).

4.3.3 ATP/ADP conversion standard curve and FI window

The ATP/ADP conversion standard curve is needed for the quantification of product formed assuming a 1:1 (ADP) : (phosphorylated product) ratio. For the Transcreener® ADP^2 FI Assay, the standard curve is particularly necessary to ensure ≤ 10% substrate conversion for optimal assay responsiveness (*Transcreener® ADP FI Assay Technical Manual*, 2023). A standard curve of ATP + ADP mixtures mimicking ATP-to-ADP conversions of 0% to 60% was generated (the detailed protocol is available is **Section 3.8.3**). For instance, the [ATP] in the enzymatic reaction is 10 μM, meaning that at 10% conversion 1 μM ADP is produced. From the standard curve, two parameters were chosen to assess assay sensitivity: 1) the ratio between the FI signals generated at 60% ATP/ADP conversion and 4% ATP/ADP conversion ("60/4 ratio"); and 2) the spread between the FI signals at these points (*i.e.*, FI at 60% ATP/ADP conversion minus FI at 4% ATP/ADP conversion, "60-4 spread"). A small 60/4 ratio or 60-4 spread can be interpreted as insufficient amounts of antibody in the reaction mixture, leading to similar quenching rates of the ADP-fluorophore at low (4%) and high (60%) ADP conversion. On the other hand, an optimal supply of ADP^2 Antibody–IRDye® QC-1 provides adequate quenching rates of the ADP-fluorophore that are inversely proportional to ADP produced in the reaction, (a detailed explanation on the Transcreener® ADP FI Assay technology is available in S**ection 1.4**).

Initial attempts to generate an ATP/ADP standard curve employed the amount of ADP antibody calculated by **Equation 1**, 5 μg/mL. Considering that the results obtained were non-satisfactory, the concentration of ADP antibody was increased to 6 μg/mL as suggested by the

technical support staff of the Transcreener® ADP FI Assay supplier (M. Kumar, personal communication, December 14, 2021). Despite this modification, the obtained ATP/ADP standard curve repeatedly displayed a 60-4 spread of just above 200,000 RFU (**Figure 26B**), which is poor considering that the FI signal for 4% ATP conversion is typically around 1,000,000 RFU in the conditions employed. Following the ADP antibody titration (S**section 4.3.2**), the ATP/ADP standard curve produced with the optimal antibody concentration (8.88 μg/mL) was improved based on one trial with four technical repeats: the 60/4 ratio increased by ~ 23% and the 60-4 spread by 117% (**Figures 26A** and **26B**, squares and circles). Importantly, these measurements were performed in the presence of the same substrate, 0.2 mg/mL PI:PS SUVs. To assess if the ATP/ADP standard curve would be affected by a different lipid substrate, and to enable product quantification in activity assays employing LUVs, a new standard curve was run with 0.2 mg/mL (50:25:25) PI:PC:PS LUVs (200 nm) but maintaining the ATP and ADP antibody concentrations used previously. The almost identical 60/4 ratio and mildly reduced 60-spread (**Figures 26A** and **26B**, triangles and squares) suggest that the ATP/ADP standard curve is indifferent to SUVs and LUVs in the conditions tested.

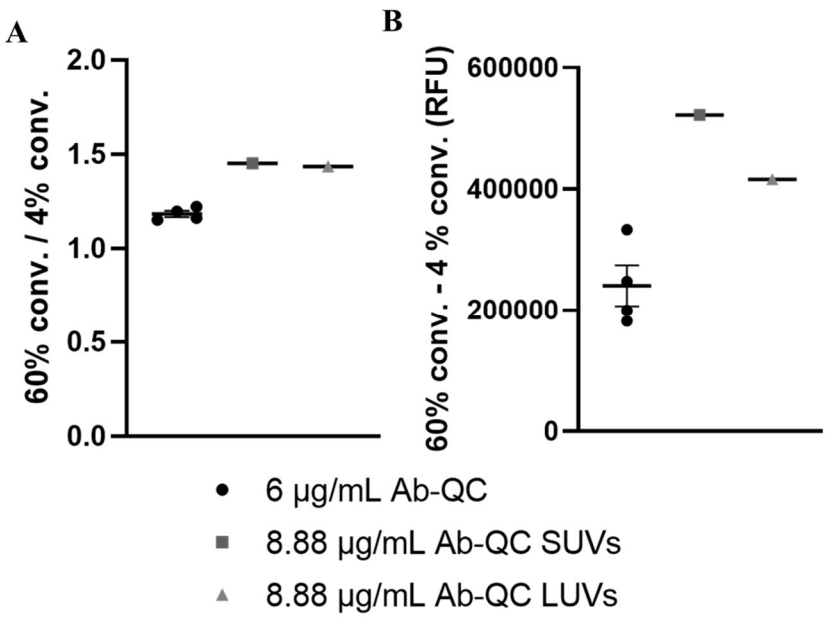

Figure 26: The effect of optimal ADP antibody concentration and liposome size in the ATP/ADP standard curve. ATP/ADP standard curves ranging from 0 to 60% ATP conversion (100% ATP conversion = 10 µM ADP) were run with 4 nM ADP-fluorophore and 0.2 mg/mL lipid substrate in 1X assay buffer. The empirically determined ADP antibody concentration, 8.88 µg/mL, led to an increased ratio between the FI signal at 60% and 4% ATP conversion, as well as an increase FI spread between these two points when compared to standard curves generated with 6 µg/mL ADP antibody (**26A** and **26B**, squares and circles). 200 nm LUVs did not seem to affect the 60/4 ratio and 60-4 spread observed with SUVs under the same conditions (**26A** and **26B**, triangles and squares). Ab-QC = ADP^2 Antibody–IRDye® QC-1. Error bar = SD based on 4 independent measurements, each run in quadruplicates. $N = 1$, $n = 4$ for standard curves run with 8.88 µg/mL ADP antibody.

Overall, the empirically determined ADP antibody concentration assured an assay with improved sensitivity-quantifying parameters, as shown in **Figure 26**. The ATP/ADP standard curves obtained are seen below:

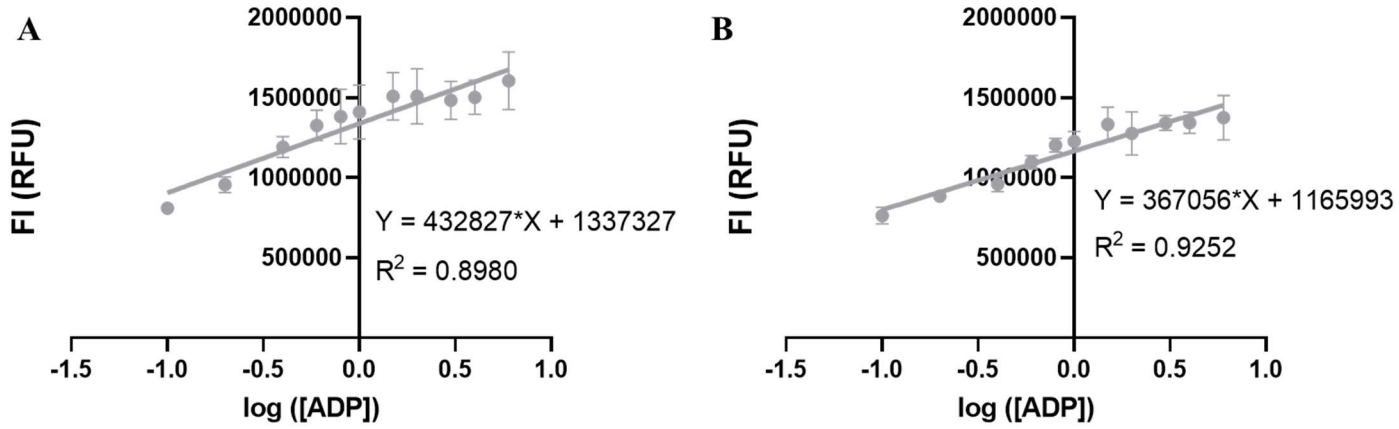

Figure 27: ATP/ADP standard curves with optimized conditions. 11 ATP + ADP mixtures were made to mimic ATP-to-ADP conversions ranging from 1 to 60% (100% ATP conversion = 10 µM ADP). In addition to the nucleotides, the mixtures contained 4 nM ADP-fluorophore, 8.88 µg/mL ADP antibody and lipid substrate (**27A:** 0.2 mg/mL PI:PS 50 nm SUVs, **27B:** 0.2 mg/mL (50:25:25) PI : PS : PC 200 nm LUVs) in 1X assay buffer. Error bars = SD based on four technical replicates.

Another important parameter for the Transcreener® ADP FI Assay is the maximum FI window, obtained by subtracting the lowest FI signal (ADP-fluorophore + ADP antibody) from the highest FI signal (ADP-fluorophore alone). Although absolute RFU readings are plate reader- and plate type-specific, a ratio between the highest and the lowest FI signals greater than 5.0 indicates that two key components of the assay, the ADP-fluorophore and the ADP antibody, are operating as expected in a given reaction buffer (*Transcreener® ADP FI Assay Technical Manual*, 2023). Overall, the optimal ADP antibody concentration appeared to improve the FI window (**Figure 28A**), increasing it by ~36% based on one trial with four technical repeats. The obtained window for a minimum FI mixture containing 8.88 µg/mL ADP antibody is seen in **Figure 28B**:

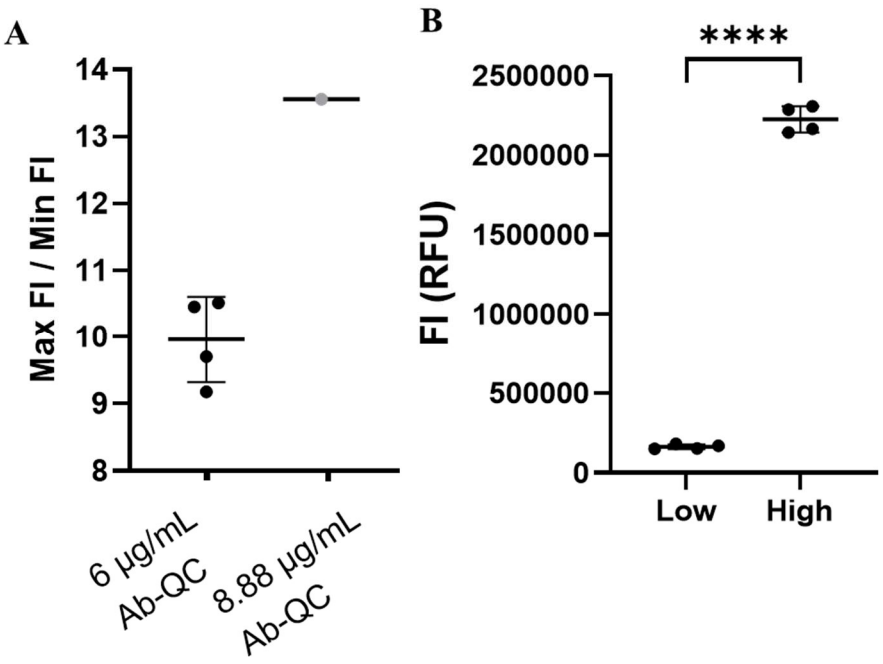

Figure 28: The effect of the optimized ADP[2] Antibody–IRDye® QC-1 in the FI assay window. 28A: Comparison between (max FI / min FI) ratios with 6 µg/mL ADP antibody ("Ab-QC", black circle, $N = 4$, $n = 4$) and the empirically derived ADP antibody concentration, 8.88 µg/mL (grey circle, $N = 1$, $n = 4$) in the FI assay window. A marked increase in the (max FI / min FI) ratio is observed with the higher ADP antibody concentration. **28B:** FI assay window readings ($N = 1$, $n = 4$) for the minimum FI reading (4 nM ADP-fluorophore + 8.88 µg/mL ADP antibody) and maximum FI reading (4 nM ADP-fluorophore), both in 1X assay buffer.

4.3.4 Optimizing the protocol

The protocol for the time-resolved version of the Transcreener® ADP FI Assay initially developed by previous members of the Atkinson group (Meehan, 2019) was the founding cornerstone that inspired the present study. To further improve its performance and to allow the eventual, previously untested addition of protein partners (*i.e.*, PITPs and Frq1), the assay protocol was optimized. Briefly, the seminal procedure included an assay mix whereby ADP[2] Antibody–IRDye® QC-1 and ADP Alexa Fluor® 594 Tracer were initially equilibrated in assay buffer, followed by the addition of ATP and acceptor substrate. Once the proper volume of assay mix was added to the plate wells, the reaction was initiated by the addition of the appropriate

amount of PI-kinase diluted in autoclaved mQ H_2O (**Figure 29**). Using the initial setup, introduction of PITPs would either take place in the assay mix or in the lipid kinase dilution. In the first scenario, PITPs would equilibrate with lipid vesicles before being exposed to the lipid kinase. This approach is theoretically sound if testing the proposed lipid presentation model by PITPs to lipid kinases, and has been employed previously (Hubner et al., 1998; Panaretou et al., 1997). However, this would also expose PITPs to ATP (also present in the original protocol's assay mix) prior to addition of lipid kinase, thereby allowing hydrolysis of this nucleotide by contaminating ATP-consuming bacterial chaperones inherently present in the LTPs fractions. Alternatively, PITPs could be introduced in the assay with the lipid kinase, which prevents the initial incubation with lipid vesicles mentioned above.

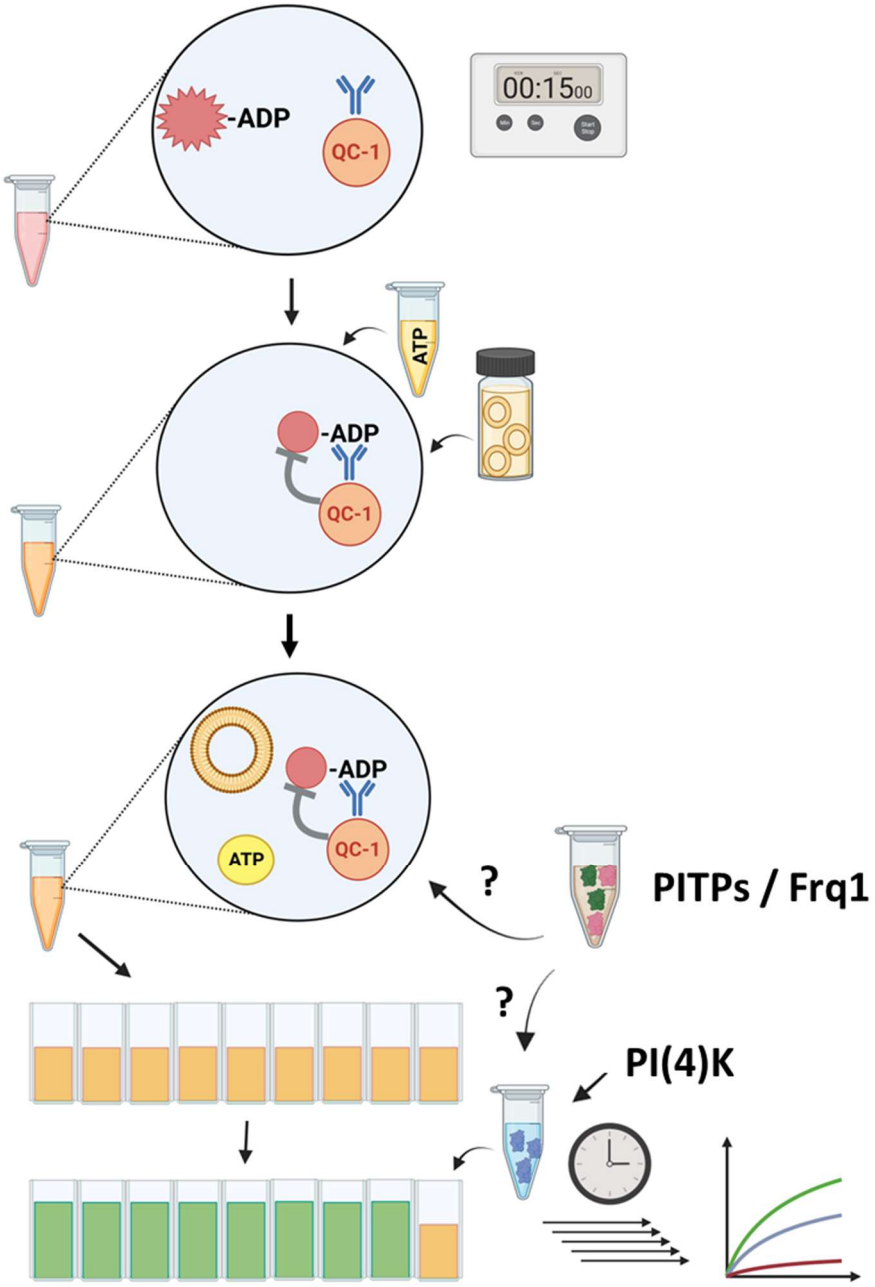

Figure 29: Initial protocol for the Transcreener® ADP^2 FI Assay in time-resolved mode. The protocol developed by a former member of the Atkinson group (Meehan, 2019) to run the Transcreener® ADP^2 FI Assay in time-resolved mode included initial incubation of ADP antibody and ADP-fluorophore in assay buffer. To the same tube, ATP and lipid vesicles were added. This mixture was pipetted into plate wells, and the reaction was started by addition of the lipid kinase (blue tube) to the wells. The plate was inserted into an appropriate plate reader and the FI signal was read over a given period at prescribed intervals, thus allowing the generation of enzyme progression curves. PITPs/Frq1 would either be added to the assay in the assay mix or with the lipid kinase. Created with BioRender.com.

In trying to address the aforementioned challenges, the protocol was modified to include three pre-mixes:

1) Assay Mix: contained lipid substrate, PI-kinases, and protein partners (when appropriate) in 0.8X assay buffer (prepared first);
2) Detection Mix: ADP^2 Antibody–IRDye® QC-1 and ADP Alexa Fluor® 594 Tracer in 0.2X assay buffer (prepared second, only added to the assay mix tube following antibody-tracer equilibration);
3) ATP (added last and directly to the well plate).

The optimized protocol (**Figure 30**) prevents the dilution of the enzyme and protein partners in non-buffered, low ionic strength systems (*i.e.*, water), thereby preserving protein native structure and function (Salis & Monduzzi, 2016). Additionally, switching to an ATP-initiated reaction (revised protocol) rather than an enzyme-initiated reaction (initial protocol) allows a pre-equilibration of PITPs with lipid substrate in the absence of ATP, thereby minimizing the non-productive ATPase activity by bacterial chaperones that co-purified with the recombinant expressed PITPs employed in this study (**Sections 4.2.2-3**). In fact, starting lipid or protein kinase reactions by the addition of ATP is commonly the method of choice (Flanagan & Thorner, 1992; H. Li et al., 2009; Panaretou et al., 1997; Schaaf et al., 2008). Furthermore, the new procedure also minimizes exposure of ADP^2 Antibody–IRDye® QC-1 to ATP, which is advantageous as this antibody also recognizes triphosphates (Hong et al., 2009; H. Li et al., 2009). Lastly, the assay volume was reduced from 50 to 20 μL to reduce reagent usage. For this, 384-well plates replaced the previously used 96-well plates.

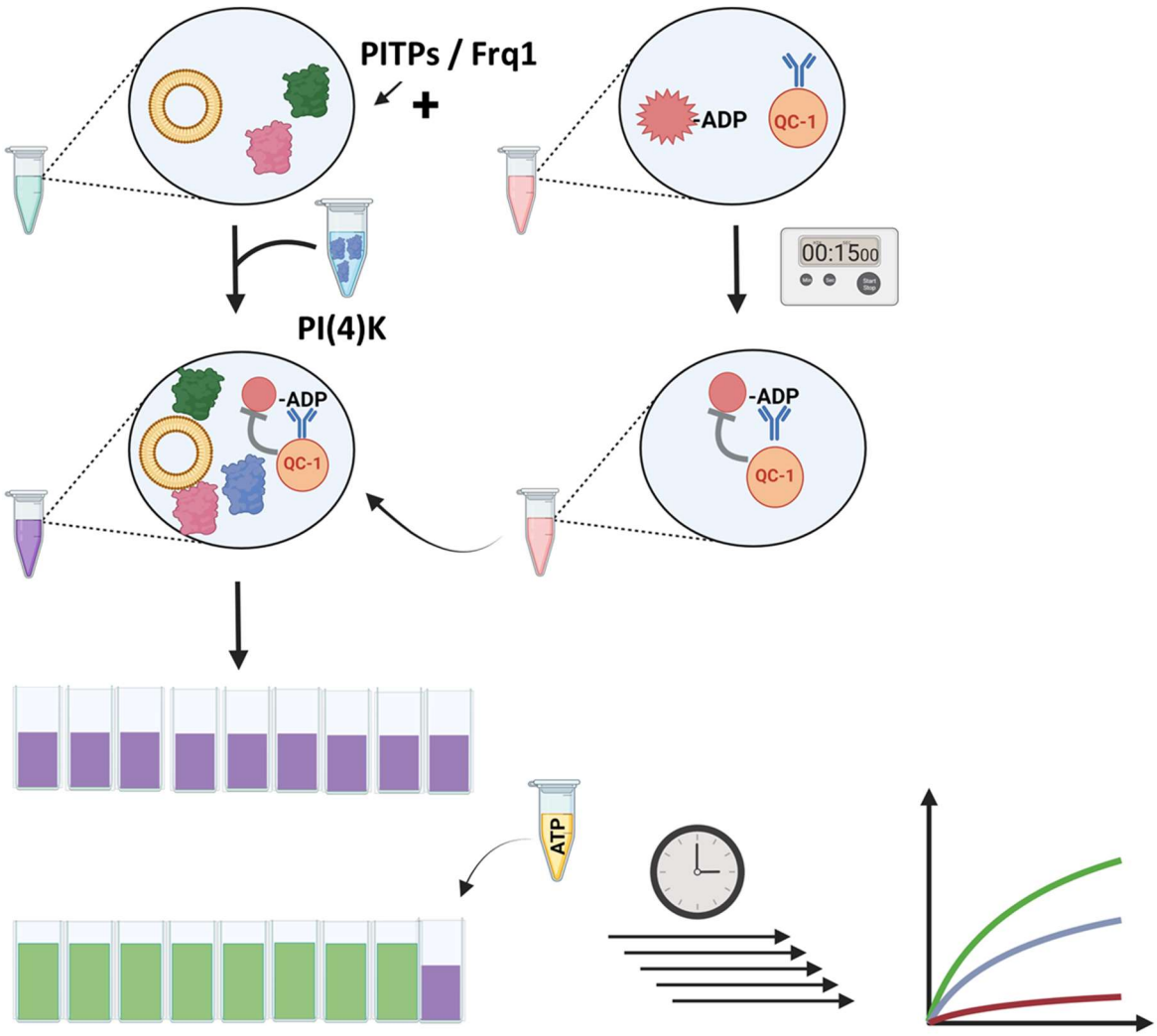

Figure 30: Optimized protocol for the Transcreener® ADP^2 FI Assay in time-resolved mode. The optimized protocol developed in the present study requires the initial incubation of lipid vesicles and lipid binding proteins (when appropriate) in 0.8X assay buffer, followed by addition of the lipid kinase. The ADP antibody and ADP-fluorophore are allowed to equilibrate in 0.2X assay buffer in a separate tube, after which they are mixed with the reaction mixture. This mixture is pipetted into plate wells, and the reaction is started with the addition of ATP. The plate is inserted into an appropriate plate reader and the FI signal is read over a given time period at prescribed intervals, thus allowing the generation of enzyme progression curves. Created with BioRender.com.

4.3.5 Comparison of PI4K-IIIβ constructs

Upon ensuring that basic parameters of the assay (*i.e.*, the ATP/ADP standard curve and the FI assay window, **Section 4.3.3**) displayed the expected behaviour, and having an optimized assay protocol (**Section 4.3.4**), the activity of PI4K-IIIβ could be assessed with confidence.

First, the PI4K-IIIβ constructs needed to be assayed to establish whether the deletion mutants (described in **Section 4.1.4**) produced PI(4)P at similar rates when compared to the wt. In reactions containing 110 nM lipid kinase, 0.2 mg/mL PI:PS SUVs and 10 μM ATP, the FI signal produced by the C and L deletion mutants were comparable to that produced by the wt PI4K-IIIβ (**Figure 31B, 31C and 31A**, green, pink, and blue curves, respectively). However, when contrasting these signals to those produced in the same conditions but without the lipid substrate (NL control, **Figure 31A-C**, lighter-coloured curves), the biggest gap is seen with the wt PI4K-IIIβ. In trying to quantify the contribution of substrate-independent ATP hydrolysis, the signal for the NL control at t = 40 min was normalized to the matching FI signal for the lipid-containing reaction. This time point was chosen to determine and compare initial rates of kinase activity in the present study. As shown in **Figure 31D**, wt PI4K-IIIβ (blue bar) displayed the lowest non-productive ATPase activity when compared to the C (green bar) and L (pink bar) deletion mutants. Therefore, it can be inferred that the true lipid kinase activity was reduced in PI4K-IIIβ constructs with deleted disordered loops, a trend observed previously (Fowler et al., 2016; Klima et al., 2016) but without acknowledgement to lipid-independent controls. It remains unclear the mechanism by which removing disordered loops that lie upstream of the lipid kinase domain in PI4K-IIIβ negatively impact lipid kinase activity, but perhaps the absence of these loops may prevent the protein from adopting its optimal, native conformation. Considering our

observations, wt PI4K-IIIβ was selected as the construct to move forward with for activity assays.

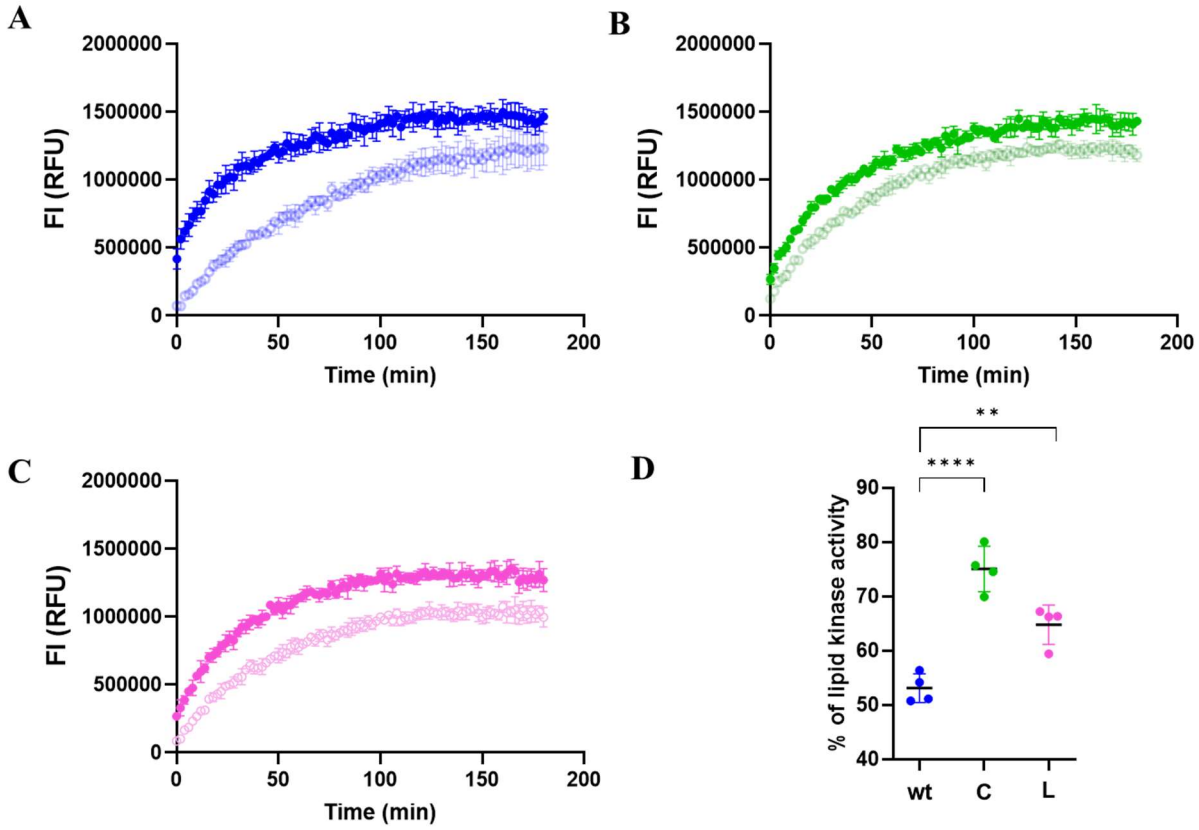

Figure 31: PI-containing and PI-independent activity assays with different PI4K-IIIβ constructs. The time-resolved activity of PI4K-IIIβ constructs (**31A:** wt; **31B:** "C" Δ453-511; **31C:** "L" Δ408-507) was assessed in reactions containing 110 nM lipid kinase, 10 μM ATP, with and without 0.2 mg/mL PI:PS SUVs. The FI signal generated by PI-containing reactions is represented by solid colours, whereas PI-independent reactions is shown in matching, lighter colours. The curves were corrected for the assay background (*i.e.*, no protein control). **31D:** comparison of the FI signal generated by PI4K-IIIβ without PI at t = 40 min normalized to the matching FI signal for reactions containing PI. Error bar = SD based on 4 technical repeats.

4.3.6 Assaying PI4K-IIIβ on its own

4.3.6.1 Titration of PI4K-IIIβ

The concentration dependence of PI4K-IIIβ activity was assessed with the goal of determining the optimal dosage in the assays. A range of 0-110 nM wt PI4K-IIIβ was tested with

0.2 mg/mL PI:PS and 10 µM ATP. The obtained results (**Figure 32**) demonstrated that the FI signal produced by PI4K-IIIβ in our optimized, vesicle-based, real-time assay is dose-dependent.

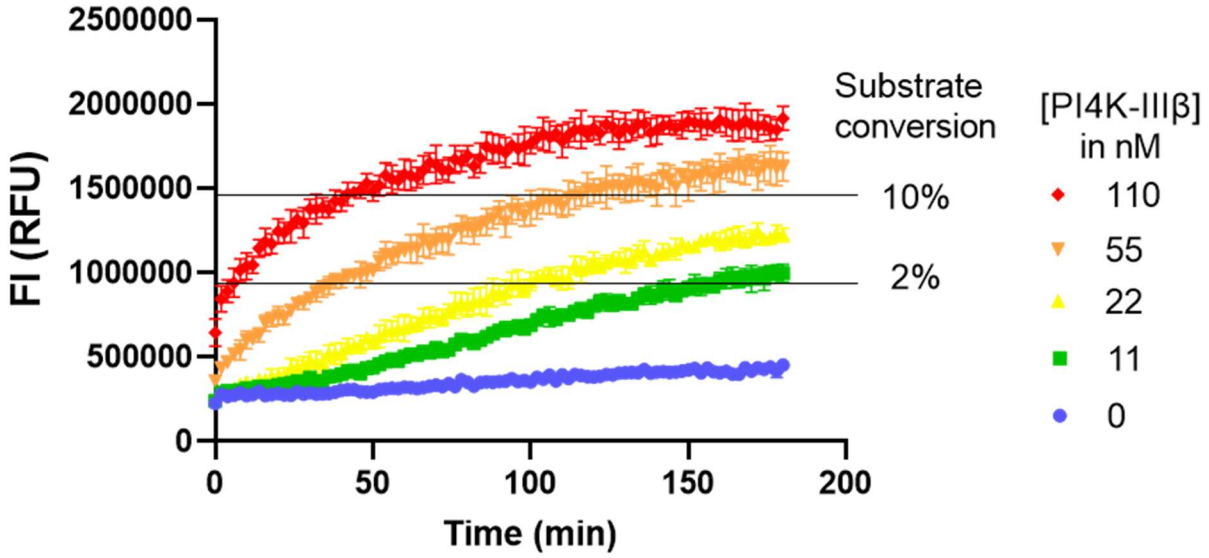

Figure 32: PI4K-IIIβ titration. Lipid kinase concentrations ranging from 0 to 110 nM were assayed for 180 min with 0.2 mg/mL PI:PS and 10 µM ATP in the time-resolved version of the Transcreener® ADP^2 FI Assay developed in this study. A dose-dependent response is observed between concentration of enzyme and product formation as judged by the FI signal produced. 2% and 10% substrate conversion, as previously determined by a standard curve (Figure 27A), are indicated. Error bar = SD based on 4 technical repeats.

According to the behaviour noticed above, 22 nM PI4K-IIIβ was selected as the concentration of lipid kinase to be used henceforth. Of importance, the assay supplier suggests using enzyme concentrations that produce between 50 and 80% change in FI signal (*Transcreener® ADP FI Assay Technical Manual*, 2023). With 110 nM PI4K-IIIβ, the FI signal produced approached the max FI determined previously (**Section 4.3.3**), ~ 2.2 x 10^6 RFUs (**Figure 32**, red curve). Following this rationale, ~ 1.1 x 10^6 RFUs would correspond to approximately 50% FI signal, which is reached by 22 nM PI4K-IIIβ at later time points (**Figure 32**, yellow curve). Moreover, 22 nM of lipid kinase produced a FI signal below 10% substrate conversion for the entirety of the assay, and below 2% substrate conversion if focusing on initial

reaction rates. This is relevant as the Transcreener® ADP^2 FI Assay reliably monitors enzymatic activity at low substrate conversion, *i.e.*, up to 10% (preferably ≤ 2.5%) (*Transcreener® ADP FI Assay Technical Manual*, 2023). Since previous studies reported a 3-fold stimulation in the activity of PI4K-IIIβ and its homologue PIK3C3 when exposed to Sec14p (Panaretou et al., 1997; Schaaf et al., 2008), the chosen concentration of lipid kinase should allow enough room to monitor a potentially enhanced activity that would still be detected where this assay promises the best sensitivity.

4.3.6.2 The effect of the inhibitor wortmannin

Before adding proposed positive regulators of PI4K-IIIβ activity (*i.e.*, PITPs and Frq1) to the assay, a negative regulator was tested to verify that the predicted effect would be observed. The fungal metabolite wortmannin is a known inhibitor of PI3Ks and type III PI4Ks (Fruman et al., 1998). A previous study demonstrated that 1 μM wortmannin reduced the production of PI(4)P by recombinant GST-PI4K-IIIβ to approximately 10% of the uninhibited reaction (Meyers & Cantley, 1997). Mimicking those conditions, the activity of native PI4K-IIIβ was clearly reduced by wortmannin, but only to 30-40% of the uninhibited reaction (**Figure 33**, black and red curves). A possible explanation for this difference relies on varying results obtained by others when assessing the inhibitory effects of wortmannin on lipid kinases. Particularly, wortmannin IC_{50} values of 100, 125 and 300 nM have been determined for PI4K-IIIβ (Meyers & Cantley, 1997; Suer et al., 2001; X.-H. Zhao et al., 2000), suggesting an assay dependent variability. Alternatively, if considering that the wortmannin treatment reduced PI4K-IIIβ's activity to the levels observed in the NL control (red and green curves), an argument could be made that wortmannin in fact reproduced its potent inhibition on the production of PI(4)P by PI4K-IIIβ. Since wortmannin does not inhibit all ATP-hydrolyzing enzymes, the remaining FI

signal seen in the inhibitor-treated reaction (red curve) could be generated by ATP-consuming chaperones that remained bound to PI4K-IIIβ even after the HSP Removal Wash treatment (**Section 4.2.1**). Overall, these results demonstrated that negative regulation of PI4K-IIIβ's activity by wortmannin is observable in our assay conditions.

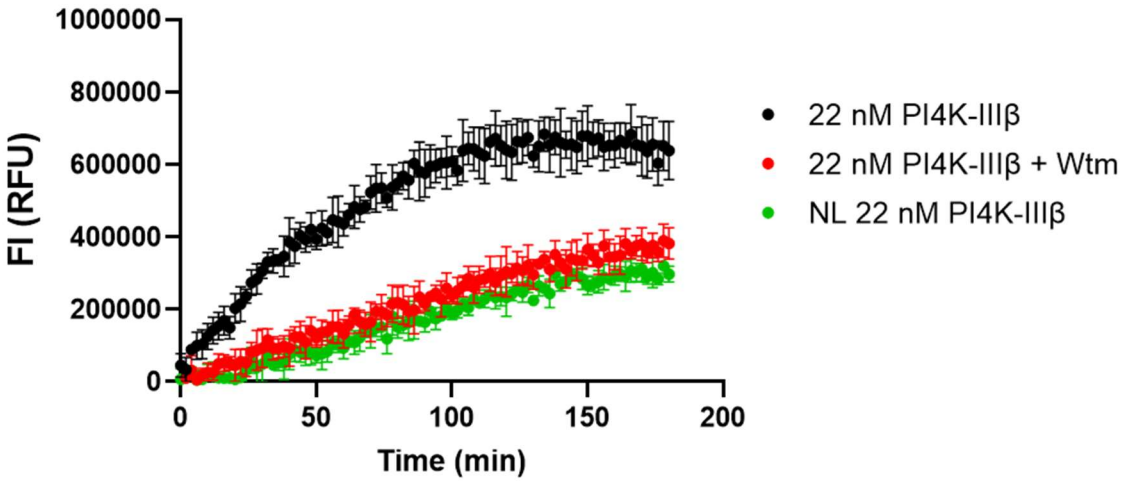

Figure 33: Wortmannin inhibition of PI4K-IIIβ's lipid kinase activity. Addition of 1 μM wortmannin ("Wtm") to a reaction containing 22 nM native PI4K-IIIβ, 0.2 mg/mL (50:25:25) PI:PS:PC 200 nm LUVs and 10 μM ATP (red curve) reduced the FI signal produced to 30-40% of the uninhibited reaction (black curve). The FI signal observed in the wortmannin-inhibited reaction is similar to that produced by PI4K-IIIβ in the absence of lipid substrate ("NL", green curve). Error bar = SD based on 4 technical repeats.

4.3.6.3 Comparison with insect cell expressed PI4K-IIIβ

The activity of recombinant PI4K-IIIβ expressed in bacteria for the present study was compared to the commercially sourced PI4K-IIIβ expressed in baculovirus infected *Spodoptera frugiperda* (Sf9) cells (**Figure 34**). This testing was done to assess what effect post-translational modifications (PTMs), possible in eukaryotic but not in prokaryotic expression systems, would have on the activity of PI4K-IIIβ. Of importance, phosphorylation of PI4K-IIIβ at Ser_{294} by

members of the PKD family has been reported to increase PI(4)P production by 60% when compared to a non-phosphorylatable mutant (Hausser et al., 2005).

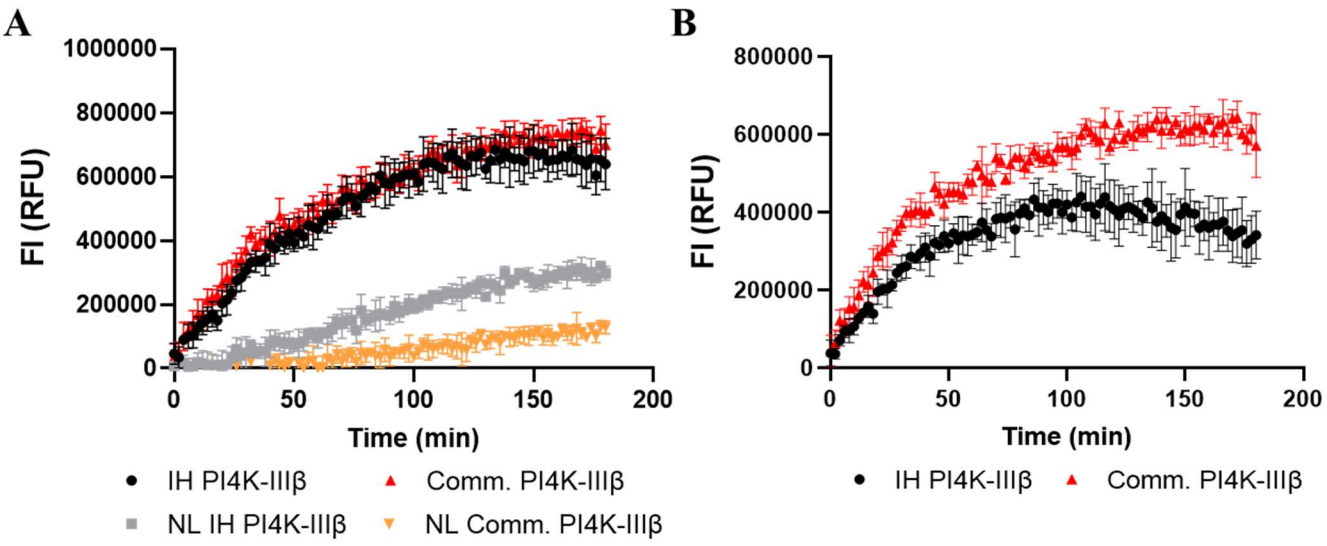

Figure 34: Comparison of bacteria- and insect cells-expressed recombinant PI4K-IIIβ. **34A:** Enzyme progression curves for lipid-containing and no-substrate (NL, no-lipid) controls for in-house prepared, bacteria expressed recombinant PI4K-IIIβ ("IH") and its commercially available, insect cells derived counterpart ("Comm."). **34B:** Activity of the same preparations of recombinant PI4K-IIIβ corrected for non-productive ATP hydrolysis. Reactions contained 22 nM of lipid kinase, 10 µM ATP, and 0.2 mg/mL (50:25:25) PI:PS:PC 200 nm LUVs. The lipid substrate was replaced by mQ H_2O in the NL control. Error bar = SD based on 4 technical repeats.

As seen in **Figure 34A**, the FI signal produced by recombinant PI4K-IIIβ in the PI-containing reactions is similar for both bacteria expressed, in-house purified ("IH", black curve) and commercially sourced, insect cell expressed PI4K-IIIβ ("Comm.", red curve). However, the FI signal generated by the NL controls of the two enzyme preparations is significantly different (grey and orange curves). This difference could stem from a lower degree of chaperone contamination in the commercially sourced recombinant PI4K-IIIβ when compared to the IH produced lipid kinase. If correcting for non-productive ATP hydrolysis, the observed activity of

recombinant insect cells produced PI4K-IIIβ is ~ 45% higher when contrasted to the same parameter displayed by the enzyme prepared in-house if initial rates are considered (*i.e.*, t = 40 min) (**Figure 34B**). This behaviour could result from the activating impact of PTMs (Hausser et al., 2006) when employing eukaryotic expression systems.

Seven residues other than Ser_{294} are phosphorylatable in PI4K-IIIβ, which has been associated with its cellular localization (Szivak et al., 2006). Therefore, it can be inferred that PTMs are required for optimal functioning of this lipid kinase *in vivo*. For this reason, testing insect cell expressed PI4K-IIIβ may also be relevant when trying to reproduce more complex molecular interactions even *in vitro*, such as the lipid presentation model by PITPs to the lipid kinase. Furthermore, the negligible FI signal of the NL control produced by insect cell-derived PI4K-IIIβ (**Figure 34A**, orange curve) particularly at early times (≤ 75 min), allows assaying this lipid kinase without accounting for non-productive ATPase activity thus minimizing reagent expenditure and simplifying the workload.

4.3.7 Assaying PI4K-IIIβ with protein partners

4.3.7.1 Testing bacterial expressed PI4K-IIIβ with protein partners

Initial testing of the effect of PITPs on the lipid kinase activity of PI4K-IIIβ employed recombinant expressed PITPβ. Not only is this the human PITP isoform with higher affinity for membranes and ligand transfer rates when compared to PITPα, but also it mostly localizes to the Golgi complex and ER (Baptist et al., 2016), like PI4K-IIIβ (Balla & Balla, 2006; Szivak et al., 2006). Considering that the proposed PI presentation mechanism is based on the PI/PC heterotypic exchange performed by PITPs (Schaaf et al., 2008), the liposome composition was modified from PI:PS to include PC. Assays were initially performed with 0.2 mg/mL (50:25:25) PC:PS:PI SUVs, 10 μM ATP and 2:1 PITPβ:PI4K-IIIβ. Unexpectedly, no PITPβ-caused

enhancement of the activity of PI4K-IIIβ was observed (**Figure 35A**). Hoping to maximize the encounters of PI-carrying PITPβ and the lipid kinase, the ratio of PITPβ to PI4K-IIIβ was increased to 10:1 in a subsequent attempt, while maintaining the other conditions. Again, PITPβ demonstrated no effect on the activity of PI4K-IIIβ (**Figure 35B**). Next, the liposomes' content was further optimized to more closely resemble the lipid composition of Golgi membranes, which is where both PI4K-IIIβ and PITPβ mostly act *in vivo* (Balla & Balla, 2006; Baptist et al., 2016). The lipid mixture used herein mimics a Golgi lipid preparation used elsewhere (Burke et al., 2014) - 45% PC, 25% PE, 10% PS, 10% PI, 10% cholesterol - which agrees with ratios seen in other works (Casares et al., 2019; Van Meer et al., 2008) despite minor variations. Additionally, we thought of switching to 200 nm LUVs on the grounds that SUVs offer a highly curved, stressed surface that poorly accommodates spatial changes. In fact, a previous report indicated that LUVs are significantly less impacted than SUVs by the electrostatic charge and increased headgroup size triggered by the phosphorylation of PI (Hubner et al., 1998). Although theoretically sound, the experiment with the 200 nm LUVs Golgi lipid mixture did not produce the anticipated stimulation of PI4K-IIIβ activity (**Figure 35C**). Finally, Frq1 was included in the assay hoping that it would increase the effective concentration of lipid substrate around PI4K-IIIβ. Frq1 is known to recruit PI4K-IIIβ's yeast orthologue, Pik1, to the Golgi membrane (Strahl et al., 2007). Moreover, the Frq1 homologue in humans, NCS-1, has been shown to perform an analogous recruiting function on PI4K-IIIβ in human cells (Haynes et al., 2005). Lastly, the sequence region of Pik1 recognized by Frq1 is partially conserved in PI4K-IIIβ (McPhail & Burke, 2023), suggesting that yeast Frq1 may bind the human PI4-kinase and elicit a similar effect to that observed with yeast Pik1. Notwithstanding four independent repeats of the assay

under these conditions, each in quadruplicates, no reproducible enhancement in the production of PI(4)P by PI4K-IIIβ was noticed (**Figure 35D**).

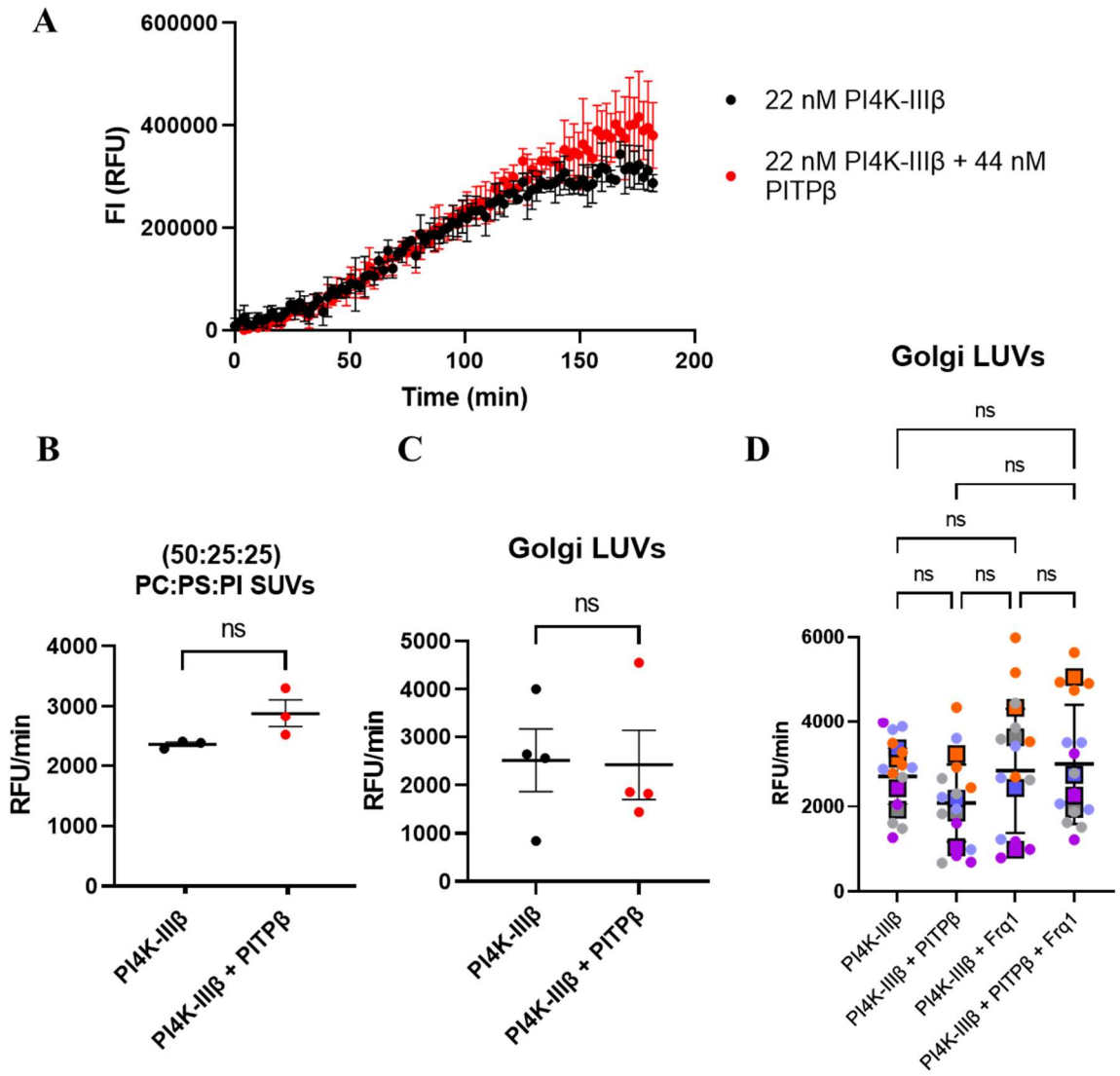

Figure 35: Effect of PITPβ and Frq1 in the lipid kinase activity of PI4K-IIIβ. 35A: Assay of PI4K-IIIβ alone and with a 1-fold molar excess of PITPβ using 0.2 mg/mL (50:25:25) PC:PS:PI SUVs as the lipid substrate. **35B:** Change in FI, in RFU/min, produced by PI4K-IIIβ for 40 min alone and with the addition of 9-fold molar excess of PITPβ using 0.2 mg/mL (50:25:25) PC:PS:PI SUVs as the lipid substrate. **35C:** Change in FI, in RFU/min, produced by PI4K-IIIβ for 40 min alone and with the addition of 9-fold molar excess of PITPβ using 0.2 mg/mL 200 nm LUVs Golgi lipid mixture. **35D:** Change in FI, in RFU/min, produced by PI4K-IIIβ for 40 min alone and with the addition of equimolar amounts of Frq1 and/or 9-fold molar excess of PITPβ using 0.2 mg/mL 200 nm LUVs Golgi lipid mixture. All reactions employed 22 nM PI4K-IIIβ. Error bar = SD based on 4 technical repeats, except for **35D**, where 4 independent experiments (colour-coded) were run, each in quadruplicates. Circles represent individual data points, while squares represent the mean of a given independent experiment.

Next, Sec14p was tested with PI4K-IIIβ. A previous study demonstrated that Sec14 led to a 3-fold increase in the PI(4)P production by PI4K-IIIβ (Schaaf et al., 2008). Also, heterologous expression of PITPβ in yeast rescued the defects caused by ablation of Sec14p activity (Skinner et al., 1993), altogether demonstrating a degree of functional interchangeability between the human and the yeast PITP. Our Sec14p containing assays were performed on (50:25:25) PI:PC:PS 200 nm LUVs as the lipid substrate, in an effort to maximize PI in the liposomes while maintaining PC in the mixture. If correcting for substrate-independent ATP hydrolysis, Sec14p appears to stimulate the lipid kinase activity of PI4K-IIIβ by ~ 40% if the initial rate (up to t = 40 min) is considered (**Figure 36**). However, the observed large standard deviations make it challenging to securely infer the effect promoted by Sec14p in the activity of PI4K-IIIβ can lead to multifold increases in PI(4)P production (as previously reported (Schaaf et al., 2008)), even though $p = 0.0308$ between the initial reaction rates.

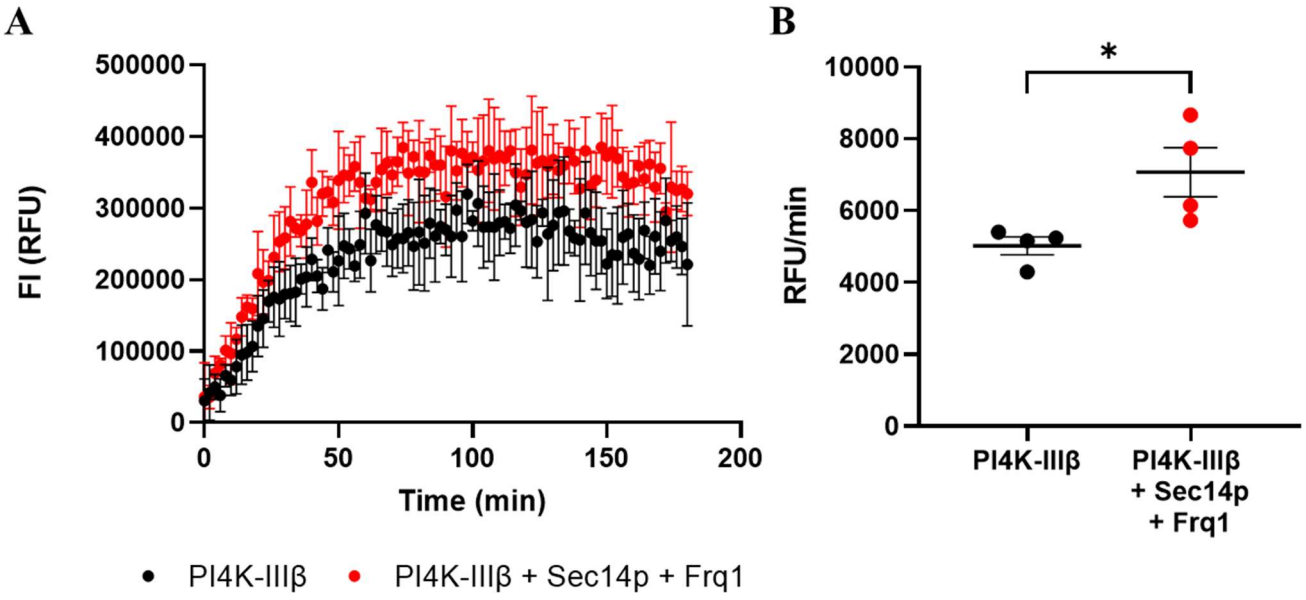

Figure 36: Effect of Sec14p in PI4K-IIIβ's activity. 36A: Enzyme progression curves of reactions containing PI4K-IIIβ only (black curve) and PI4K-IIIβ + Frq1 + Sec14p (red curve) in the presence of (50:25:25) PI:PC:PS 200 nm LUVs and 10 μM ATP. Reactions contained 22 nM lipid kinase, equimolar amount of Frq1 and 9-fold excess Sec14p. The signal was corrected for non-productive ATP hydrolysis. **36B:** Quantification of initial rates (up to t = 40 min) of the same reactions, in RFU/min, demonstrate an approximate 40% increase in the activity of PI4K-IIIβ stimulated by Sec14p. Error bar = SD based on 4 technical repeats.

4.3.7.2 Verifying that PITPs and Frq1 were "active"

To ensure that the lack of reproducible, significant enhancement on the activity of PI4K-IIIβ promoted by PITPs and Frq1 was not due to instability of these proteins, their ligand binding was tested in fluorescence-based assays. NBD-labelled lipids are excellent probes to study lipid-involving processes like membrane fusion and lipid transfer. NBD is a reliable reporter of change in chemical environment since its fluorescence intensity in polar environments is much lower than in a hydrophobic environment such as a protein's binding pocket (Chattopadhyay, 1990). Binding of PITPs to the PC analogue NDB-PC was performed in the present study to verify that these proteins were "healthy", *i.e.*, able to bind one of their cognate ligands. As seen in **Figure 37A**, all tested PITPs (PITPα, PITPβ and Sec14p) exhibited the expected binding profile to NBD-PC: initially a fast, first-order type association, followed by slower binding until plateauing at saturation. The rate constants of the first-order association, K_{fast}, for PITPβ (0.02073 s^{-1}) and Sec14p (0.03364 s^{-1}) were approximately 2- and 3-fold higher, respectively, than that displayed by PITPα (0.01073 s^{-1}). A previous study showed that both PITPβ and Sec14p transferred NBD-PC to vesicles *in vitro* at faster rates than PITPα (Panagabko et al., 2019). Our experiments demonstrated that all tested PITPs were able to bind NDB-PC.

As for Frq1, its intrinsic tryptophan fluorescence spectra were obtained in two different conditions: without Ca^{2+} and at saturating concentrations of this metal. Three of Frq1's four EF-hands, a domain widely conserved in Ca^{2+}-binding proteins, bind calcium (Strahl et al., 2007). Previous studies with NCS-1, the human homologue of Frq1, reported an increase in the fluorescence emission intensity upon binding to saturating concentrations of Ca^{2+} (Tsvetkov et al., 2018). We observed a similar pattern when performing an analogous test with Frq1 (**Figure 37B**), which was expected given that NCS-1 and Frq1 share 75% of residues that are either

identical or conservatively replaced (Bourne et al., 2001). Importantly, Ca^{2+} binding has been shown to be relevant but not essential for the activation of Pik1, the yeast homologue of PI4K-IIIβ's (Strahl et al., 2007). Altogether, our results support functional binding of Frq1 to Ca^{2+}.

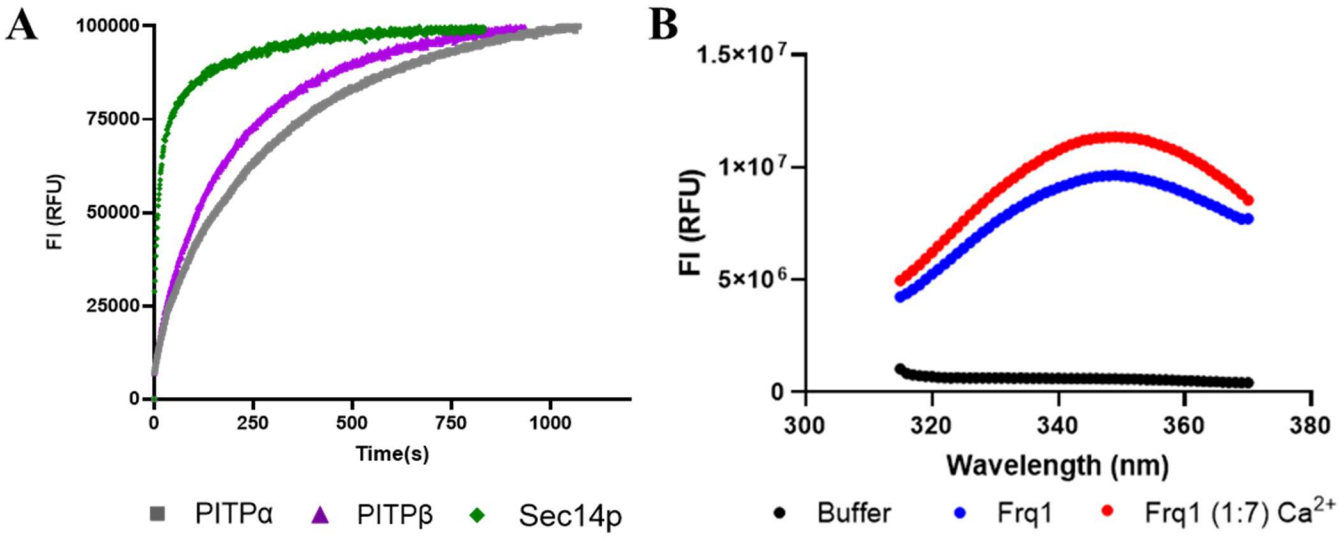

Figure 37: Binding curves for PITPs and intrinsic tryptophan fluorescence of Frq1 upon Ca^{2+} binding. 37A: The binding of PITPα (grey), PITPβ (purple), and Sec14p (green) to the fluorescent PC analogue, NBD-PC, was monitored in a fluorimeter. 150 nM NBD-PC was added to 220 nM PITPs in 1X TKE buffer. Fluorescence readings (λ_{EX} = 469 nm, λ_{EM} = 527 nm) were taken for 5-7 min, and the data was fitted to an exponential, two phase association curve using GraphPad Prism. **37B:** Intrinsic tryptophan fluorescence spectra of 13 μM Frq1 with a 6-fold molar excess of Ca^{2+} (red curve) and without this metal (blue curve) monitored in a microplate reader. The fluorescence emission was measured between 315 and 370 nm with λ_{EX} = 295 nm. Calcium-containing and calcium-free buffer controls (25 mM HEPES, 150 mM NaCl, pH 7.5, black line) displayed identical behaviours.

4.3.7.3 Testing insect cell expressed PI4K-IIIβ with protein partners

The hypothesized PI presentation model was tested with insect cell expressed recombinant PI4K-IIIβ. This was done on the premise that the lack of PTMs on the bacterially expressed lipid kinase could prevent its optimal performance, including the activation by PITPs. In fact, the true lipid kinase activity of the Sf9 cells derived PI4K-IIIβ was shown in the present study to be higher than that produced in bacteria (**Figure 34**). 22 nM PI4K-IIIβ was tested with an equimolar amount of Frq1 and 10 μM ATP. PITPα, PITPβ and Sec14p were in 9-fold excess,

and their effect on lipid kinase activity was assessed alone or in combination with Frq1. All assays employed 0.2 mg/mL 200 nm LUVs (50:25:25) PI:PC:PS as the lipid substrate (**Figure 38**). Unexpectedly, neither PITPs nor Frq1 caused enhancement on the PI(4)P production by PI4K-IIIβ, especially if initial rates are considered (**Figure 38D**).

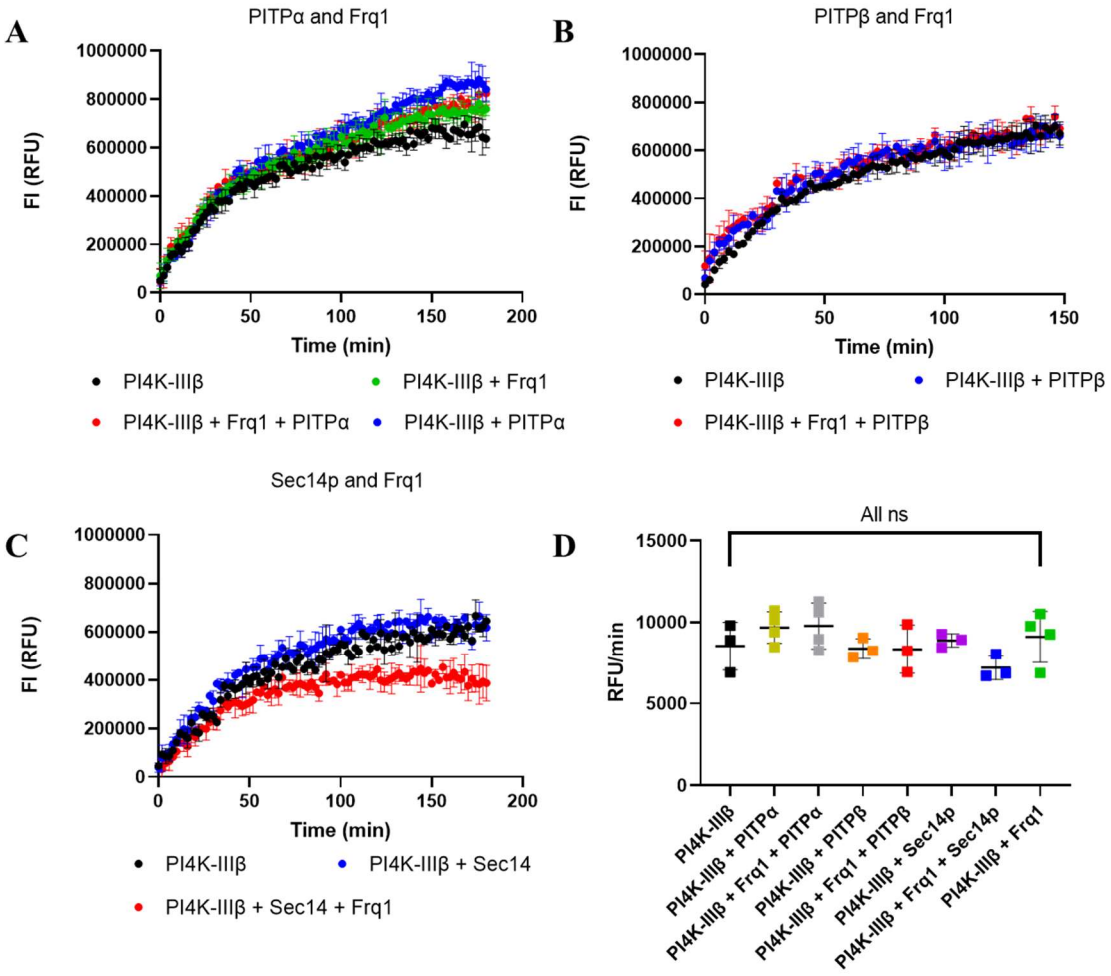

Figure 38: Effect of PITPα, PITPβ, Sec14p and Frq1 on the activity of commercially sourced PI4K-IIIβ. The activity of Sf9 cells expressed recombinant PI4K-IIIβ was assessed in the presence and absence of PITPα and Frq1 (**38A**), PITPβ and Frq1 (**38B**) and Sec14p and Frq1 (**38C**). All reactions contained 22 nM PI4K-IIIβ, 0.2 mg/mL 200 nm LUVs (50:25:25) PI:PC:PS, and 10 μM ATP in 1X assay buffer. PITPs were present in 9-fold molar excess, whereas Frq1 was equimolar to the lipid kinase. The assays with Sec14p were corrected for lipid-independent ATP hydrolysis. **38D:** Summary of initial rates measured in RFU/min, for reactions run until t = 40 min. None of the protein partners tested elicited a statistically significant effect on PI4K-IIIβ's activity. Error bar = SD based on 4 or 3 technical repeats.

Variations in the assay conditions were attempted, hoping to detect the proposed enhanced in lipid kinase activity promoted by PITPs. Namely, the molar ratio PI4K-IIIβ:Sec14p was decreased from 1:10 (previous assays) to 1:3, thus reproducing the proportion used in a previous study where the PI(4)P production of PI4K-IIIβ was enhanced by Sec14p (Schaaf et al., 2008). Unable to observe the same effect in our assays, we next altered the total protein concentration in the assay while maintaining the amounts of lipid and nucleotide substrates. Lower total protein in the assay should decrease the substrate conversion rate, thereby potentially increasing the assay sensitivity. On the other hand, a higher total protein concentration maximizes the number of collisions between enzyme, substrate, and protein partners, which could allow us to monitor activity stimulation. In fact, higher protein concentrations in the assay lower the molar ratio between proteins and substrates to ranges used by others when studying the effect of protein partners on PI4K-IIIβ's (Fowler et al., 2016; Schaaf et al., 2008) and PI-3 kinases' activity (Kular et al., 2002; Panaretou et al., 1997). A summary of these molar ratios and how they are in range with the ones employed in the present study is seen on **Table 15**. Despite repeated attempts, assays run with varied total protein concentrations did not reveal a significant enhancement in the activity of PI4K-IIIβ promoted by PITPs.

Table 15: Molar ratio of proteins and substrates in reactions involving homologous lipid kinases and PITPs. Ratios are normalized to the molar concentration of recombinant lipid kinase used in the assay, except for when this parameter was not disclosed. In the latter case, ratios are normalized to the molar concentration of PITPs.

Source	PI-kinase	PI	ATP	PITP
Present study (at 5.5 nM PI4K-IIIβ)	1	20000	5000	10
Present study at 22 nM PI4K-IIIβ)	1	5000	500	≤ 10
Present study (at 55 nM PI4K-IIIβ)	1	2000	200	≤ 10
(Fowler et al., 2016)	1	2500	50	N/A
(Panaretou et al., 1997)	? (Resin-immobilized)	1000	40000	1
(Kular et al., 2002)	1	13000	4000	10
(Schaaf et al., 2008)	1	~ 400	~ 300	3

In another experiment, the same lipid recipe (0.2 mg/mL (50:25:25) PI:PC:PS) was presented as SUVs instead of 200 nm LUVs. Previous reports demonstrated that PITPα and PITPβ transfer ligands at much faster rates when the acceptor vesicles are small, as phospholipids in highly curved membranes are more susceptible to lipid and protein insertion thus making it easier for deposition and retrieval of ligands by PITPs (Baptist et al., 2016). We hypothesized that by promoting a faster ligand transfer rate, we could maximize encounters between PI-carrying PITPs and PI4K-IIIβ (**Figure 39A**). In another set of experiments, we included 0.4% Triton X-100 (herein denoted as Triton) in the assay buffer (**Figure 39B**) as this non-ionic detergent is known to activate PI4K-IIIβ (Sasaki et al., 2009). Considering that Triton is not present in cells, such an activation can be deemed artifactual and irrelevant to the enzyme's *in vivo* functioning. Phospholipids in detergent-mixed micelles are more loosely packed than in true bilayers (Stillwell, 2016), which likely supports the claim that PI becomes more accessible to lipid kinases in the presence of Triton. Overall, no PITP-elicited enhancement

in the activity of PI4K-IIIβ was detected, regardless of substrate presentation as SUVs or in Triton-mixed micelles. However, the activity of PI4K-IIIβ alone was ~ 60% higher in the presence of detergent then with SUVs (**Figure 39C-D**) or LUVs (**Figure 38D**, black bar), supporting previous observations (Meyers & Cantley, 1997; Suer et al., 2001).

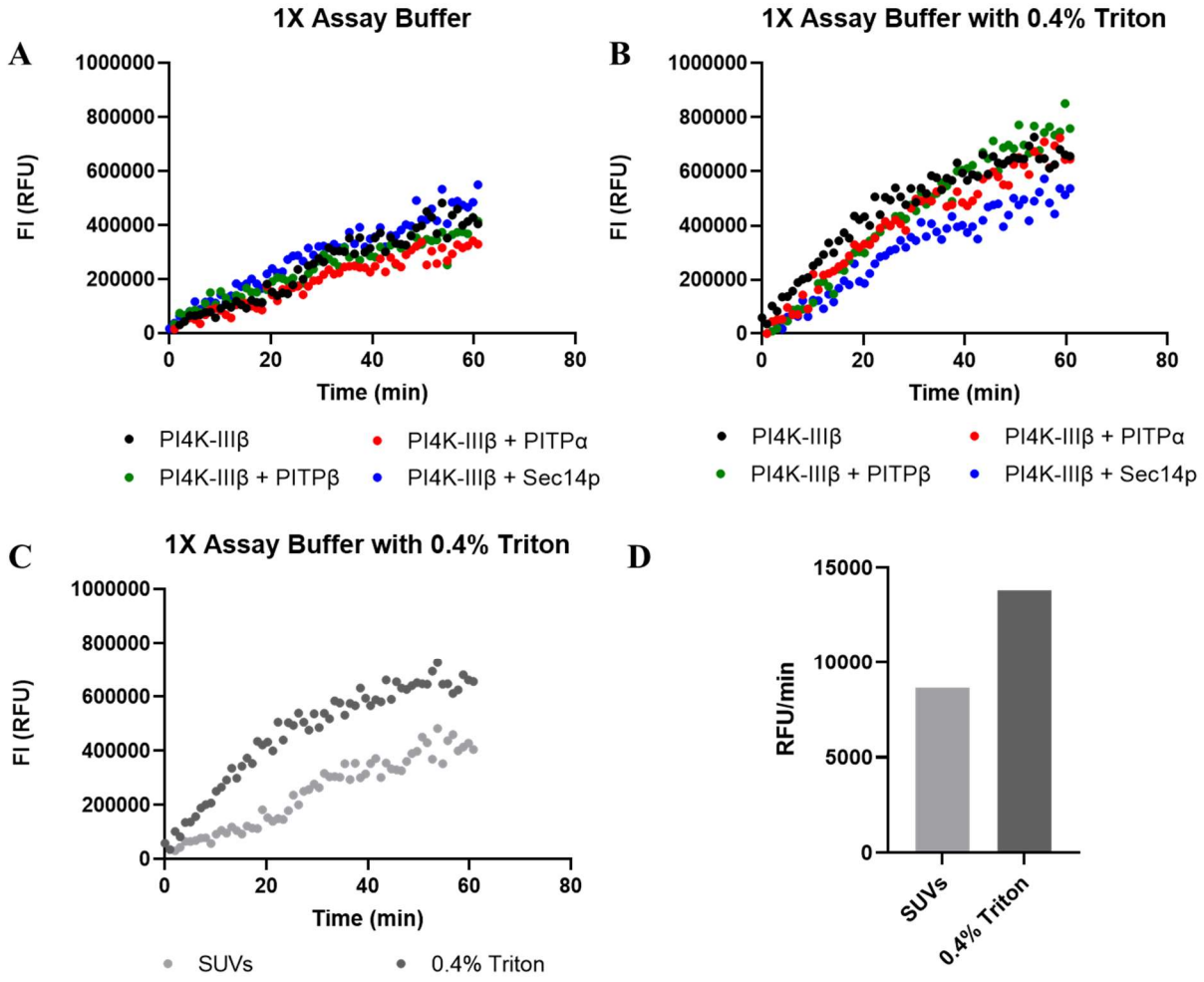

Figure 39: Activity assays of PI4K-IIIβ using SUVs and detergent-mixed micelles as substrates. 22 nM PI4K-IIIβ was assayed with 10 μM ATP and 0.2 mg/mL (50:25:25) PI:PC:PS either presented as SUVs (**39A**) or in 0.4% Triton X-100 containing buffer (**39B**). Addition of PITPα, PITPβ and Sec14p to the reaction mixture was also tested but elicited no apparent increase in enzyme activity. **39C:** Activity of PI4K-IIIβ alone, corrected for the assay background, using SUVs and Triton-mixed micelles as the substrate. **39D:** Comparison of initial reaction rates (up to t = 40 min) for the same reaction described in **39C**. Low enzyme stocks prevented running these assays in replicates.

In a final attempt, we ensured that the lack of observable PITP stimulation on the activity of PI4K-IIIβ was not due to our in-house developed, time-resolved format assay. Specifically, in the time-resolved format, the ADP antibody and ADP-fluorophore are both present in the assay mixture during the lipid kinase reaction (**Section 4.3.4**). In the original, endpoint format the lipid kinase reaction is allowed to proceed for a given time period, and then it is stopped by the addition of EGTA-containing Detection Mixture, which also harbours the ADP antibody and ADP-fluorophore (*Transcreener® ADP FI Assay Technical Manual*, 2023). Assaying PI4K-IIIβ and PITPs in the endpoint format produced the same results observed by the time-resolved assay developed in the present stud (**Figure 40**). Due to reagents availability, this experiment was only performed once, with two technical replicates.

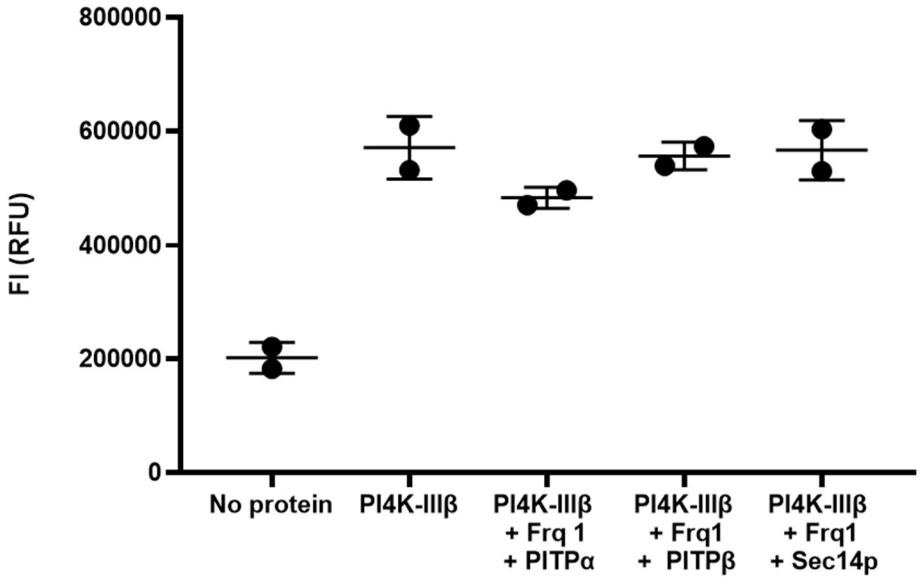

Figure 40: PI4K-IIIβ assay using the endpoint format. 22 nM PI4K-IIIβ was assayed alone and with an equimolar amount of Frq1 + 2-fold molar excess PITPs using the Transcreener® ADP^2 FI Assay in its original, endpoint format. The reactions ran for 1 hour and contained 10 μM ATP and 0.2 mg/mL (50:25:25) PI:PC:PS SUVs in 1X Assay Buffer. No effect on the lipid kinase activity of PI4K-IIIβ was elicited by the protein partners. Error bar = SD based on two technical replicates.

4.3.8 Comparison with PIK3C3

Considering the lack of observable enhancement of PI4K-IIIβ activity by PITPs, we next tested a different lipid kinase to confirm that those results were not PI4K-IIIβ specific. The activity of commercially sourced, insect cells expressed recombinant PIK3C3 was assayed in the presence of PITPs to assess whether any enhancement on the activity of the lipid kinase would be detected. PITPα, PITPβ and Sec14p have been shown to stimulate the production of PI(3)P by PIK3C3 by approximately 300% *in vitro* (Panaretou et al., 1997), or by almost 10-fold in a different study with Sec14p and the same lipid kinase (Hubner et al., 1998). Interestingly, yet another report demonstrated that the PITPα-led augmentation in PI3K activity was substrate dependent. PI3Ks can phosphorylate PI, PI(4)P and PI(4,5)P_2, and the addition of PITPα to the lipid kinase reaction only led to a slight increase in PI(3)P production, contrasting previous studies, whereas a 9- and 18-fold enhancement in the production of PI(3,4)P_2 and PIP_3 were observed (Kular et al., 2002). However, in all three reports the enhancement in PI3K activity was dependent on the PITP concentration, whereby too high a dosage of PITP had inhibitory effects on the activity of the lipid kinase.

In an attempt to reproduce the above observations, different concentrations of PITPs were added to reactions involving PIK3C3. Nevertheless, no significant stimulation in lipid kinase activity was observed for any of the three PITPs tested (**Figure 41**). In a final experiment, SUVs replaced LUVs as the lipid substrate while maintaining the vesicle's chemical composition, (50:25:25) PI:PC:PS. Justifying this change is a previous observation that PIK3C3's activity increases by 5-fold when its substrate is presented in highly curved membranes versus in 200 nm LUVs (Hubner et al., 1998). We hypothesized that by providing PIK3C3 with SUVs the lipid

kinase would perform optimally, perhaps improving the chances of observing a PITP stimulation of kinase activity. However, no such stimulation was detected.

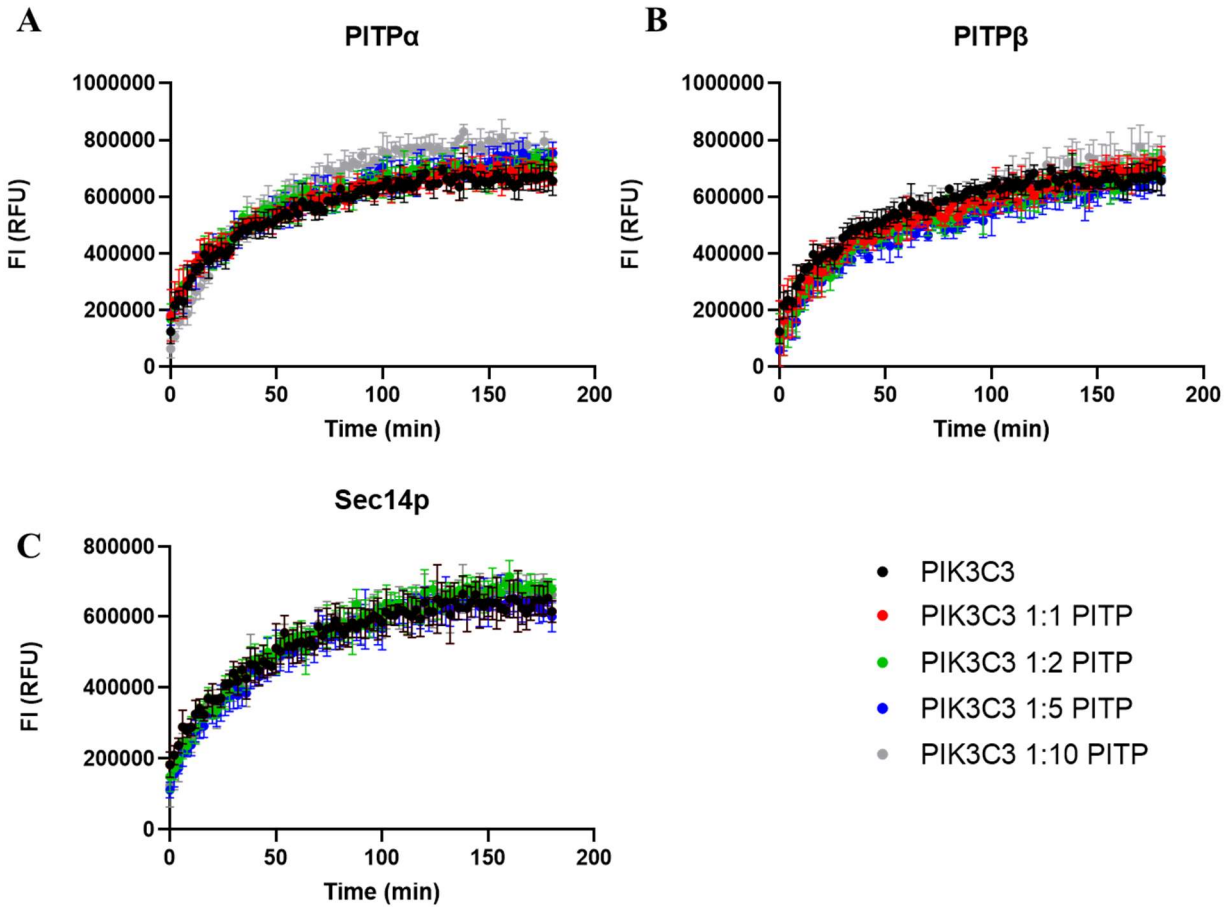

Figure 41: Activity of PIK3C3 in the presence of growing concentrations of PITPs. The activity of 22 nM PIK3C3 was assayed in the presence of 1 to 10 molar equivalents of PITPα (**41A**), PITPβ (**41B**) and Sec14p (**41C**). Reactions contained 0.2 mg/mL (50:25:25) PI:PC:PS and 10 µM ATP in 1X Assay Buffer. No significant effect on the lipid kinase activity was elicited by the protein partners at any of the concentrations tested. Error bar = SD based on 4 technical repeats.

5 CONCLUSION AND FUTURE DIRECTIONS

In addition to the expression and improved purification of recombinant PI4K-IIIβ, PITPα, PITPβ and Sec14p, the present study describes the optimization of a time-resolved, vesicle-based fluorescence intensity assay originally designed for an endpoint format. Importantly, our approach allows the monitoring of lipid kinase activity using liposomes, a substrate that much better mimics the physical features of biological membranes compared to widely employed lipid-detergent mixed micelles. Challenges previously observed in the assay such as unexpected behaviour of controls and high signal levels caused by non-productive ATP hydrolysis were addressed here by an optimized protocol, empirically finding an [ATP] that was optimal for our conditions, as well as removing co-purifying chaperones from our protein preparations. Also, the assay sensitivity and max FI window were improved by adjusting the concentration of ADP antibody to an experimentally determined concentration and by monitoring very low substrate conversion rates. With these settings, we obtained an *in vitro* assay that produces a time-resolved FI-signal proportional to the concentration of active enzyme used, and where both a negative (wortmannin) and a positive (Triton X-100) regulator of PI4K-IIIβ activity reproduced the behaviours previously documented (Balla & Balla, 2006).

Notwithstanding these successes, our assay could not detect any significant enhancement in the lipid kinase activity of PI4K-IIIβ and PIK3C3 caused by PITPs. Although we observed a 40% increase in the activity of *E. coli* expressed PI4K-IIIβ by Sec14p, similar results were not reproduced when using the insect cell derived lipid kinase. Since the commercially sourced enzyme is more active than its in-house produced counterpart, it was expected that a similar (or greater) activity stimulation by PITPs would be noticed in some of the various conditions tested.

Estimates suggest that Sec14p could execute as many as 10 ligand exchange cycles every 2 seconds (Bankaitis et al., 2010), implying that even if we consider early reaction times (up to t = 40 min), there is more than enough time for PI-carrying Sec14p (or the other tested PITPs) to collide with PI4K-IIIβ *in vitro*. Assuming that an encounter between these proteins is thus very probable, the lack of observable enhancement on the activity of the lipid kinase in the present work may speak to the difficulty in testing the proposed lipid presentation model *in vitro*. In fact, this difficulty was expressed by others (Lipp et al., 2020; Nile et al., 2010). Perhaps the addition of other protein partners (NCS-1, ABDC3, 14-3-3, etc.) that are essential for PI4K-IIIβ activity *in vivo* (Bourne et al., 2001; Hausser et al., 2006; Klima et al., 2016) could offer a better scaffold for *in vitro* testing of the presentation model by PITPs (**Figure 43A**). Alternatively, relying on the direct monitoring of PI(4)P production rather than on the ADP by-product (as is the case in the present study) may offer enhanced sensitivity when assessing PI4K activity. Indeed, all studies reporting enhancement in the lipid kinase activity of PI3Ks or PI4K-IIIβ resorted to direct PIP detection (Hubner et al., 1998; Kular et al., 2002; Panaretou et al., 1997; Schaaf et al., 2008), although employing currently undesirable radiolabelled reagents. The much safer Transcreener® ADP^2 FI Assay technology, on the other hand, suffers from a non-linear relationship between generated ADP and FI signal, which was also noticed by others (Hong et al., 2009; H. Li et al., 2009).

That PITPs are essential to maintaining the homeostasis of PI/PC in the cell is unquestionable, as repeatedly shown and reviewed elsewhere (Bankaitis et al., 2010; Cockcroft & Carvou, 2007; Lipp et al., 2020). However, the same level of evidence is still lacking for a PI presentation mechanism based on the heterotypic ligand exchange. Arguing against this model is the observation that a Sec14p mutant devoid of PC-binding (and thus of performing PI/PC

exchange) elicited the same enhancement on PI4K-IIIβ activity as the wt Sec14p (Schaaf et al., 2008). In light of this evidence, and if PITPs *de facto* stimulate the activity of PI4Ks *in vivo*, this could be effected rather by a PI-priming mechanism whereby PITPs render PI more accessible a substrate to the lipid kinase than when this ligand is embedded into vesicles (Schaaf et al., 2008). In a more simplistic hypothesis, the impact of Sec14p and other PITPs on the activity of PI4Ks would solely rely on ensuring that adequate levels of PI are available in membranes. The results of the present work may offer supporting evidence of this hypothesis. As previously shown, the lack of proper Sec14p activity resulted in reduced levels of PI(4)P at the Golgi surface and a 2-fold decrease of the aforementioned PIP in the cell (Schaaf et al., 2008).

Membrane-spanning PI (bola-PI) would be an ideal probe to test the lipid presentation mechanism proposed by others if this mechanism truly takes place. Since the two headgroups are connected in bolalipids, lifting such a molecule from the lipid bilayer is prevented by the polar nature of the opposing headgroup, which cannot enter the hydrophobic zone (**Figure 42**). The Atkinson group has recently synthesized a photocleavable version of bola-PC (Wilson et al., 2023), which following conversion to an inositol headgroup will be an invaluable tool in a time-resolved PI4K-IIIβ assay as this bolalipid is easily cleavable into a “normal” chain length phospholipid by exposure to a specific wavelength of light. Added to ongoing efforts by our group on developing an assay that directly detects PI(4)P production, tests with bola-PI containing vesicles should offer unequivocal insights on whether and how a heterotypic exchange-based presentation mechanism happens *in vitro*.

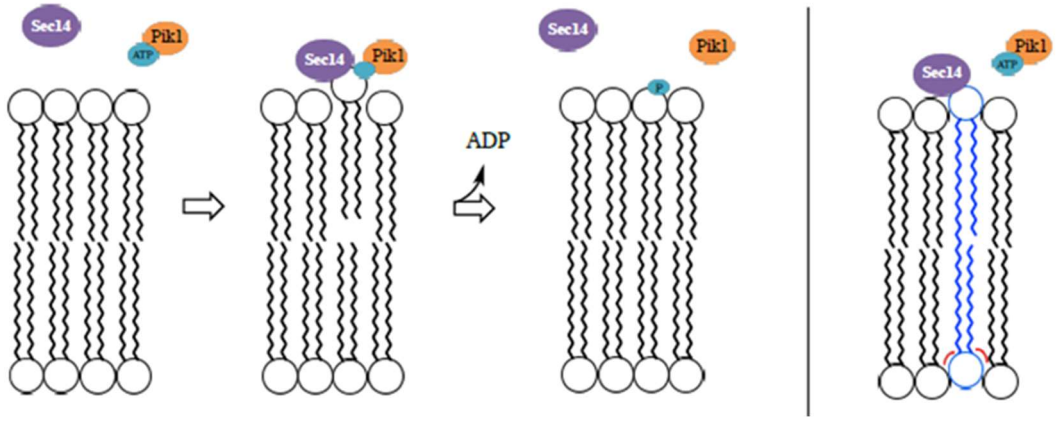

Figure 42: Testing the proposed PI presentation mechanism with membrane-spanning bola-PI. The heterotypic exchange-based presentation mechanism posits that Sec14p lifts PI from a phospholipid bilayer, thus presenting it to the yeast PI4K Pik1. Bola-PI cannot be lifted from the lipid bilayer as the inositol headgroup, linked by a membrane-spanning acyl chain to another inositol headgroup, cannot enter the lipid bilayer hydrophobic zone.

Of importance, some evidence suggests that the regulation of PI/PC and PIP homeostasis might be more complex than once thought. Early studies showed that a Sec14p mutant that could bind PC, but not PI, rescued lethality in yeast thus indicating that Sec14p's main function may not be that of PI binding/transfer (Phillips et al., 1999). In a recent report, pharmacological inhibition of PITPα and PITPβ in human cell culture reduced plasma membrane PI(4)P levels, without affecting PI(4)P at the Golgi membrane (F.-L. Li et al., 2022). In the above conditions, PI pools at the Golgi membrane might have been maintained by vesicular trafficking from ER and/or by other PITPs such as class II PITP Nir2 in humans (also called PITPnm1), which has been shown to localize to the Golgi and ER membranes (Lete et al., 2020). **Figure 43B** illustrates a scenario whereby PITPs other than PITPα/β in humans might contribute to sufficient PI pools at the Golgi membrane, thus enabling PI(4)P synthesis by PI4K-IIIβ.

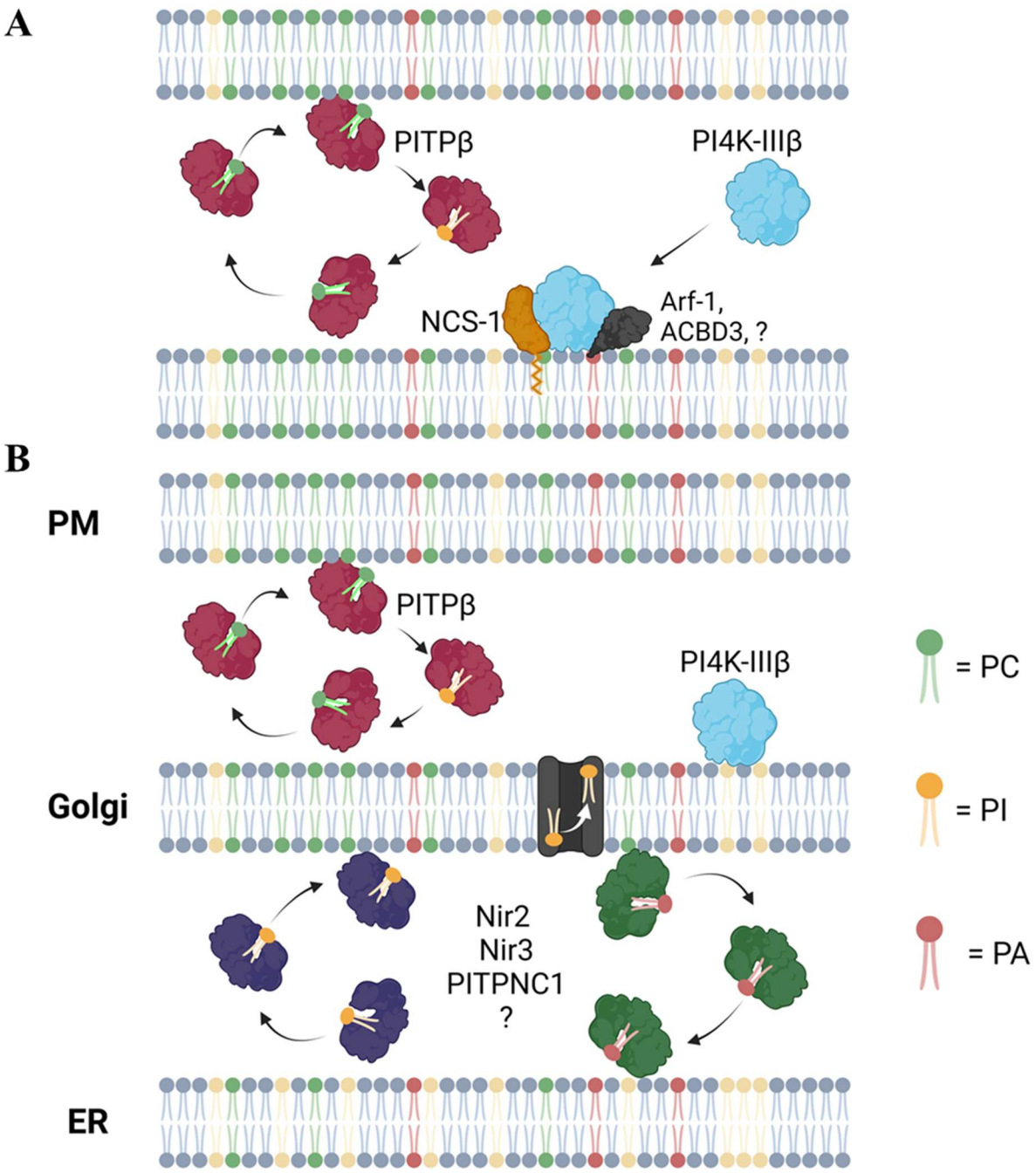

Figure 43: Alternatives to the proposed heterotypic lipid exchange-based enhancement of PI4K-IIIβ activity. 43A: PI4K-IIIβ may need binding human partners like NCS-1, Arf-1, ACBD3, etc. to be properly recruited to membranes. Only then may the *in vitro* assay employed in the present study report an enhancement in lipid kinase activity elicited by PITPs. **43B:** In humans, adequate supplies of PI at the Golgi membrane may also be secured by class II PITPs like Nir2, Nir3, PITPNC1. Created with Biorender.com.

Current medicinal chemistry efforts elsewhere include targeting both PI4K-IIIβ (Boura & Nencka, 2015; Burke et al., 2022) and PITPs (Bankaitis et al., 2022; Nile et al., 2014), which is not surprising given the importance of phosphoinositide signalling for the normal functioning of eukaryotic cells (including pathogenic fungi) and the involvement of PIPs in viral replication. However, better understanding of the regulation of PI4Ks and the effect, if any, of PITPs on lipid kinase activities remain a goal in the scientific community. Even though the present study was unable to report the anticipated lipid kinase activity stimulation, the results offer insight to analytical approaches to test lipid kinases and their potential protein regulators. Moreover, the protocol established herein may be useful when testing other kinases, which are numerous and indispensable in health and disease (Cohen, 2002), in a time-resolved manner.

6 REFERENCES

Adams, J. A. (2001). Kinetic and Catalytic Mechanisms of Protein Kinases. *Chemical Reviews*, *101*(8), 2271–2290. https://doi.org/10.1021/cr000230w

ADP-Glo™ Lipid Kinase Systems—Technical Manual. (2022). Promega. https://www.promega.ca/-/media/files/resources/protocols/technical-manuals/101/adp-glo-lipid-kinase-assay-protocol.pdf?rev=cd91960fd7fe4e2793ed2d10dd6709bf&sc_lang=en

Alb, J. G., Cortese, J. D., Phillips, S. E., Albin, R. L., Nagy, T. R., Hamilton, B. A., & Bankaitis, V. A. (2003). Mice Lacking Phosphatidylinositol Transfer Protein-α Exhibit Spinocerebellar Degeneration, Intestinal and Hepatic Steatosis, and Hypoglycemia. *Journal of Biological Chemistry*, *278*(35), 33501–33518. https://doi.org/10.1074/jbc.M303591200

Alb, J. G., Phillips, S. E., Rostand, K., Cui, X., Pinxteren, J., Cotlin, L., Manning, T., Guo, S., York, J. D., Sontheimer, H., Collawn, J. F., & Bankaitis, V. A. (2002). Genetic Ablation of Phosphatidylinositol Transfer Protein Function in Murine Embryonic Stem Cells. *Molecular Biology of the Cell*, *13*(3), 739–754. https://doi.org/10.1091/mbc.01-09-0457

Balla, A., & Balla, T. (2006). Phosphatidylinositol 4-kinases: Old enzymes with emerging functions. *Trends in Cell Biology*, *16*(7), 351–361. https://doi.org/10.1016/j.tcb.2006.05.003

Bankaitis, V. A., Mousley, C. J., & Schaaf, G. (2010). The Sec14 superfamily and mechanisms for crosstalk between lipid metabolism and lipid signaling. *Trends in Biochemical Sciences*, *35*(3), 150–160. https://doi.org/10.1016/j.tibs.2009.10.008

Bankaitis, V. A., Tripathi, A., Chen, X.-R., & Igumenova, T. I. (2022). New strategies for combating fungal infections: Inhibiting inositol lipid signaling by targeting Sec14 phosphatidylinositol transfer proteins. *Advances in Biological Regulation*, *84*, 100891. https://doi.org/10.1016/j.jbior.2022.100891

Baptist, M. (2016). *The Ligand and Membrane-binding Behaviour of the Phosphatidylinositol Transfer Proteins (PITPa & PITPb)* [Brock University]. http://hdl.handle.net/10464/8575

Baptist, M., Panagabko, C., Cockcroft, S., & Atkinson, J. (2016). Ligand and membrane-binding behavior of the phosphatidylinositol transfer proteins PITPα and PITPβ. *Biochemistry and Cell Biology*, *94*(6), 528–533. https://doi.org/10.1139/bcb-2015-0152

Belval, L., Marquette, A., Mestre, P., Piron, M.-C., Demangeat, G., Merdinoglu, D., & Chich, J.-F. (2015). A fast and simple method to eliminate Cpn60 from functional recombinant proteins produced by E. coli Arctic Express. *Protein Expression and Purification*, *109*, 29–34. https://doi.org/10.1016/j.pep.2015.01.009

Boura, E., & Nencka, R. (2015). Phosphatidylinositol 4-kinases: Function, structure, and inhibition. *Experimental Cell Research*, *337*(2), 136–145. https://doi.org/10.1016/j.yexcr.2015.03.028

Bourne, Y., Dannenberg, J., Pollmann, V., Marchot, P., & Pongs, O. (2001). Immunocytochemical Localization and Crystal Structure of Human Frequenin (Neuronal Calcium Sensor 1). *Journal of Biological Chemistry*, *276*(15), 11949–11955. https://doi.org/10.1074/jbc.M009373200

Bradford, M. M. (1976). A rapid and sensitive method for the quantitation of microgram quantities of protein utilizing the principle of protein-dye binding. *Analytical Biochemistry*, *72*(1–2), 248–254. https://doi.org/10.1016/0003-2697(76)90527-3

Burke, J. E., Inglis, A. J., Perisic, O., Masson, G. R., McLaughlin, S. H., Rutaganira, F., Shokat, K. M., & Williams, R. L. (2014). Structures of PI4KIIIβ complexes show simultaneous recruitment of Rab11 and its effectors. *Science*, *344*(6187), 1035–1038. https://doi.org/10.1126/science.1253397

Burke, J. E., Triscott, J., Emerling, B. M., & Hammond, G. R. V. (2022). Beyond PI3Ks: Targeting phosphoinositide kinases in disease. *Nature Reviews Drug Discovery*. https://doi.org/10.1038/s41573-022-00582-5

Candiano, G., Bruschi, M., Musante, L., Santucci, L., Ghiggeri, G. M., Carnemolla, B., Orecchia, P., Zardi, L., & Righetti, P. G. (2004). Blue silver: A very sensitive colloidal Coomassie G-250 staining for proteome analysis. *ELECTROPHORESIS*, *25*(9), 1327–1333. https://doi.org/10.1002/elps.200305844

Carpenter, C. L., & Cantley, L. C. (1990). Phosphoinositide kinases. *Biochemistry*, *29*(51), 11147–11156. https://doi.org/10.1021/bi00503a001

Carvou, N., Holic, R., Li, M., Futter, C., Skippen, A., & Cockcroft, S. (2010). Phosphatidylinositol- and phosphatidylcholine-transfer activity of PITPβ is essential for COPI-mediated retrograde transport from the Golgi to the endoplasmic reticulum. *Journal of Cell Science*, *123*(8), 1262–1273. https://doi.org/10.1242/jcs.061986

Casares, D., Escribá, P. V., & Rosselló, C. A. (2019). Membrane Lipid Composition: Effect on Membrane and Organelle Structure, Function and Compartmentalization and Therapeutic Avenues. *International Journal of Molecular Sciences*, *20*(9), 2167. https://doi.org/10.3390/ijms20092167

Chalupska, D., Eisenreichova, A., Różycki, B., Rezabkova, L., Humpolickova, J., Klima, M., & Boura, E. (2017). Structural analysis of phosphatidylinositol 4-kinase IIIβ (PI4KB) – 14-3-3 protein complex reveals internal flexibility and explains 14-3-3 mediated protection from degradation in vitro. *Journal of Structural Biology*, *200*(1), 36–44. https://doi.org/10.1016/j.jsb.2017.08.006

Chalupska, D., Różycki, B., Humpolickova, J., Faltova, L., Klima, M., & Boura, E. (2019). Phosphatidylinositol 4-kinase IIIβ (PI4KB) forms highly flexible heterocomplexes that include ACBD3, 14-3-3, and Rab11 proteins. *Scientific Reports*, *9*(1), 567. https://doi.org/10.1038/s41598-018-37158-6

Chattopadhyay, A. (1990). Chemistry and biology of N-(7-nitrobenz-2-oxa-1,3-diazol-4-yl)-labeled lipids: Fluorescent probes of biological and model membranes. *Chemistry and Physics of Lipids*, *53*(1), 1–15. https://doi.org/10.1016/0009-3084(90)90128-E

Chen, G., Porter, M. D., Bristol, J. R., Fitzgibbon, M. J., & Pazhanisamy, S. (2000). Kinetic Mechanism of the p38-α MAP Kinase: Phosphoryl Transfer to Synthetic Peptides. *Biochemistry*, *39*(8), 2079–2087. https://doi.org/10.1021/bi9919495

Christensen, S., Rämisch, S., & André, I. (2022). DnaK response to expression of protein mutants is dependent on translation rate and stability. *Communications Biology*, *5*(1), 597. https://doi.org/10.1038/s42003-022-03542-2

Cockcroft, S., & Carvou, N. (2007). Biochemical and biological functions of class I phosphatidylinositol transfer proteins. *Biochimica et Biophysica Acta (BBA) - Molecular and Cell Biology of Lipids*, *1771*(6), 677–691. https://doi.org/10.1016/j.bbalip.2007.03.009

Cockcroft, S., & Raghu, P. (2016). Topological organisation of the phosphatidylinositol 4,5-bisphosphate–phospholipase C resynthesis cycle: PITPs bridge the ER–PM gap. *Biochemical Journal*, *473*(23), 4289–4310. https://doi.org/10.1042/BCJ20160514C

Cohen, P. (2002). Protein kinases—The major drug targets of the twenty-first century? *Nature Reviews Drug Discovery*, *1*(4), 309–315. https://doi.org/10.1038/nrd773

De Craene, J.-O., Bertazzi, D., Bär, S., & Friant, S. (2017). Phosphoinositides, Major Actors in Membrane Trafficking and Lipid Signaling Pathways. *International Journal of Molecular Sciences*, *18*(3), 634. https://doi.org/10.3390/ijms18030634

De Matteis, M. A., Wilson, C., & D'Angelo, G. (2013). Phosphatidylinositol-4-phosphate: The Golgi and beyond: Prospects & Overviews. *BioEssays*, *35*(7), 612–622. https://doi.org/10.1002/bies.201200180

De Vries, K. J., Heinrichs, A. A. J., Cunningham, E., Brunink, F., Westerman, J., Somerharju, P. J., Cockcroft, S., Wirtz, K. W. A., & Snoek, G. T. (1995). An isoform of the phosphatidylinositol-transfer protein transfers sphingomyelin and is associated with the Golgi system. *Biochemical Journal*, *310*(2), 643–649. https://doi.org/10.1042/bj3100643

Demian, D. J., Clugston, S. L., Foster, M. M., Rameh, L., Sarkes, D., Townson, S. A., Yang, L., Zhang, M., & Charlton, M. E. (2009). High-Throughput, Cell-Free, Liposome-Based Approach for Assessing In Vitro Activity of Lipid Kinases. *SLAS Discovery*, *14*(7), 838–844. https://doi.org/10.1177/1087057109339205

Dornan, G. L., McPhail, J. A., & Burke, J. E. (2016). Type III phosphatidylinositol 4 kinases: Structure, function, regulation, signalling and involvement in disease. *Biochemical Society Transactions*, *44*(1), 260–266. https://doi.org/10.1042/BST20150219

Downing, G. J., Kim, S., Nakanishi, S., Catt, K. J., & Balla, T. (1996). Characterization of a Soluble Adrenal Phosphatidylinositol 4-Kinase Reveals Wortmannin Sensitivity of Type III

Phosphatidylinositol Kinases. *Biochemistry*, *35*(11), 3587–3594. https://doi.org/10.1021/bi9517493

Drozdetskiy, A., Cole, C., Procter, J., & Barton, G. J. (2015). JPred4: A protein secondary structure prediction server. *Nucleic Acids Research*, *43*(W1), W389–W394. https://doi.org/10.1093/nar/gkv332

Fahy, E., Subramaniam, S., Murphy, R. C., Nishijima, M., Raetz, C. R. H., Shimizu, T., Spener, F., van Meer, G., Wakelam, M. J. O., & Dennis, E. A. (2009). Update of the LIPID MAPS comprehensive classification system for lipids. *Journal of Lipid Research*, *50*, S9–S14. https://doi.org/10.1194/jlr.R800095-JLR200

Flanagan, C. A., & Thorner, J. (1992). Purification and characterization of a soluble phosphatidylinositol 4-kinase from the yeast Saccharomyces cerevisiae. *The Journal of Biological Chemistry*, *267*(33), 24117–24125.

Fowler, M. L., McPhail, J. A., Jenkins, M. L., Masson, G. R., Rutaganira, F. U., Shokat, K. M., Williams, R. L., & Burke, J. E. (2016). Using hydrogen deuterium exchange mass spectrometry to engineer optimized constructs for crystallization of protein complexes: Case study of PI4KIIIβ with Rab11: HDX-MS to Crystallize PI4KIIIβ with Rab11. *Protein Science*, *25*(4), 826–839. https://doi.org/10.1002/pro.2879

Francis, D. M., & Page, R. (2010). Strategies to Optimize Protein Expression in *E. coli*. *Current Protocols in Protein Science*, *61*(1). https://doi.org/10.1002/0471140864.ps0524s61

Fruman, D. A., Meyers, R. E., & Cantley, L. C. (1998). PHOSPHOINOSITIDE KINASES. *Annual Review of Biochemistry*, *67*(1), 481–507. https://doi.org/10.1146/annurev.biochem.67.1.481

Gao, T., Gu, S., Mu, C., Zhang, M., Yang, J., Liu, P., & Li, G. (2017). Electrochemical assay of lipid kinase activity facilitated by liposomes. *Electrochimica Acta*, *252*, 362–367. https://doi.org/10.1016/j.electacta.2017.08.190

Gericke, A., Leslie, N. R., Lösche, M., & Ross, A. H. (2013). PtdIns(4,5)P2-Mediated Cell Signaling: Emerging Principles and PTEN as a Paradigm for Regulatory Mechanism. In D. G. S. Capelluto (Ed.), *Lipid-mediated Protein Signaling* (Vol. 991, pp. 85–104). Springer Netherlands. https://doi.org/10.1007/978-94-007-6331-9_6

Godi, A., Pertile, P., Meyers, R., Marra, P., Di Tullio, G., Iurisci, C., Luini, A., Corda, D., & De Matteis, M. A. (1999). ARF mediates recruitment of PtdIns-4-OH kinase-β and stimulates synthesis of PtdIns(4,5)P2 on the Golgi complex. *Nature Cell Biology*, *1*(5), 280–287. https://doi.org/10.1038/12993

Grabon, A., Bankaitis, V. A., & McDermott, M. I. (2019). The interface between phosphatidylinositol transfer protein function and phosphoinositide signaling in higher eukaryotes. *Journal of Lipid Research*, *60*(2), 242–268. https://doi.org/10.1194/jlr.R089730

Guzman, L. M., Belin, D., Carson, M. J., & Beckwith, J. (1995). Tight regulation, modulation, and high-level expression by vectors containing the arabinose PBAD promoter. *Journal of Bacteriology*, *177*(14), 4121–4130. https://doi.org/10.1128/jb.177.14.4121-4130.1995

Hammond, G. R. V., Fischer, M. J., Anderson, K. E., Holdich, J., Koteci, A., Balla, T., & Irvine, R. F. (2012). PI4P and PI(4,5)P $_2$ Are Essential But Independent Lipid Determinants of Membrane Identity. *Science*, *337*(6095), 727–730. https://doi.org/10.1126/science.1222483

Hausser, A., Link, G., Hoene, M., Russo, C., Selchow, O., & Pfizenmaier, K. (2006). Phospho-specific binding of 14-3-3 proteins to phosphatidylinositol 4-kinase III β protects from dephosphorylation and stabilizes lipid kinase activity. *Journal of Cell Science*, *119*(17), 3613–3621. https://doi.org/10.1242/jcs.03104

Hausser, A., Storz, P., Märtens, S., Link, G., Toker, A., & Pfizenmaier, K. (2005). Protein kinase D regulates vesicular transport by phosphorylating and activating phosphatidylinositol-4 kinase IIIβ at the Golgi complex. *Nature Cell Biology*, *7*(9), 880–886. https://doi.org/10.1038/ncb1289

Haynes, L. P., Thomas, G. M. H., & Burgoyne, R. D. (2005). Interaction of Neuronal Calcium Sensor-1 and ADP-ribosylation Factor 1 Allows Bidirectional Control of Phosphatidylinositol 4-Kinase β and trans-Golgi Network-Plasma Membrane Traffic. *Journal of Biological Chemistry*, *280*(7), 6047–6054. https://doi.org/10.1074/jbc.M413090200

He, Y., Sun, M. M., Zhang, G. G., Yang, J., Chen, K. S., Xu, W. W., & Li, B. (2021). Targeting PI3K/Akt signal transduction for cancer therapy. *Signal Transduction and Targeted Therapy*, *6*(1), 425. https://doi.org/10.1038/s41392-021-00828-5

Hilpelä, P., Vartiainen, M. K., & Lappalainen, P. (2004). Regulation of the Actin Cytoskeleton by PI(4,5)P2 and PI(3,4,5)P3. In H. Stenmark (Ed.), *Phosphoinositides in Subcellular Targeting and Enzyme Activation* (Vol. 282, pp. 117–163). Springer Berlin Heidelberg. https://doi.org/10.1007/978-3-642-18805-3_5

Holič, R., Šťastný, D., & Griač, P. (2021). Sec14 family of lipid transfer proteins in yeasts. *Biochimica et Biophysica Acta (BBA) - Molecular and Cell Biology of Lipids*, *1866*(10), 158990. https://doi.org/10.1016/j.bbalip.2021.158990

Hong, L., Quinn, C. M., & Jia, Y. (2009). Evaluating the utility of the HTRF® Transcreener™ ADP assay technology: A comparison with the standard HTRF assay technology. *Analytical Biochemistry*, *391*(1), 31–38. https://doi.org/10.1016/j.ab.2009.04.033

Hubner, S., Couvillon, A. D., Kas, J. A., Bankaitis, V. A., Vegners, R., Carpenter, C. L., & Janmey, P. A. (1998). Enhancement of phosphoinositide 3-kinase (PI 3-kinase) activity by membrane curvature and inositol-phospholipid-binding peptides. *European Journal of Biochemistry*, *258*(2), 846–853. https://doi.org/10.1046/j.1432-1327.1998.2580846.x

Ile, K. E., Schaaf, G., & Bankaitis, V. A. (2006). Phosphatidylinositol transfer proteins and cellular nanoreactors for lipid signaling. *Nature Chemical Biology*, *2*(11), 576–583. https://doi.org/10.1038/nchembio835

Jencks, W. P. (2006). Binding Energy, Specificity, and Enzymic Catalysis: The Circe Effect. In A. Meister (Ed.), *Advances in Enzymology—And Related Areas of Molecular Biology* (pp. 219–410). John Wiley & Sons, Inc. https://doi.org/10.1002/9780470122884.ch4

Jia, B., & Jeon, C. O. (2016). High-throughput recombinant protein expression in *Escherichia coli*: Current status and future perspectives. *Open Biology*, *6*(8), 160196. https://doi.org/10.1098/rsob.160196

Klima, M., Tóth, D. J., Hexnerova, R., Baumlova, A., Chalupska, D., Tykvart, J., Rezabkova, L., Sengupta, N., Man, P., Dubankova, A., Humpolickova, J., Nencka, R., Veverka, V., Balla, T., & Boura, E. (2016). Structural insights and in vitro reconstitution of membrane targeting and activation of human PI4KB by the ACBD3 protein. *Scientific Reports*, *6*(1), 23641. https://doi.org/10.1038/srep23641

Klink, T. A., Kleman-Leyer, K. M., Kopp, A., Westermeyer, T. A., & Lowery, R. G. (2008). Evaluating PI3 Kinase Isoforms Using Transcreener™ ADP Assays. *SLAS Discovery*, *13*(6), 476–485. https://doi.org/10.1177/1087057108319864

Kular, G. S., Chaudhary, A., Prestwich, G., Swigart, P., Wetzker, R., & Cockcroft, S. (2002). Co-operation of phosphatidylinositol transfer protein with phosphoinositide 3-kinase γ in vitro. *Advances in Enzyme Regulation*, *42*, 53–61. https://doi.org/10.1016/S0065-2571(01)00023-1

Kumar, M. (2021, December 14). *Transcreener ADP2 FI Assay—Troubleshooting* [Personal communication].

Lete, M. G., Tripathi, A., Chandran, V., Bankaitis, V. A., & McDermott, M. I. (2020). Lipid transfer proteins and instructive regulation of lipid kinase activities: Implications for inositol lipid signaling and disease. *Advances in Biological Regulation*, *78*, 100740. https://doi.org/10.1016/j.jbior.2020.100740

Li, F.-L., Fu, V., Liu, G., Tang, T., Konradi, A. W., Peng, X., Kemper, E., Cravatt, B. F., Franklin, J. M., Wu, Z., Mayfield, J., Dixon, J. E., Gerwick, W. H., & Guan, K.-L. (2022). Hippo pathway regulation by phosphatidylinositol transfer protein and phosphoinositides. *Nature Chemical Biology*, *18*(10), 1076–1086. https://doi.org/10.1038/s41589-022-01061-z

Li, H., Totoritis, R. D., Lor, L. A., Schwartz, B., Caprioli, P., Jurewicz, A. J., & Zhang, G. (2009). Evaluation of an Antibody-Free ADP Detection Assay: ADP-Glo. *ASSAY and Drug Development Technologies*, *7*(6), 598–605. https://doi.org/10.1089/adt.2009.0221

Li, X., Rivas, M. P., Fang, M., Marchena, J., Mehrotra, B., Chaudhary, A., Feng, L., Prestwich, G. D., & Bankaitis, V. A. (2002). Analysis of oxysterol binding protein homologue Kes1p function in regulation of Sec14p-dependent protein transport from the yeast Golgi complex. *Journal of Cell Biology*, *157*(1), 63–78. https://doi.org/10.1083/jcb.200201037

Liébecq, C., International Union of Biochemistry and Molecular Biology, & International Union of Biochemistry and Molecular Biology (Eds.). (1992). *Biochemical nomenclature and related documents: A compendium* (2nd ed). Portland Press.

Lipp, N.-F., Ikhlef, S., Milanini, J., & Drin, G. (2020). Lipid Exchangers: Cellular Functions and Mechanistic Links With Phosphoinositide Metabolism. *Frontiers in Cell and Developmental Biology*, *8*, 663. https://doi.org/10.3389/fcell.2020.00663

Lo, W.-T., Zhang, Y., Vadas, O., Roske, Y., Gulluni, F., De Santis, M. C., Zagar, A. V., Stephanowitz, H., Hirsch, E., Liu, F., Daumke, O., Kudryashev, M., & Haucke, V. (2022). Structural basis of phosphatidylinositol 3-kinase C2α function. *Nature Structural & Molecular Biology*, *29*(3), 218–228. https://doi.org/10.1038/s41594-022-00730-w

Lowery, R. G., & Kleman-Leyer, K. (2006). Transcreener™: Screening enzymes involved in covalent regulation. *Expert Opinion on Therapeutic Targets*, *10*(1), 179–190. https://doi.org/10.1517/14728222.10.1.179

Matos, C., Moutinho, C., & Lobão, P. (2012). Liposomes as a Model for the Biological Membrane: Studies on Daunorubicin Bilayer Interaction. *The Journal of Membrane Biology*, *245*(2), 69–75. https://doi.org/10.1007/s00232-011-9414-2

Mazal, H., Aviram, H., Riven, I., & Haran, G. (2018). Effect of ligand binding on a protein with a complex folding landscape. *Physical Chemistry Chemical Physics*, *20*(5), 3054–3062. https://doi.org/10.1039/C7CP03327C

McPhail, J. A., & Burke, J. E. (2023). Molecular mechanisms of PI4K regulation and their involvement in viral replication. *Traffic*, *24*(3), 131–145. https://doi.org/10.1111/tra.12841

Meehan, K. (2019). *The Development of a Time-Resolved, Vesicle-Based, Fluorescence Assay for the Activity of the Lipid Kinase Pik1*. Brock University. http://hdl.handle.net/10464/14556

Mejdrová, I., Chalupská, D., Kögler, M., Šála, M., Plačková, P., Baumlová, A., Hřebabecký, H., Procházková, E., Dejmek, M., Guillon, R., Strunin, D., Weber, J., Lee, G., Birkus, G., Mertlíková-Kaiserová, H., Boura, E., & Nencka, R. (2015). Highly Selective Phosphatidylinositol 4-Kinase IIIβ Inhibitors and Structural Insight into Their Mode of Action. *Journal of Medicinal Chemistry*, *58*(9), 3767–3793. https://doi.org/10.1021/acs.jmedchem.5b00499

Meyers, R., & Cantley, L. C. (1997). Cloning and Characterization of a Wortmannin-sensitive Human Phosphatidylinositol 4-Kinase. *Journal of Biological Chemistry*, *272*(7), 4384–4390. https://doi.org/10.1074/jbc.272.7.4384

Morales, E. S., Parcerisa, I. L., & Ceccarelli, E. A. (2019). A novel method for removing contaminant Hsp70 molecular chaperones from recombinant proteins. *Protein Science*, *28*(4), 800–807. https://doi.org/10.1002/pro.3574

Mukherjee, P., Madarati, H., Ridgway, N. D., & Atkinson, J. (2018). Lipid and membrane recognition by the oxysterol binding protein and its phosphomimetic mutant using dual polarization interferometry. *Biochimica et Biophysica Acta (BBA) - Biomembranes*, *1860*(11), 2356–2365. https://doi.org/10.1016/j.bbamem.2018.05.022

Nakatsu, F., Baskin, J. M., Chung, J., Tanner, L. B., Shui, G., Lee, S. Y., Pirruccello, M., Hao, M., Ingolia, N. T., Wenk, M. R., & De Camilli, P. (2012). PtdIns4P synthesis by PI4KIIIα at the plasma membrane and its impact on plasma membrane identity. *Journal of Cell Biology*, *199*(6), 1003–1016. https://doi.org/10.1083/jcb.201206095

Nile, A. H., Bankaitis, V. A., & Grabon, A. (2010). Mammalian diseases of phosphatidylinositol transfer proteins and their homologs. *Clinical Lipidology*, *5*(6), 867–897. https://doi.org/10.2217/clp.10.67

Nile, A. H., Tripathi, A., Yuan, P., Mousley, C. J., Suresh, S., Wallace, I. M., Shah, S. D., Pohlhaus, D. T., Temple, B., Nislow, C., Giaever, G., Tropsha, A., Davis, R. W., St. Onge, R. P., & Bankaitis, V. A. (2014). PITPs as targets for selectively interfering with phosphoinositide signaling in cells. *Nature Chemical Biology*, *10*(1), 76–84. https://doi.org/10.1038/nchembio.1389

Panagabko, C., Baptist, M., & Atkinson, J. (2019). In vitro lipid transfer assays of phosphatidylinositol transfer proteins provide insight into the in vivo mechanism of ligand transfer. *Biochimica et Biophysica Acta (BBA) - Biomembranes*, *1861*(3), 619–630. https://doi.org/10.1016/j.bbamem.2018.12.003

Panagabko, C., Morley, S., Hernandez, M., Cassolato, P., Gordon, H., Parsons, R., Manor, D., & Atkinson, J. (2003). Ligand Specificity in the CRAL-TRIO Protein Family. *Biochemistry*, *42*(21), 6467–6474. https://doi.org/10.1021/bi034086v

Panaretou, C., Domin, J., Cockcroft, S., & Waterfield, M. D. (1997). Characterization of p150, an Adaptor Protein for the Human Phosphatidylinositol (PtdIns) 3-Kinase. *Journal of Biological Chemistry*, *272*(4), 2477–2485. https://doi.org/10.1074/jbc.272.4.2477

Payrastre, B., Missy, K., Giuriato, S., Bodin, S., Plantavid, M., & Gratacap, M.-P. (2001). Phosphoinositides: Key players in cell signalling, in time and space. *Cellular Signalling*, *13*(6), 377–387. https://doi.org/10.1016/S0898-6568(01)00158-9

Phillips, S. E., Sha, B., Topalof, L., Xie, Z., Alb, J. G., Klenchin, V. A., Swigart, P., Cockcroft, S., Martin, T. F. J., Luo, M., & Bankaitis, V. A. (1999). Yeast Sec14p Deficient in Phosphatidylinositol Transfer Activity Is Functional In Vivo. *Molecular Cell*, *4*(2), 187–197. https://doi.org/10.1016/S1097-2765(00)80366-4

Plotkin, J. B., & Kudla, G. (2011). Synonymous but not the same: The causes and consequences of codon bias. *Nature Reviews Genetics*, *12*(1), 32–42. https://doi.org/10.1038/nrg2899

Posor, Y., Jang, W., & Haucke, V. (2022). Phosphoinositides as membrane organizers. *Nature Reviews Molecular Cell Biology*, *23*(12), 797–816. https://doi.org/10.1038/s41580-022-00490-x

Rathinaswamy, M. K., Jenkins, M. L., Zhang, X., Stariha, J. T., Ranga-Prasad, H., Dalwadi, U., Fleming, K. D., Yip, C. K., Williams, R. L., & Burke, J. E. (2022). *Molecular basis for differential activation of p101 and p84 complexes of PI3Kγ by Ras and GPCRs* [Preprint]. Biochemistry. https://doi.org/10.1101/2022.07.29.502076

Raucher, D., Stauffer, T., Chen, W., Shen, K., Guo, S., York, J. D., Sheetz, M. P., & Meyer, T. (2000). Phosphatidylinositol 4,5-Bisphosphate Functions as a Second Messenger that Regulates Cytoskeleton–Plasma Membrane Adhesion. *Cell*, *100*(2), 221–228. https://doi.org/10.1016/S0092-8674(00)81560-3

Reinisch, K. M., & Prinz, W. A. (2021). Mechanisms of nonvesicular lipid transport. *Journal of Cell Biology*, *220*(3), e202012058. https://doi.org/10.1083/jcb.202012058

Reiss, S., Harak, C., Romero-Brey, I., Radujkovic, D., Klein, R., Ruggieri, A., Rebhan, I., Bartenschlager, R., & Lohmann, V. (2013). The Lipid Kinase Phosphatidylinositol-4 Kinase III Alpha Regulates the Phosphorylation Status of Hepatitis C Virus NS5A. *PLoS Pathogens*, *9*(5), e1003359. https://doi.org/10.1371/journal.ppat.1003359

Reuberson, J., Horsley, H., Franklin, R. J., Ford, D., Neuss, J., Brookings, D., Huang, Q., Vanderhoydonck, B., Gao, L.-J., Jang, M.-Y., Herdewijn, P., Ghawalkar, A., Fallah-Arani, F., Khan, A. R., Henshall, J., Jairaj, M., Malcolm, S., Ward, E., Shuttleworth, L., … Allen, R. (2018). Discovery of a Potent, Orally Bioavailable PI4KIIIβ Inhibitor (UCB9608) Able To Significantly Prolong Allogeneic Organ Engraftment *in Vivo*. *Journal of Medicinal Chemistry*, *61*(15), 6705–6723. https://doi.org/10.1021/acs.jmedchem.8b00521

Rial, D. V., & Ceccarelli, E. A. (2002). Removal of DnaK contamination during fusion protein purifications. *Protein Expression and Purification*, *25*(3), 503–507. https://doi.org/10.1016/S1046-5928(02)00024-4

Rivas, M. P., Kearns, B. G., Xie, Z., Guo, S., Sekar, M. C., Hosaka, K., Kagiwada, S., York, J. D., & Bankaitis, V. A. (1999). Pleiotropic Alterations in Lipid Metabolism in Yeast *sac1* Mutants: Relationship to "Bypass Sec14p" and Inositol Auxotrophy. *Molecular Biology of the Cell*, *10*(7), 2235–2250. https://doi.org/10.1091/mbc.10.7.2235

Romier, C., Ben Jelloul, M., Albeck, S., Buchwald, G., Busso, D., Celie, P. H. N., Christodoulou, E., De Marco, V., Van Gerwen, S., Knipscheer, P., Lebbink, J. H., Notenboom, V., Poterszman, A., Rochel, N., Cohen, S. X., Unger, T., Sussman, J. L., Moras, D., Sixma, T. K., & Perrakis, A. (2006). Co-expression of protein complexes in prokaryotic and eukaryotic hosts: Experimental procedures, database tracking and case studies. *Acta Crystallographica Section D Biological Crystallography*, *62*(10), 1232–1242. https://doi.org/10.1107/S0907444906031003

Rudiger, S. (1997). Substrate specificity of the DnaK chaperone determined by screening cellulose-bound peptide libraries. *The EMBO Journal*, *16*(7), 1501–1507. https://doi.org/10.1093/emboj/16.7.1501

Rutaganira, F. U., Fowler, M. L., McPhail, J. A., Gelman, M. A., Nguyen, K., Xiong, A., Dornan, G. L., Tavshanjian, B., Glenn, J. S., Shokat, K. M., & Burke, J. E. (2016). Design and Structural Characterization of Potent and Selective Inhibitors of Phosphatidylinositol 4 Kinase IIIβ. *Journal of Medicinal Chemistry*, *59*(5), 1830–1839. https://doi.org/10.1021/acs.jmedchem.5b01311

Ryan, M. M., Temple, B. R. S., Phillips, S. E., & Bankaitis, V. A. (2007). Conformational Dynamics of the Major Yeast Phosphatidylinositol Transfer Protein Sec14p: Insight into the Mechanisms of Phospholipid Exchange and Diseases of Sec14p-Like Protein Deficiencies. *Molecular Biology of the Cell*, *18*(5), 1928–1942. https://doi.org/10.1091/mbc.e06-11-1024

Salis, A., & Monduzzi, M. (2016). Not only pH. Specific buffer effects in biological systems. *Current Opinion in Colloid & Interface Science*, *23*, 1–9. https://doi.org/10.1016/j.cocis.2016.04.004

Sasaki, T., Takasuga, S., Sasaki, J., Kofuji, S., Eguchi, S., Yamazaki, M., & Suzuki, A. (2009). Mammalian phosphoinositide kinases and phosphatases. *Progress in Lipid Research*, *48*(6), 307–343. https://doi.org/10.1016/j.plipres.2009.06.001

Schaaf, G., Ortlund, E. A., Tyeryar, K. R., Mousley, C. J., Ile, K. E., Garrett, T. A., Ren, J., Woolls, M. J., Raetz, C. R. H., Redinbo, M. R., & Bankaitis, V. A. (2008). Functional Anatomy of Phospholipid Binding and Regulation of Phosphoinositide Homeostasis by Proteins of the Sec14 Superfamily. *Molecular Cell*, *29*(2), 191–206. https://doi.org/10.1016/j.molcel.2007.11.026

Sha, B., Phillips, S. E., Bankaitis, V. A., & Luo, M. (1998). Crystal structure of the Saccharomyces cerevisiae phosphatidylinositol- transfer protein. *Nature*, *391*(6666), 506–510. https://doi.org/10.1038/35179

Shemesh, T., Luini, A., Malhotra, V., Burger, K. N. J., & Kozlov, M. M. (2003). Prefission Constriction of Golgi Tubular Carriers Driven by Local Lipid Metabolism: A Theoretical Model. *Biophysical Journal*, *85*(6), 3813–3827. https://doi.org/10.1016/S0006-3495(03)74796-1

Simons, J. P., Al-Shawi, R., Minogue, S., Waugh, M. G., Wiedemann, C., Evangelou, S., Loesch, A., Sihra, T. S., King, R., Warner, T. T., & Hsuan, J. J. (2009). Loss of phosphatidylinositol 4-kinase 2alpha activity causes late onset degeneration of spinal cord axons. *Proceedings of the National Academy of Sciences of the United States of America*, *106*(28), 11535–11539. https://doi.org/10.1073/pnas.0903011106

Skinner, H. B., Alb, J. G., Whitters, E. A., Helmkamp, G. M., & Bankaitis, V. A. (1993). Phospholipid transfer activity is relevant to but not sufficient for the essential function of the yeast SEC14 gene product. *The EMBO Journal*, *12*(12), 4775–4784. https://doi.org/10.1002/j.1460-2075.1993.tb06166.x

Somlyo, A. P., & Somlyo, A. V. (1994). Signal transduction and regulation in smooth muscle. *Nature*, *372*(6503), 231–236. https://doi.org/10.1038/372231a0

Srinivasan, S., Di Luca, A., John Peter, A. T., Gehin, C., Lone, M. A., Hornemann, T., D'Angelo, G., & Vanni, S. (2023). *Conformational dynamics of lipid transfer domains provide a general framework to decode their functional mechanism* [Preprint]. Biophysics. https://doi.org/10.1101/2023.04.11.536463

Stack, J. H., & Emr, S. D. (1994). Vps34p required for yeast vacuolar protein sorting is a multiple specificity kinase that exhibits both protein kinase and phosphatidylinositol-specific PI 3-kinase activities. *The Journal of Biological Chemistry*, *269*(50), 31552–31562.

Stillwell, W. (2016). *An introduction to biological membranes: Composition, structure and function* (Second edition). Academic Press is an imprint of Elsevier.

Stothard, P. (2000). The Sequence Manipulation Suite: JavaScript Programs for Analyzing and Formatting Protein and DNA Sequences. *BioTechniques*, *28*(6), 1102–1104. https://doi.org/10.2144/00286ir01

Strahl, T., Huttner, I. G., Lusin, J. D., Osawa, M., King, D., Thorner, J., & Ames, J. B. (2007). Structural Insights into Activation of Phosphatidylinositol 4-Kinase (Pik1) by Yeast Frequenin (Frq1). *Journal of Biological Chemistry*, *282*(42), 30949–30959. https://doi.org/10.1074/jbc.M705499200

Strahl, T., & Thorner, J. (2007). Synthesis and function of membrane phosphoinositides in budding yeast, Saccharomyces cerevisiae. *Biochimica et Biophysica Acta (BBA) - Molecular and Cell Biology of Lipids*, *1771*(3), 353–404. https://doi.org/10.1016/j.bbalip.2007.01.015

Structural Genomics Consortium, Architecture et Fonction des Macromolécules Biologiques, Berkeley Structural Genomics Center, China Structural Genomics Consortium, Integrated Center for Structure and Function Innovation, Israel Structural Proteomics Center, Joint Center for Structural Genomics, Midwest Center for Structural Genomics, New York Structural GenomiX Research Center for Structural Genomics, Northeast Structural Genomics Consortium, Oxford Protein Production Facility, Protein Sample Production Facility, Max Delbrück Center for Molecular Medicine, RIKEN Structural Genomics/Proteomics Initiative, & SPINE2-Complexes. (2008). Protein production and purification. *Nature Methods*, *5*(2), 135–146. https://doi.org/10.1038/nmeth.f.202

Studier, F. W. (2005). Protein production by auto-induction in high-density shaking cultures. *Protein Expression and Purification*, *41*(1), 207–234. https://doi.org/10.1016/j.pep.2005.01.016

Suer, S., Sickmann, A., Meyer, H. E., Herberg, F. W., & Heilmeyer, L. M. G. (2001). Human phosphatidylinositol 4-kinase isoform PI4K92: **Expression of the recombinant enzyme and determination of multiple phosphorylation sites**. *European Journal of Biochemistry*, *268*(7), 2099–2106. https://doi.org/10.1046/j.1432-1327.2001.02089.x

Szivak, I., Lamb, N., & Heilmeyer, L. M. G. (2006). Subcellular Localization and Structural Function of Endogenous Phosphorylated Phosphatidylinositol 4-Kinase (PI4K92). *Journal of Biological Chemistry*, *281*(24), 16740–16749. https://doi.org/10.1074/jbc.M511645200

Szoka, F., & Papahadjopoulos, D. (1980). Comparative Properties and Methods of Preparation of Lipid Vesicles (Liposomes). *Annual Review of Biophysics and Bioengineering*, *9*(1), 467–508. https://doi.org/10.1146/annurev.bb.09.060180.002343

Tilley, S. J., Skippen, A., Murray-Rust, J., Swigart, P. M., Stewart, A., Morgan, C. P., Cockcroft, S., & McDonald, N. Q. (2004). Structure-Function Analysis of Phosphatidylinositol Transfer

Protein Alpha Bound to Human Phosphatidylinositol. *Structure*, *12*(2), 317–326. https://doi.org/10.1016/j.str.2004.01.013

Transcreener® ADP FI Assay Technical Manual. (2023). Bellbrook Labs. https://www.bellbrooklabs.com/wp-content/uploads/2023/05/Tech-Manual-ADP2-FI-v050223.pdf

Tsvetkov, P. O., Roman, A. Yu., Baksheeva, V. E., Nazipova, A. A., Shevelyova, M. P., Vladimirov, V. I., Buyanova, M. F., Zinchenko, D. V., Zamyatnin, A. A., Devred, F., Golovin, A. V., Permyakov, S. E., & Zernii, E. Yu. (2018). Functional Status of Neuronal Calcium Sensor-1 Is Modulated by Zinc Binding. *Frontiers in Molecular Neuroscience*, *11*, 459. https://doi.org/10.3389/fnmol.2018.00459

Van Durme, J., Maurer-Stroh, S., Gallardo, R., Wilkinson, H., Rousseau, F., & Schymkowitz, J. (2009). Accurate Prediction of DnaK-Peptide Binding via Homology Modelling and Experimental Data. *PLoS Computational Biology*, *5*(8), e1000475. https://doi.org/10.1371/journal.pcbi.1000475

Van Meer, G., Voelker, D. R., & Feigenson, G. W. (2008). Membrane lipids: Where they are and how they behave. *Nature Reviews Molecular Cell Biology*, *9*(2), 112–124. https://doi.org/10.1038/nrm2330

Volinia, S., Dhand, R., Vanhaesebroeck, B., MacDougall, L. K., Stein, R., Zvelebil, M. J., Domin, J., Panaretou, C., & Waterfield, M. D. (1995). A human phosphatidylinositol 3-kinase complex related to the yeast Vps34p-Vps15p protein sorting system. *The EMBO Journal*, *14*(14), 3339–3348. https://doi.org/10.1002/j.1460-2075.1995.tb07340.x

Vordtriede, P. B., Doan, C. N., Tremblay, J. M., Helmkamp, G. M., & Yoder, M. D. (2005). Structure of PITPβ in Complex with Phosphatidylcholine: Comparison of Structure and Lipid Transfer to Other PITP Isoforms ‡. *Biochemistry*, *44*(45), 14760–14771. https://doi.org/10.1021/bi051191r

Wandinger, S. K., Richter, K., & Buchner, J. (2008). The Hsp90 Chaperone Machinery. *Journal of Biological Chemistry*, *283*(27), 18473–18477. https://doi.org/10.1074/jbc.R800007200

Wang, Y., Hanrahan, G., Abou Azar, F., & Mittermaier, A. (2022). Binding interactions in a kinase active site modulate background ATP hydrolysis. *Biochimica et Biophysica Acta (BBA) - Proteins and Proteomics*, *1870*(1), 140720. https://doi.org/10.1016/j.bbapap.2021.140720

Ward, N. E., & O'Brian, C. A. (1992). The intrinsic ATPase activity of protein kinase C is catalyzed at the active site of the enzyme. *Biochemistry*, *31*(25), 5905–5911. https://doi.org/10.1021/bi00140a029

Wilson, S., Panagabko, C., Laleye, T., Robinson, M., Jagas, S., Bowman, D., & Atkinson, J. (2023). Synthesis of a photocleavable bola-phosphatidylcholine. *Bioorganic & Medicinal Chemistry*, *93*, 117465. https://doi.org/10.1016/j.bmc.2023.117465

Wood, D. W. (2014). New trends and affinity tag designs for recombinant protein purification. *Current Opinion in Structural Biology*, *26*, 54–61. https://doi.org/10.1016/j.sbi.2014.04.006

Zhang, X., Vadas, O., Perisic, O., Anderson, K. E., Clark, J., Hawkins, P. T., Stephens, L. R., & Williams, R. L. (2011). Structure of Lipid Kinase p110β/p85β Elucidates an Unusual SH2-Domain-Mediated Inhibitory Mechanism. *Molecular Cell*, *41*(5), 567–578. https://doi.org/10.1016/j.molcel.2011.01.026

Zhao, L., & Vogt, P. K. (2008). Class I PI3K in oncogenic cellular transformation. *Oncogene*, *27*(41), 5486–5496. https://doi.org/10.1038/onc.2008.244

Zhao, X.-H., Bondeva, T., & Balla, T. (2000). Characterization of Recombinant Phosphatidylinositol 4-Kinase β Reveals Auto- and Heterophosphorylation of the Enzyme. *Journal of Biological Chemistry*, *275*(19), 14642–14648. https://doi.org/10.1074/jbc.275.19.14642

Zwier, J. M., Roux, T., Cottet, M., Durroux, T., Douzon, S., Bdioui, S., Gregor, N., Bourrier, E., Oueslati, N., Nicolas, L., Tinel, N., Boisseau, C., Yverneau, P., Charrier-Savournin, F., Fink, M., & Trinquet, E. (2010). A Fluorescent Ligand-Binding Alternative Using Tag-lite® Technology. *SLAS Discovery*, *15*(10), 1248–1259. https://doi.org/10.1177/1087057110384611

7 APPENDIX

4/22/22, 3:34 PM Sequence Manipulation Suite

Codon Usage results

Results for 2406 residue sequence "PI4K-IIIb " starting "atgggagata"

AmAcid	Codon	Number	/1000	Fraction	..
Arg	AGG	8.00	9.98	0.17	
Arg	AGA	6.00	7.48	0.13	
Arg	CGG	14.00	17.46	0.29	
Gly	GGG	15.00	18.70	0.33	
Gly	GGA	4.00	4.99	0.09	
Gly	GGT	4.00	4.99	0.09	
Gly	GGC	23.00	28.68	0.50	
Ile	ATA	3.00	3.74	0.07	
Ile	ATT	17.00	21.20	0.38	
Ile	ATC	25.00	31.17	0.56	
Leu	TTG	12.00	14.96	0.14	
Leu	TTA	0.00	0.00	0.00	
Leu	CTG	36.00	44.89	0.42	
Leu	CTA	6.00	7.48	0.07	
Leu	CTT	11.00	13.72	0.13	
Leu	CTC	20.00	24.94	0.24	
Pro	CCG	2.00	2.49	0.05	
Pro	CCA	9.00	11.22	0.21	
Pro	CCT	13.00	16.21	0.30	
Pro	CCC	19.00	23.69	0.44	

Figure 16: Codon usage by bacteria for the human PI4K-IIIβ coding sequence. Analysis of the coding sequence of human PI4K-IIIβ by the Sequence Manipulation Suite (http://www.ualberta.ca/~stothard/javascrip) for codon usage by bacteria. Rare codons for which extra tRNAs are supplied in Rosetta 2(DE3) cells are enclosed by the red rectangles, alongside the number of times said codon appears in PI4K-IIIβ's sequence ("Number"), the proportion a given codon is used normalized to a 1000-amino acid sequence ("1000"), and the proportion of usage of synonymous codons by the organism of choice ("Fraction"). The Rosetta 2(DE3) cells-supplied tRNAs for the scarce codons CCC (Pro), CGG and AGG (Arg) are the most impactful for expression of PI4K-IIIβ in bacteria, as these codons appear 19, 14 and 8 times, respectively.

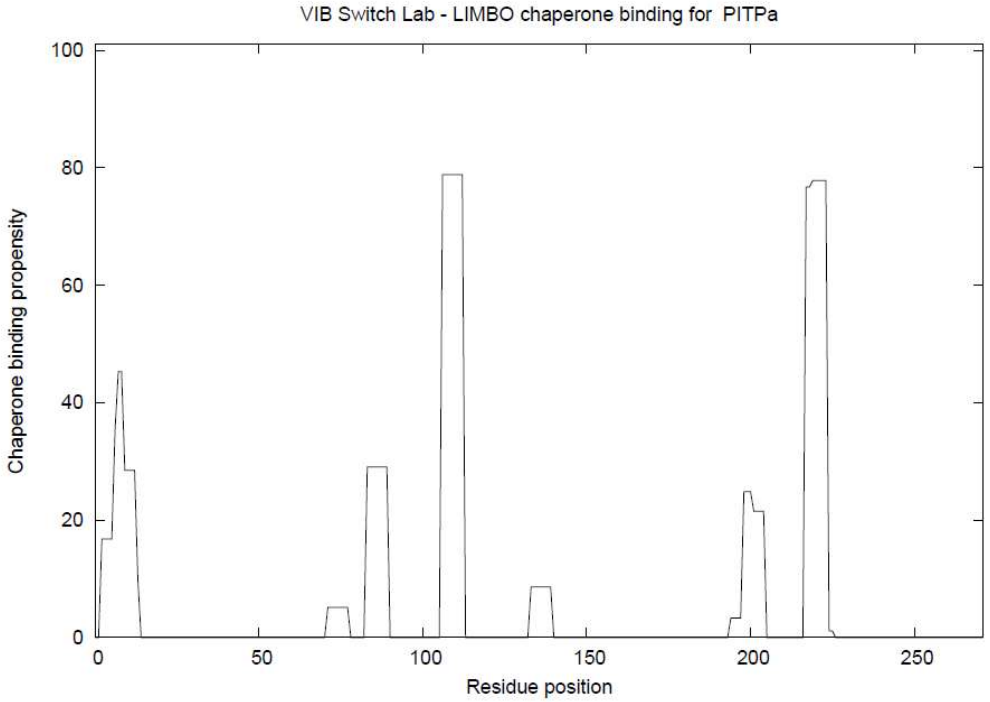

DnaK binding propensity report for PITPα. Generated by the algorithm described in (Van Durme et al., 2009).

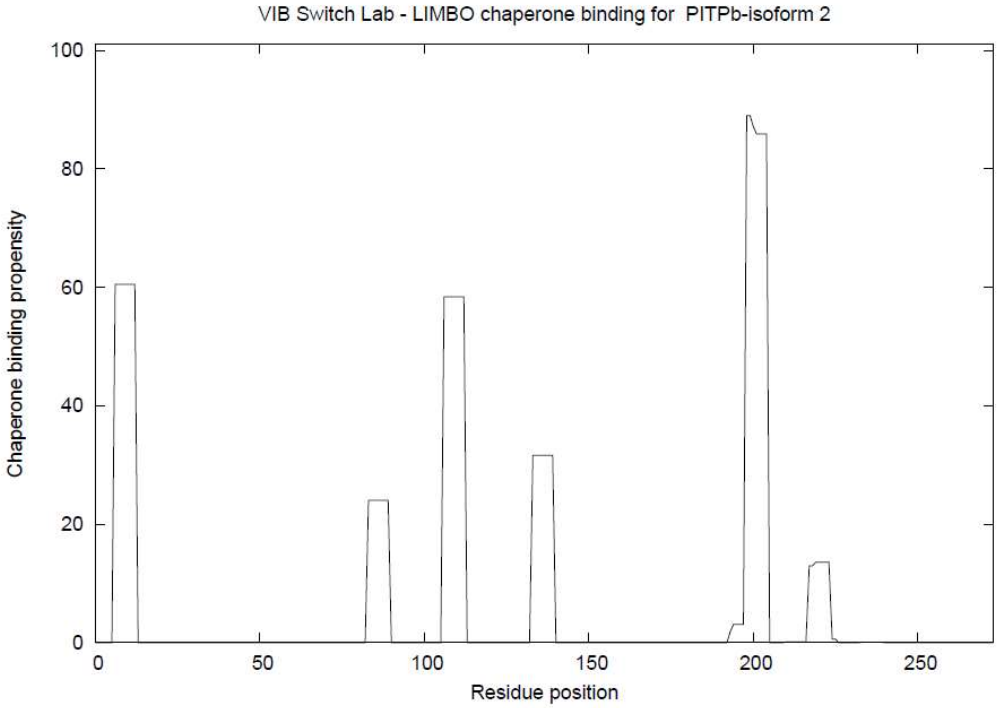

DnaK binding propensity report for PITPβ. Generated by the algorithm described in (Van Durme et al., 2009).

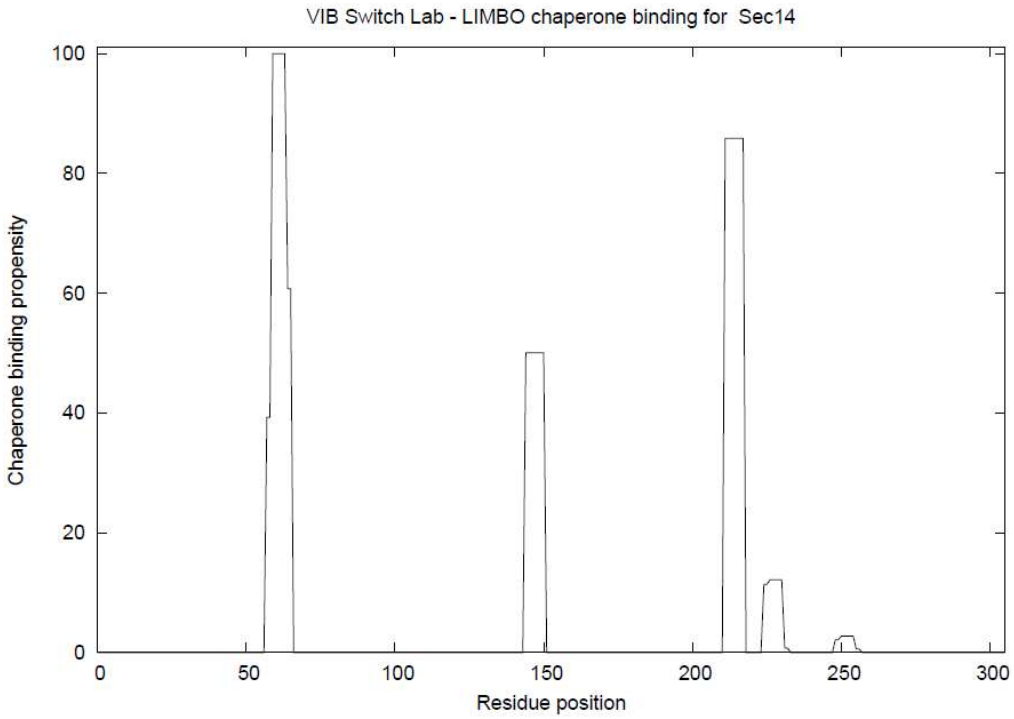

DnaK binding propensity report for Sec14p. Generated by the algorithm described in (Van Durme et al., 2009).

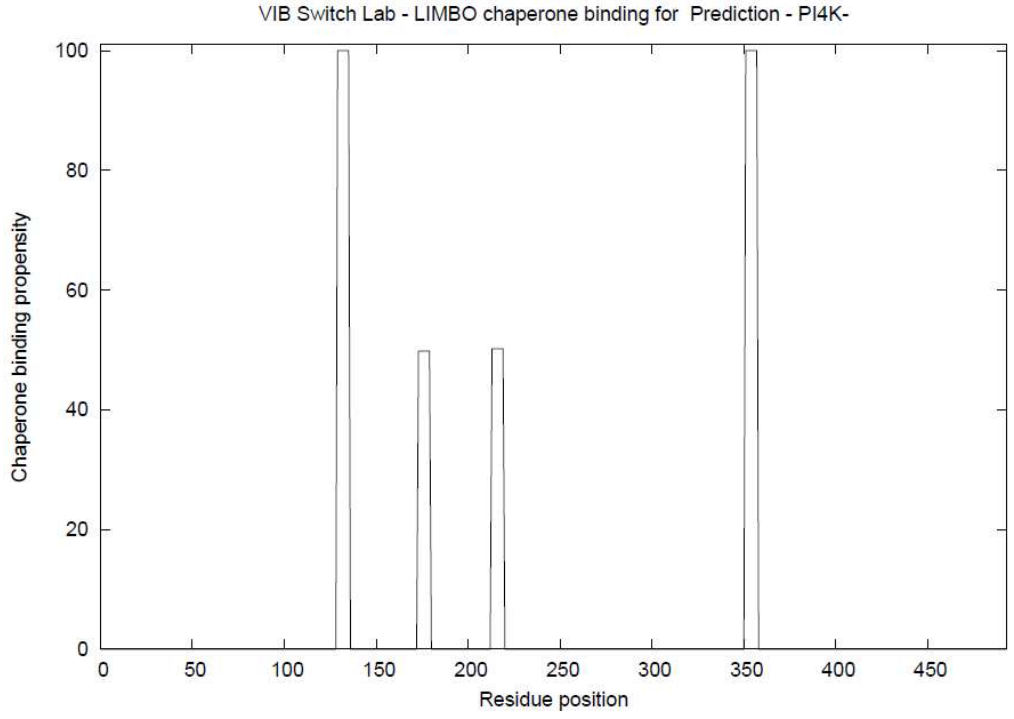

DnaK binding propensity report for PI4K-IIIβ (residues 1-500). Generated by the algorithm described in (Van Durme et al., 2009).

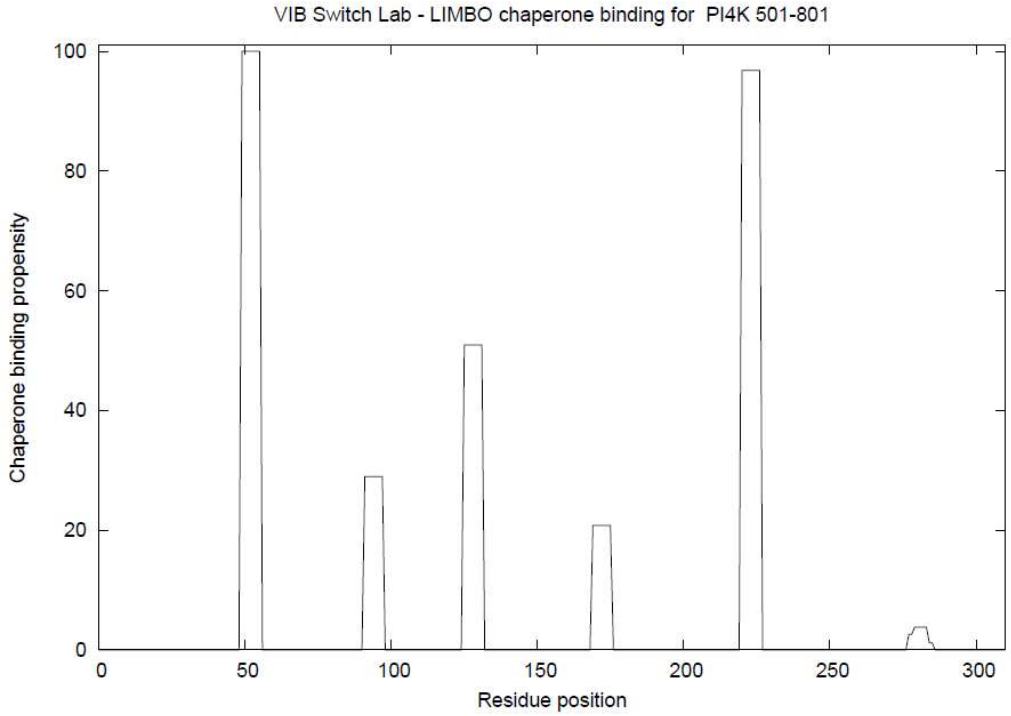

DnaK binding propensity report for PI4K-IIIβ (residues 501-801). Generated by the algorithm described in (Van Durme et al., 2009).

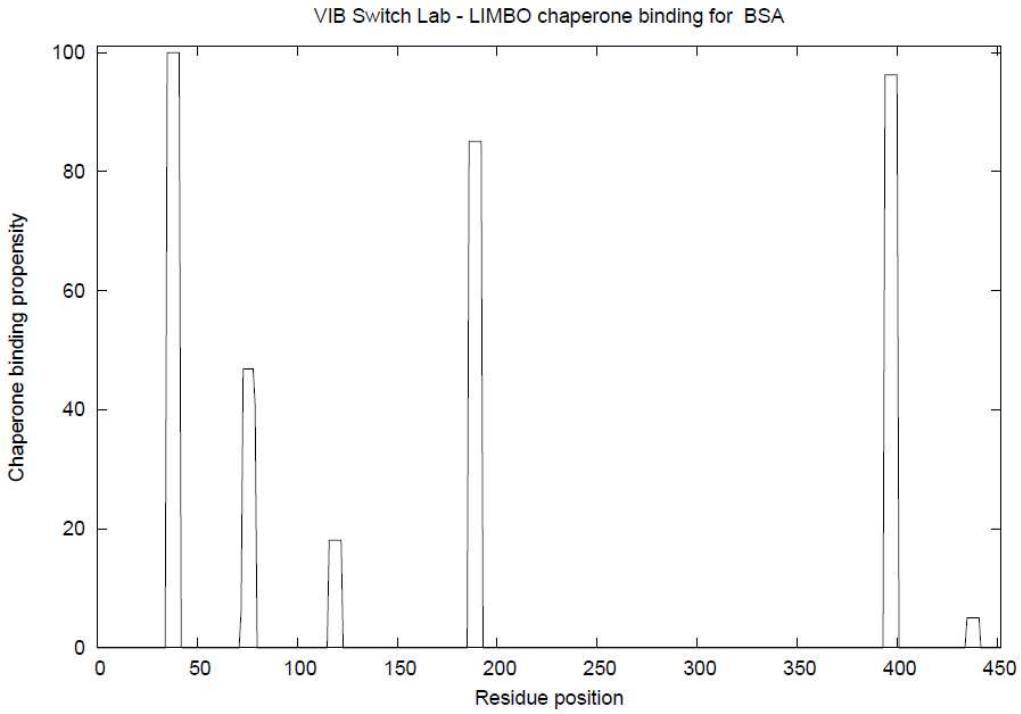

DnaK binding propensity report for BSA. Generated by the algorithm described in (Van Durme et al., 2009).

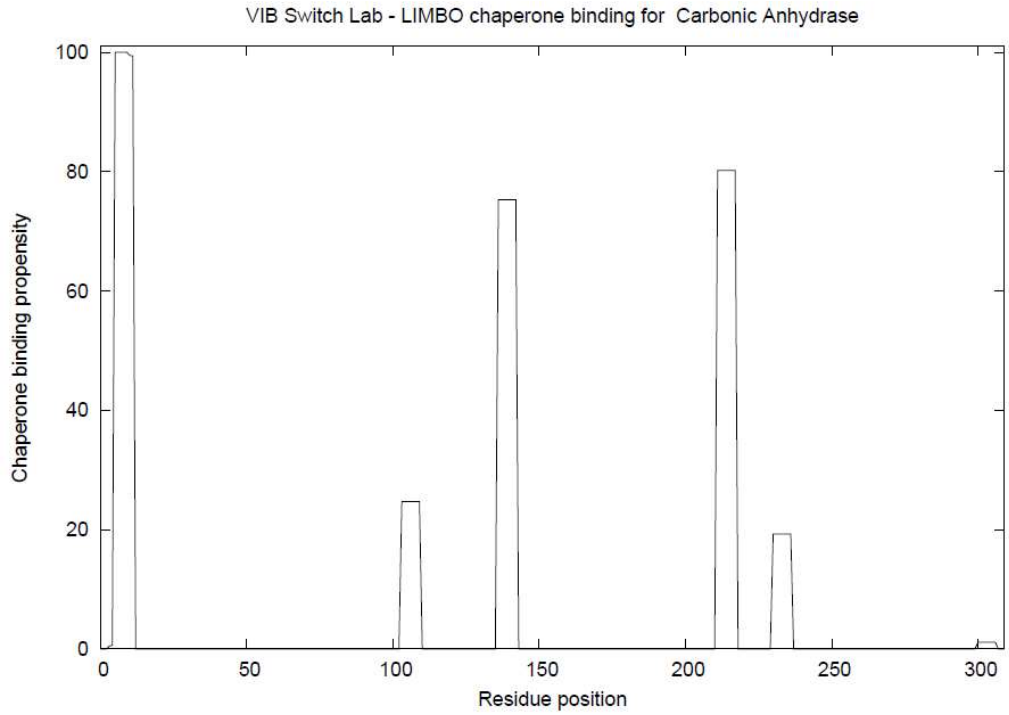

DnaK binding propensity report for Carbonic Anhydrase. Generated by the algorithm described in (Van Durme et al., 2009).

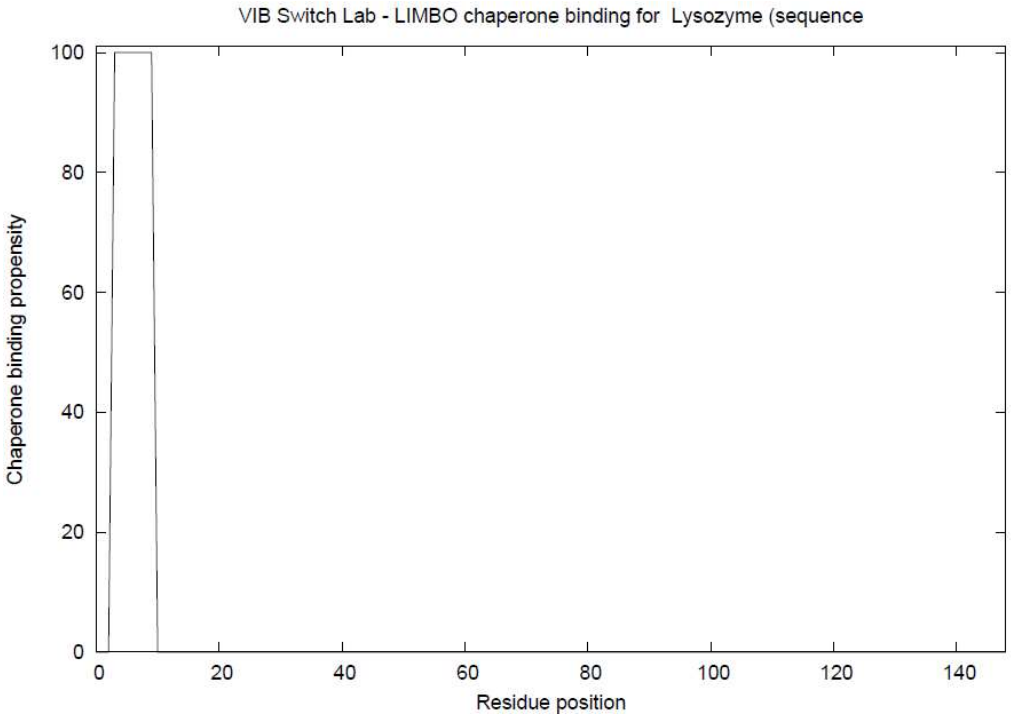

DnaK binding propensity report for Lysozyme. Generated by the algorithm described in (Van Durme et al., 2009).

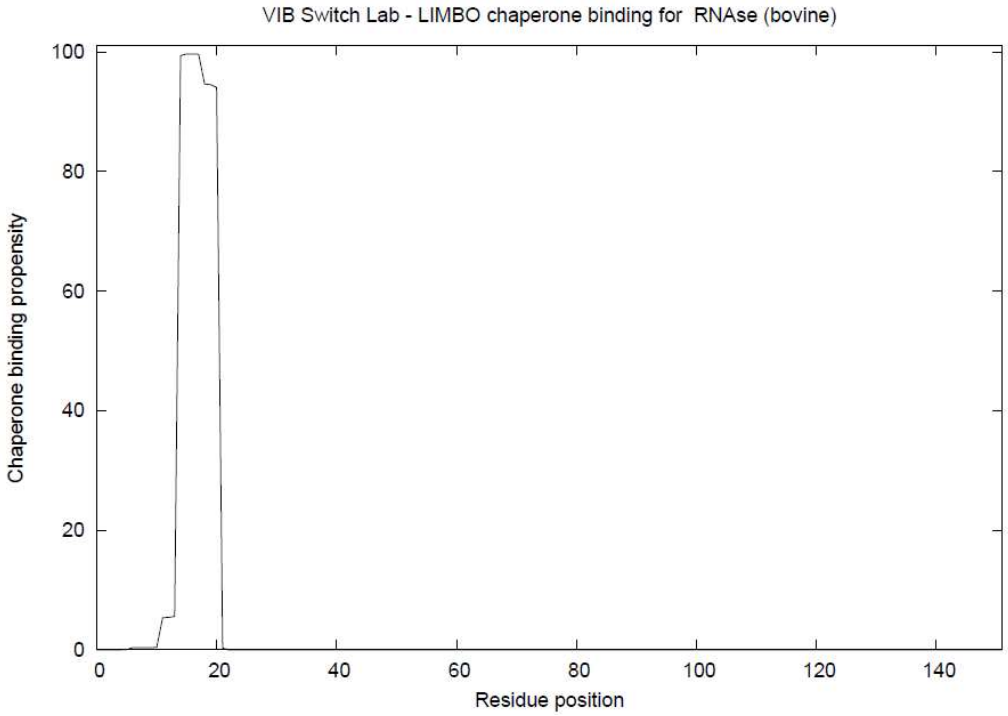

DnaK binding propensity report for bovine RNAse. Generated by the algorithm described in (Van Durme et al., 2009).